Biosensors Embedded in Contact Lenses for Human Health Monitoring

Huanfen Yao

A dissertation
submitted in partial fulfillment of the
requirements for the degree of

Doctor of Philosophy

University of Washington
2013

Reading Committee:
Karl F. Böhringer, Chair
Babak Amirparviz
Brian P. Otis

Program Authorized to Offer Degree:
Electrical Engineering

University of Washington

Abstract

Biosensors Embedded in Contact Lenses for Human Health Monitoring

Huanfen Yao

Chair of the Supervisory Committee:
Professor Karl F. Böhringer
Department of Electrical Engineering

This dissertation covers my graduate research about the development of micro biosensors which are embedded in soft contact lenses for human health monitoring in University of Washington. The work mainly focuses on two parts: the glucose sensors and the microbe sensors. As there are various informative physiological chemicals in tear fluids and a lot of eye diseases are related with bacterial invasion into the eye, biosensors embedded in contact lenses could pave a way to monitor human heath levels in a continuous and non-invasive way. In this work, glucose sensors have been developed and tested. The sensors were fabricated on plastic and parylene substrates, tested using the eye mimicking molds with artificial tear fluids, and integrated with wireless communication circuit. The parylene sensors were successfully molded into soft contact lenses and showed good characteristics such as linearity, repeatability, interference rejection property, temperature stability and protein fouling protection. Meanwhile, microbe sensors have also been constructed on parylene substrate and molded in soft contact lenses. By employing the antibody-antigen interaction and electrochemical impedance spectroscopy, the microbe sensors were tested for different concentrations of *E.coli* and *P. aeruginosa*, and further validated by biofilms. For the development of both glucose and microbe sensors, further work is necessary to make these biosensors more practical, such as optimizing the sensor design, improving the wireless

transmission efficiency, realizing comfortable contact lenses and validating the sensors with animal or clinical experiment.

Table of Contents

List of Figures

List of Tables

List of Abbreviations

AC	Alternating Current
APTES	3-Aminopropyl Triethoxysilane
CE	Counter Electrode
DEGDMA	Diethylene Glycol Dimethacylate
DTT	DL-Dithiothreitol
ELISA	Enzyme-Linked Immunosorbent Assay
FAD	Flavin Adenine Dinucleotide
FET	Field-Effect Transistor
FITC-dextran	Fluorescein Isothiocyanate-dextran
GOD	Glucose Oxidase
HEMA	Hydroxyethyl Methacrylate
Parylene-C	Poly(Chloro-p-xylylene)
PCB	Printed Circuit Board
PCR	Polymerase Chain Reaction
PDMS	Polydimethylsiloxane
pHEMA	Poly(Hydroxyethyl Methacrylate)
PI	2,2-Dimethoxy-2-Phenylacetophenone
QCM	Quartz Crystal Microbalance
RE	Reference Electrode
RT-PCR	Reverse Transcriptase Polymerase Chain Reaction
sIgA	Secretory Immunoglobulin A
SPR	Surface Plasmon Resonance
sulfo-LC-SPDP	Sulfosuccinimidyl 6-3'-[2-Pyridyldithio]-Propionamido Hexanoate
TRITC-Con A	Tetramethylrhodamine Isothiocyanate-Concanavalin A
WE	Working Electrode

Acknowledgements

I would like to gratefully and sincerely thank Dr. Karl F. Böhringer and Dr. Babak A. Parviz for their guidance, understanding, and most importantly, their full support during my graduate studies at University of Washington. I would like to express my great gratitude to Dr. Buddy D. Ratner, Dr. Brian P. Otis and Dr. Tueng T. Shen for their support and advise for my graduate research.

I would like to thank the Department of Electrical Engineering at University of Washington for providing me the opportunity to work as a research assistant. I would like to specially thank the National Science Foundation for financial support and the University of Washington Microfabrication/Nanotechnology User Facility for the microfabrication facility support.

I am particularly grateful for all the colleagues in the Bionanotechnology Laboratory for their input, great support and valuable discussion.

Finally and most importantly, I would like to thank my family, especially my husband, for their unending support and encouragement.

Chapter 1 Introduction

1.1 Eye Structure and Tear Fluid

1.1.1 Basic Structure of the Human Eye

The human eye is an organ which reacts to light for several purposes. Although small in size, human eyes are one of the most important and complex organs for daily life. The basic eye structure is shown in Figure 1.1.

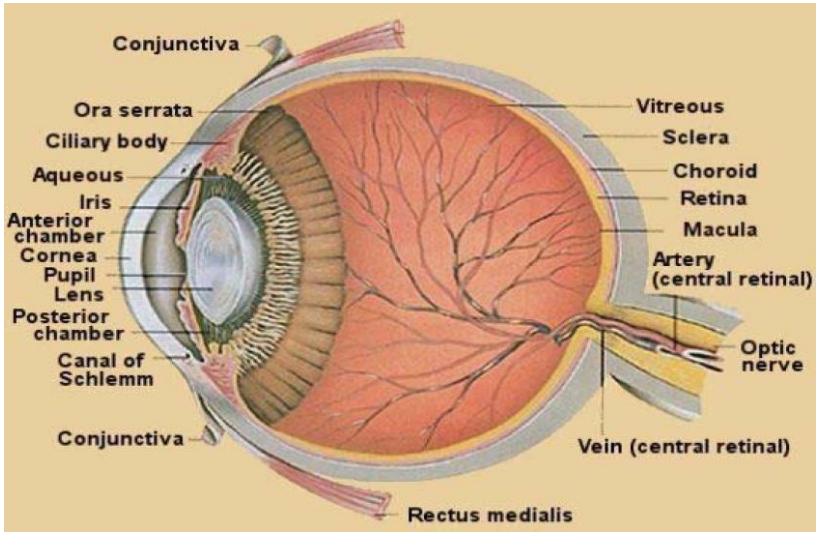

Figure 1.1 Anatomy of the eye[1]

The eye is made up of three outer coats and various inner components. The vertical size is about 2.4 cm among adults, and the horizontal distance is generally a little bit more than the vertical size. The whole volume of the eye is about 6.5 mL and the weight is 7.5 g[1].

The outermost layer is composed of the cornea and sclera[1, 2]. The smaller frontal cornea is transparent, more curved and covers the iris, pupil and anterior chamber. The cornea contributes most of the eye's focusing power, and its focus can be tuned upon the distance of objects. The larger posterior sclera is opaque, linked with the cornea, and mainly functional as a protection.

The middle layer consists of the choroid, ciliary body and iris[1, 2]. The choroid lies between the sclera and the retina. It provides oxygen and nourishment to the outer layers of the retina. The ciliary body is the circumferential tissue composed of ciliary muscle and ciliary processes, and receives parasympathetic innervation from the oculomotor nerve, responsible for shaping the lens to focus light onto the retina. The iris is a thin pigmented structure in the eye,

and has a circular opening in its center. The center opening, known as the pupil, is controlled by muscles around its edge, responsible for controlling the diameter and size of the pupil and thus the amount of light reaching the retina.

The innermost layer is the light-sensitive retina[1, 2]. The retina is a complex layer, composed largely of nerve cells. The basic process of the image creation of the retina is: light striking the retina initiates a cascade of chemical and electrical events that ultimately trigger nerve impulses, which are sent to various visual centers of the brain through the fibers of the optic nerve.

Inside these three outer layers, there are inner components, such as the anterior chamber, the lens and the vitreous body[1, 2]. The anterior chamber is fluid-filled with aqueous humor inside the eye between the iris and the cornea and exposed area of the lens. The vitreous body is the clear gel filling the space between the lens and the retina. The aqueous humor flows from ciliary body to the pupil and is absorbed through the channels in the angle of the anterior chamber. The delicate balance of liquid production and absorption controls the pressure within the eye. The lens is a transparent, biconvex structure in the eye, helps to refract light to be focused onto the retina. The adjustment of the lens is similar to the focusing of a photographic camera via movement of the lens.

1.1.2 Human Tear Fluid

The tear film ahead of the cornea forms an interface between the open air and the eyeball. There are three basic types of tears: the basal tears keep the cornea wet, nourished and lubricated continuously; the reflex tears results from eye irritation by foreign particles for environmental excitation; and the third one is psychic tears coming from crying or weeping. As the basal tears are most related to human health status, they are the targeting tears for our sensor development. And the tear fluid has many significant functions for human health as it can: (1) clean and lubricate the eyeball, (2) form a smooth layer over the corneal surface and supply nutrients for the corneal epithelium, (3) provide antibacterial agents for the ocular surface, (4) construct a vehicle for the entry of polymorphonuclear leukocytes in case of injury, and (5) dilutes and washes away toxic irritants[3].

The basic structure of the humans tear film has three distinct layers, as shown in Figure 1.2. The innermost is the mucous layer (0.02-0.04 μm), covering the cornea and providing a

hydrophobic layer. The intermediate is the aqueous layer (7 μm) composed of water and many chemicals. The outmost is the anterior lipid layer (0.1 μm), providing a hydrophobic barrier that envelops tears[3].

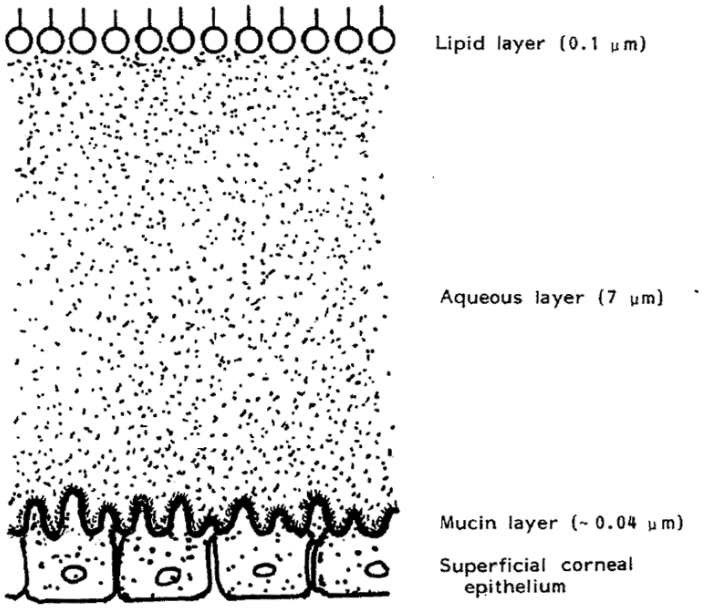

Figure 1.2 Schematic representation of the tear film[3]

There are various chemicals in the aqueous layer of the tear film, including electrolytes, organic solutes and proteins, etc. Table 1.1 shows the approximate concentrations of different key chemicals in human tear fluids[3].

Table 1.1 Major components in human tear fluid[3]

Electrolytes		Organic solutes		Proteins	
Component	Concentration (mM)	Component	Concentration (mM)	Component	Concentration (mg/mL)
Na^+	120-165	Glucose	0.1-0.6	Lysozyme	2.4±0.7
Cl^-	118-135	Urea	3.0-6.0	Lactoferrin	1.5±0.4
K^+	20-42	Lactate	2-5	Albumin	0.054
HCO_3^-	20-26	Pyruvate	0.05-0.35	sIgA	0.41±0.15
Ca^{2+}	0.4-1.1	Ascorbate	0.008-0.04	IgG	0.032
Mg^{2+}	0.5-0.9			IgM	0.0003

Besides the eyelid and eyelash, the tear fluid offers the most significant line of defense against pathogens, with its complex mixture of proteins, lipids, carbohydrates and electrolytes. Within these bactericidal or bacteriolytic activities, the principle one is the bacteriolytic

properties of lysozyme, which accounts for more than 30% of the total proteins in human tear fluid[3]. Lactoferrin, with its anti-inflammatory and antimicrobial activities, also display an essential role in maintaining ocular health. And sIgA (Secretory Immunoglubulin A) is reported as the major immunoglobulin in tears and an essential immune defense factor against infections[4]. In addition, small amounts of peroxidase have been detected in human tear fluid, and as to the biological function of peroxidase, it not only forms part of the broad spectrum of antimicrobial agents produced by the lacrimal gland, but it may also play a role in protecting the eye from potential hydrogen peroxide toxicity[4].

1.2 Diabetes and Glucose Monitoring

1.2.1 Diabetes

Diabetes mellitus, often simply referred to as diabetes, is a chronic metabolic illness with high blood glucose levels. If not treated appropriately or adequately, diabetes may cause further risk for other serious long-term complications including cardiovascular diseases, diabetic nephropathy, diabetic neuropathy and diabetic retinopathy. An estimated 285 million people, corresponding 6.4% of the world's adult population, lived with diabetes in 2010, and this number is expected to increase to 7.8% by the year 2030[5].

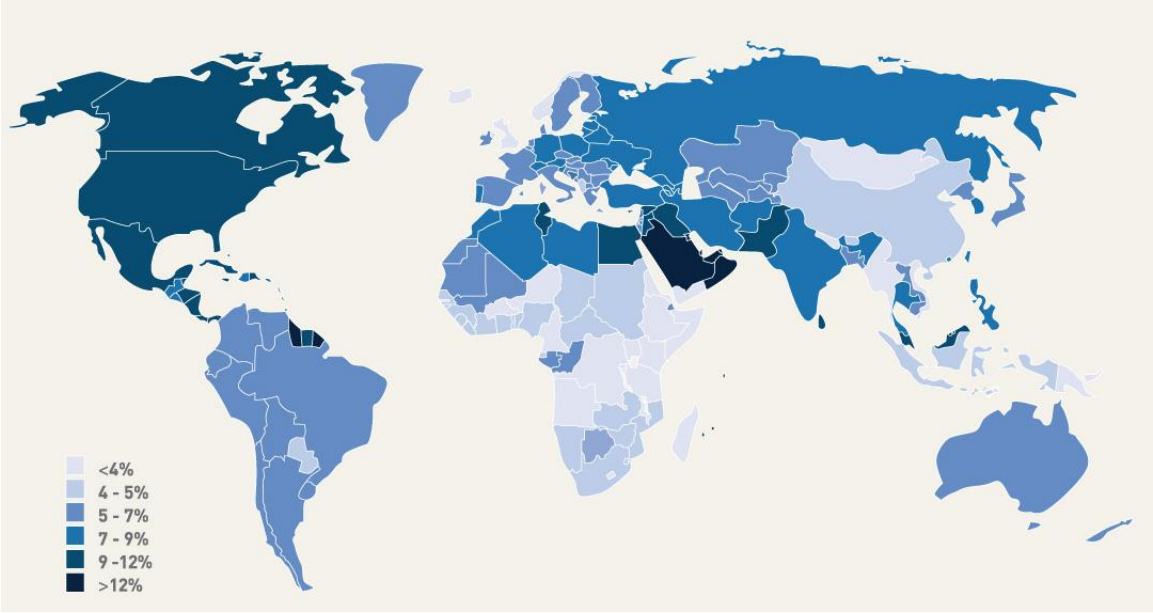

Figure 1.3 Proportion of people with diabetes (20-79 years) for the year 2010[5]

There are three main types of diabetes[6]. Type I results from the body's failure to produce insulin and presently requires the patient to inject insulin. Type II results from insulin

resistance, a condition in which cells fail to use insulin properly, sometimes combined with an absolute insulin deficiency. Type II is the most common type. Gestational diabetes is when pregnant women, who have never had diabetes before, have a high blood glucose level during pregnancy; and it may precede development of Type II.

1.2.2 Categories of Glucose Monitoring Devices

For any type of diabetes mellitus, if the amount of insulin available is insufficient, or if cells respond poorly to the effects of insulin, or if the insulin itself is defective, glucose will not have its usual effect, so it will not be absorbed properly by those body cells that require it, nor will it be stored appropriately in the liver or muscles. The net effect is persistent high levels of blood glucose, so the recurrent or persistent hyperglycemia is the main characteristic for diabetes mellitus. Based on the high glucose levels, there are some basic criteria for diabetes diagnostic, as shown in Table 1.2.

Table 1.2 Standard diabetes diagnostic criteria[7]

	Normal	Diabetes
Fasting blood glucose level	<6.1 mM two times	>7.0 mM two times
Nonfasting blood glucose level	<10.0 mM	>11.1 mM
Oral glucose tolerance test	<7.8 mM after 2 hours	>11.1 mM after 2 hours
Hemoglobin A1c test	<5.7%	>6.5%

Along with the rapid growth of modern sensing technologies and fast growth of the diabetes market, various kinds of glucose sensors have been developed depending on different mechanisms. According to whether the glucose sensors penetrates the skin and/or the sample is measured extra-corporeally, these devices can be categorized as follows[8]:

1. Totally invasive

The most typical devices are glucose sensors implanted subcutaneously[9, 10]. As implanted devices usually require an open cut, elicit a foreign body response, and suffer from biofouling-induced sensor degradation, minimally invasive devices have recently become a more desirable option for monitoring glucose levels.

2. Minimally invasive

The most common devices of recent minimally invasive monitors are the finger prick test based on microneedles. Since the first available commercial blood glucose meter Dextrostix® (Ames Company) in 1965, there have been various kinds of glucometers based on blood sample

coming into the markets, as shown in Figure 1.4. Among them, finger prick test is the most commonly used method due to its easy operation, quick response and less distress than venipuncture, so it is widely used for self-monitoring of blood glucose.

1965 Ames Dextrostix®　　LifeScan OneTouch®　　Bayer CONTOUR®

Figure 1.4 Some commercial glucometers

3. Non-invasive

Although the finger prick test is a nearly completed method, the glucometer provides only a single temporal value, and cannot follow the rapid fluctuations of blood glucose levels towards hypoglycaemic or hyperglycaemic events during diabetes medication. And this sensing method is not only invasive, requiring the direct contact between the sensor and the blood, which presents a risk from blood infection, but also painful, leading uncomfortable feeling due to its lancing devices. Therefore the attitude was initially motived toward a non-invasive continuous monitoring of glucose levels. Recent advances in portable devices and sensing techniques offer the potential of developing a non-invasive, continuous, and portable glucose sensing method for the next generation of monitoring diabetes.

An alternative route to decrease the invasive nature of glucose monitoring would be to take the measurements from urine, saliva or tear fluid. A major disadvantage of this approach is its intermittent nature: all of these fluids need to be collected before a measurement, which makes the truly *in situ* sensing not possible. Recently, however, this situation has been changed as several sensor designs have been developed that could allow continuous monitoring in tear fluid.

For instance, Gao *et al*. have reported a pH-sensitive-polymer-coated magnetoelastic glucose sensor for glucose assay in urine[11]. The sensor contains immobilized glucose oxidase (GOD), which catalyzes the conversion of glucose to gluconic acid, resulting in shrinking and corresponding mass decrease in the pH sensitive polymer, and consequently increases the resonance frequency of the magnetoelastic sensor. The test platform shows a linearity between glucose 1 mM to 15 mM, and good interference rejection for acetaminophen, lactose, saccharose, galactose, and ascorbic acid. However, this sensor also brings the complexity of collecting urine samples.

Yamaguchi *et al*. have reported an enzyme-based glucose sensor to analyze glucose as low as 5.6 μM in saliva[12]. The saliva analyzing system is composed of a flow injection instrument and an enzyme-based sensor. But an obvious drawback of this sensor is that the saliva collecting procedure is very inconvenient and time-consuming, because the process of collecting saliva is done by inserting cotton rolls onto the subjects' sublingual caruncular for more than 5 minutes and the saliva needs to be extracted by compressing the cotton rolls into syringe. Besides, an extra step is necessary for the subjects to brush their teeth and rinse their oral cavities to remove intraoral residues before every test.

Compared with urine and saliva, tear fluid is more appealing as it is easily accessible and does not need sample collection if designed appropriately, thus achieving non-invasive sensing in real. As reported (Figure 1.5), there exists a potential correlation between glucose levels in tear and blood[13, 14], although the correlation between them has not yet been fully established.

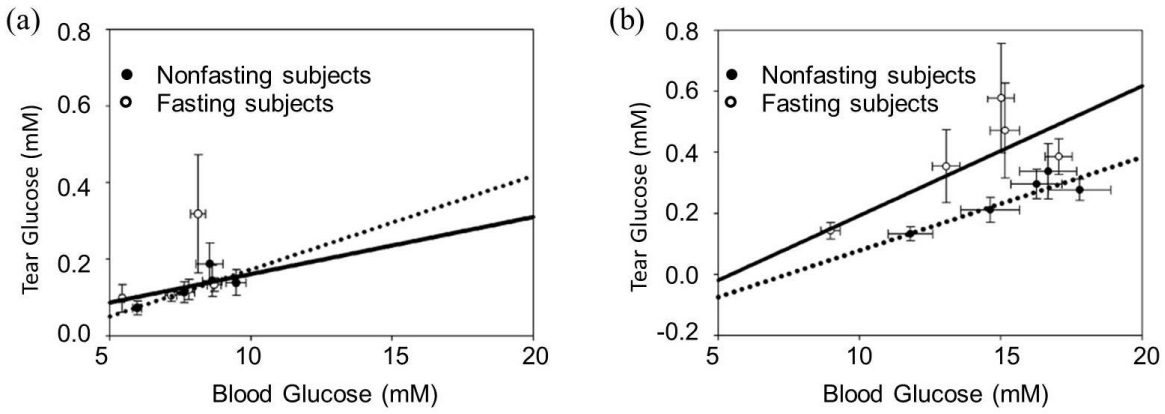

Figure 1.5 Correlation between blood and tear glucose levels for fasting and nonfasting groups[13]: (a) nondiabetic subjects (n=23); (b) diabetic subjects (n=15)

To test glucose levels of tear fluid *in situ*, a contact lens would be an ideal vehicle for non-invasive and continuous monitoring, as it can be worn for hours without discomfort. Under normal circumstances, the eye surface is continuously flushed by basal tear fluid. The fluid is generated by the lacrimal gland and is spread across the eye surface by the blinking movement of the eyelid. Spent tear fluid collects in the lacrimal lake around the bottom eyelid, where it is drawn out by lacrimal puncta. Under such conditions, the signal from a contact lens-borne glucose sensor would reflect the glucose concentration in the basal tear fluid.

March *et al.* developed the first trial of a non-invasive contact lens glucose sensor, which utilizes fluorescence to probe the tear glucose concentrations by means of a competitive binding mechanism[15]. The contact lens contains tetramethylrhodamine isothiocyanate-concanavalin A (TRITC-Con A) and fluorescein isothiocyanate-dextran (FITC-dextran) during the contact lens polymerization process. As the TRITC-Con A binds competitively with FITC-dextran and glucose, the increase of glucose will lead to less binding of FITC-dextran with TRITC-Con A. Because the FITC-dextran fluorescence is quenched through free resonance energy transfer when associated with TRITC-Con A, fluorescence increases proportionally to glucose concentration. Of course, the system needs a modulated blue LED as a light source, and another diode detector, as well as a light filter, as shown in Figure 1.6(a). Recently, Chu *et al*. have constructed a soft biosensor on the surface of a polydimethylsiloxane (PDMS) contact lens and monitored tear glucose *in situ* on a rabbit eye, as shown in Figure 1.6(b). The measurements are carried out with a bench top potentiostat, using a hard-wired connection from the sensor.

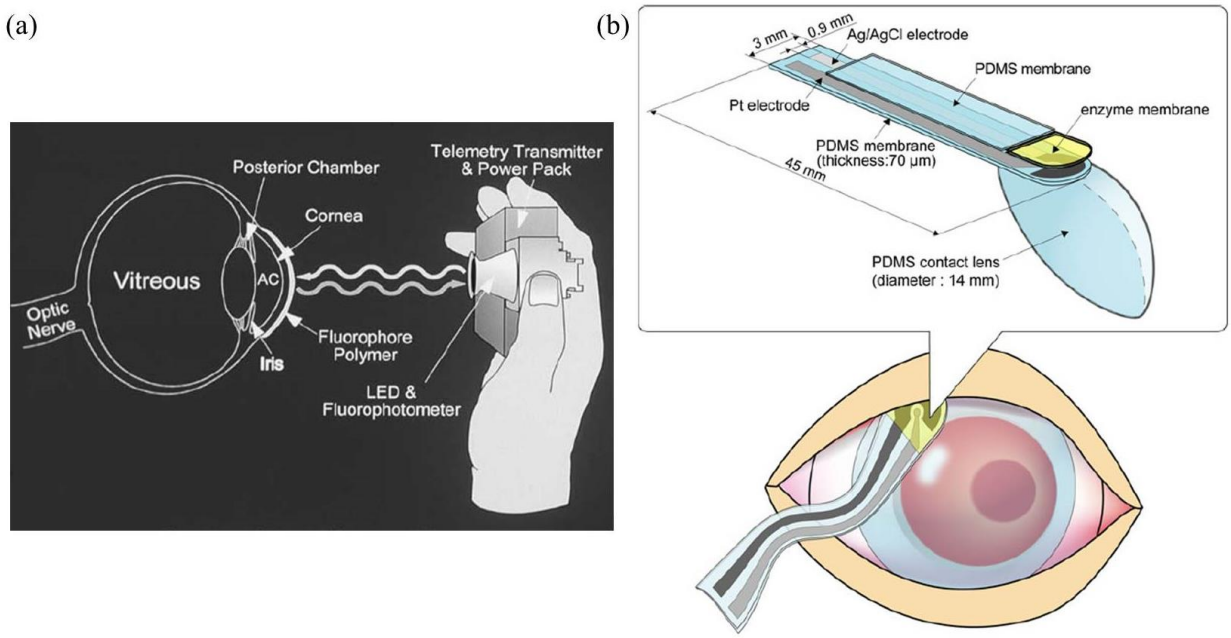

Figure 1.6 Contact lens based glucose sensors: (a) diagram of the contact lens glucose sensor using fluorescence with a hand-held photofluorometer[15]; (b) structure of the contact lens glucose sensor having an enzyme electrode on the surface of a PDMS contact lens[16]

1.2.3 Glucose Detection Methodologies

According to different mechanisms of glucose detection, there is another way to categorize various glucose sensors, such as electronic/magnetic, optical, and nano-technological methods, etc.

1. Electronic/magnetic methods.

Different electronic and/or magnetic methods have been employed to transduce the biological signals occurring at the electronic/magnetic supports, including electrochemical measurement[17-19], impedance spectroscopy[20], electromagnetic sensing[21], potential changes[22], piezoelectric transduction[23], and field-effect transistor (FET)[24], etc. Compared to other electronic techniques, electrochemical methods are relatively simple, inexpensive, and more specific to glucose. They require short acquisition times and can easily be reduced to nanoscale dimensions and incorporated into various device geometries. Thus electrochemical sensing is widely used in modern detection technologies. Since the first glucose sensor was constructed by Clark and Lyons in 1962[25], a large number of electrochemical approaches have been developed, both enzymatic and non-enzymatic.

The use of non-enzymatic electrodes as glucose sensors strives to directly oxidize glucose in the sample. With the rapid development of nanotechnologies, nanostructures are usually employed in order to improve the sensitivity and selectivity of the non-enzymatic sensors[26]. But these devices have the drawbacks of non-specificity to glucose and substantial fouling of electrodes by the products of glucose oxidation.

In contrast, enzyme-based methods benefit from their high specificity to glucose and high sensitivity. There are mainly two kinds of enzymes, glucose oxidase (GOD) and PQQ-glucose dehydrogenases[27] to catalyze glucose. Of these two alternatives, GOD exhibits superior substrate specificity and enhanced operating stability[28], and hence is widely applied in the design of glucose monitoring device. The GOD structure and the basic enzymatic reaction is shown in Figure 1.7.

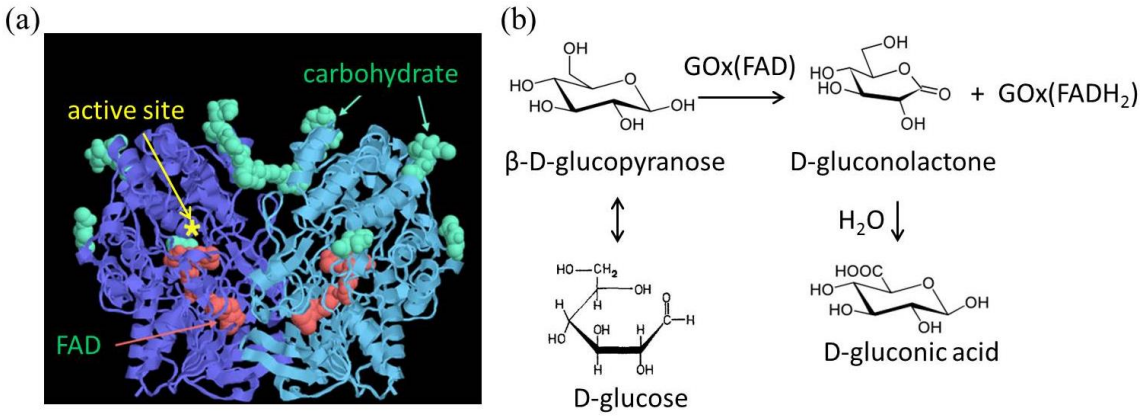

Figure 1.7 GOD and the enzymatic reaction: (a) the structure of GOD[29];
(b) the basic enzymatic reaction based on GOD

GOD consists of two equal subunits (Figure 1.7(a)), each having a molecular mass of about 80 kDa and containing one cofactor FAD (flavin adenine dinucleotide). The FAD is bound deep inside the enzyme shown in red. The active site where glucose binds is just above the FAD, in the deep pocket shown with a star. The whole enzyme is covered with carbohydrate chains outside. The enzyme size is about 6 nm × 5 nm × 4 nm[30]. The redox cofactor FAD has an oxidized form FAD and a reduced form $FADH_2$. It converts between those forms by accepting or donating electrons. GOD catalyzes a specific redox reaction where D-glucose is initially oxidized to D-gluconolactone, which can subsequently hydrolyze spontaneously to gluconic acid (Figure 1.7(b)). The oxidation of glucose is balanced by the reduction of FAD to $FADH_2$. The

reduced $FADH_2$ needs some strategy to transfer electrons in order to go back to the active form FAD. As the redox center is deep within the enzyme, such electron transfer to an external redox-active center is a major limiting factor for the glucose oxidation rate.

Based on the enzyme structure and the enzymatic reaction, three different strategies are in place to oxidize the $FADH_2$, as shown in Figure 1.8. The first one is based on direct electrical communication between the enzyme and the electrode[31], but the electron transfer is a big difficulty due to the physical separation of the electrode surface and the cofactor. The second one is applying an electron transfer mediator, which can access the cofactor and thus constructs a bridge between the electrode and the enzyme[32, 33]. But the addition of mediator is sometimes not acceptable for the sensing system, and the dissolved H_2O_2 will compete with the mediator, which causes some interference and reduces the efficiency. The third mechanism depends on relying on O_2 as a naturally occurring mediator[34, 35]. It oxidizes $FADH_2$ back to FAD, producing H_2O_2 in the process. H_2O_2 is measured on the electrode by oxidation. This method responds fast and does not require the addition of a mediator, but sometimes the dependence on O_2 brings some limitations for this method.

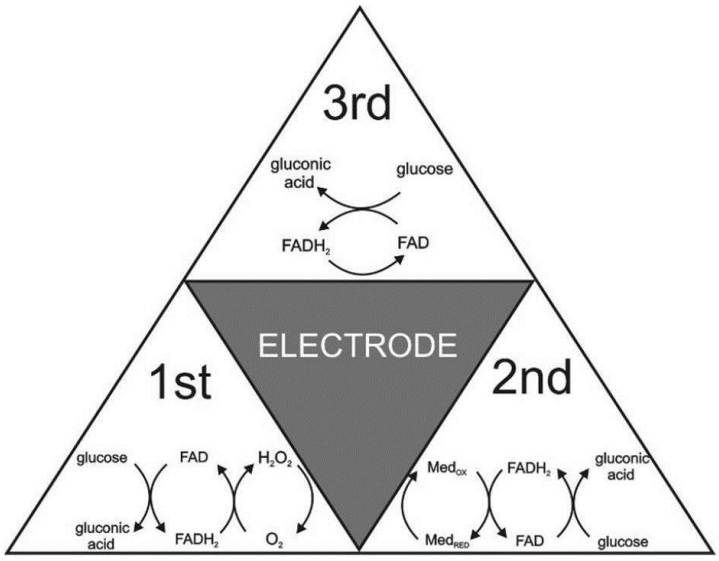

Figure 1.8 Three mechanisms of enzymatic glucose sensors[36]

2. Optical methods

Optical methods have gained attention as a non-invasive measurement procedure for biological substances. These optical methods have included measurement of the rotation of optical polarization in the aqueous humor of the eye[37] or a fluorescence contact lens measuring

in tear film[15] or the use of near-infrared spectroscopy in tissues from the finger or the lip[38]. Raman spectroscopy has also been investigated for this purpose[39]. But clinical applications have not succeeded because the in vivo optical pathways contain various constituents that interfere with the measurement, and the differences in photometric characteristics among sugars is small.

3. Glucose sensing based on nanotechnologies

Recent advances in the development of nanotechnologies revolve around the increase in different kinds of nano glucose sensors, while these nanosensors usually have to cooperate with other sensing methods, such as magnetic, electrochemical or optical strategies, to achieve the goal of sensing. For instance, a Si-based field-effect electronic transducer with Au nanoparticles and GOD has been reported to sense glucose concentrations with a high sensitivity[40]. Another nanosensor with oxygen-sensitive nanobeads by immobilization of lipophilic indicators has also shown its functionality of monitoring the consumption of oxygen during enzymatic reaction of glucose[41]. Besides, nanotubes, nanowires and other nanostructures have also been developed for glucose sensing in recent years[42, 43].

1.3 Ocular Infection, Microbe Sensing and Biofilm Monitoring

1.3.1 Basic Bacteriology

1. Bacterial architecture

Bacteria are a large domain of prokaryotic microorganisms. Compared with the super kingdom of eukaryotes, prokaryotes have many aspects of difference[44], such as no nucleus, no nucleosomes, no steroids, no cytoskeleton, no mitochondria, and cell wall with unique residues, as shown in Figure 1.9.

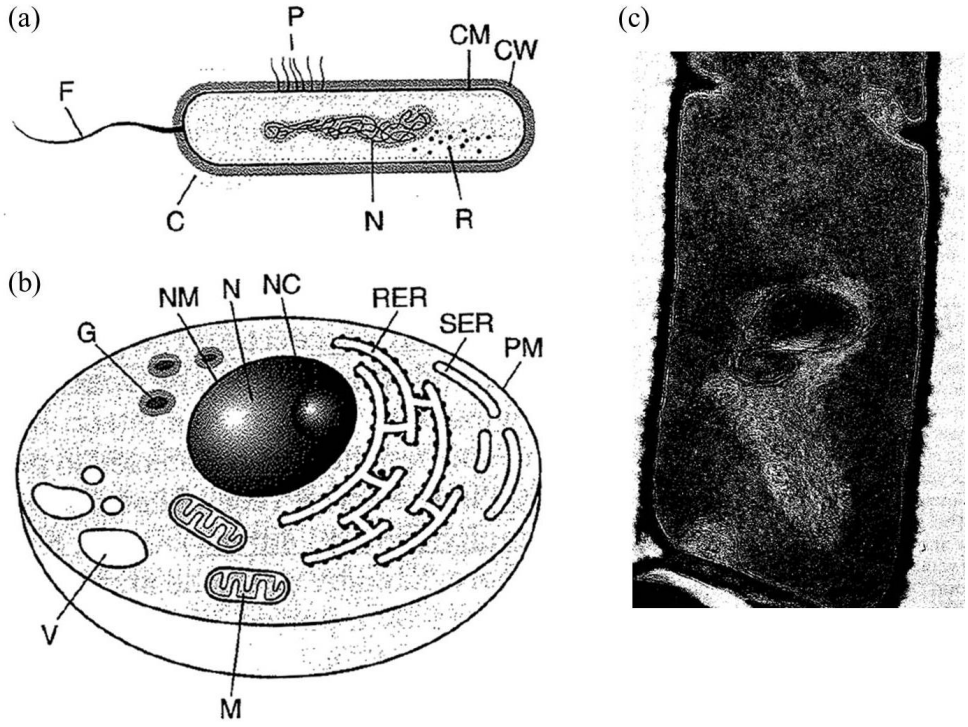

Figure 1.9 Prokaryotic and eukaryotic cells: (a) diagram of a prokaryotic bacterial cell[45]; (b) diagram of a eukaryotic cell[45]; (c) image of Bacillus subtilis[44]. CM: cell membrane; CW: cell wall; P: pili; N: nucleoid in the cytoplasm; R: ribosomes; F: flagella; C: capsules; G: storage granules; M: mitochondria; V: vacuole; N: nucleus; NM: nuclear membrane; NC: nucleolus; RER: rough endoplasmic reticulum; SER: smooth endoplasmic reticulum; PM: plasma membrane.

2. Categories of bacteria

Bacteria are traditionally categorized by the types of different cell walls. There are basically two kinds of cell wall structures in bacteria, which have been categorized according to their staining characteristics, as the gram-positive and the gram-negative types. In addition, some mycobacteria have an acid fast cell wall, and mycoplasmas have no cell wall[45]. As shown in Figure 1.10, gram-positive bacteria has a very thick peptidoglycan layer in the cell wall, thus they are stained by blue or violet by gram staining. For an opposite position, gram-negative kinds have two layers for the cell wall: the inner peptidoglycan layer is much thinner than in gram-positive cell walls; and the outside peptidoglycan layer is an additional unique membrane containing proteins, phospholipids, and lipopolysaccharide. Gram-negative bacteria do not retain crystal violet dye in the gram staining protocol[45].

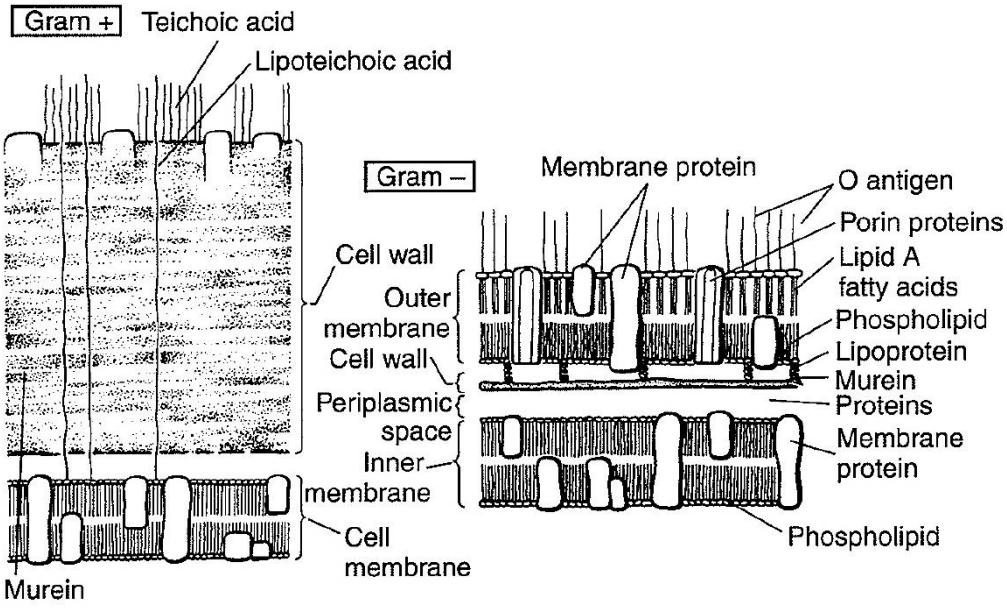

Figure 1.10 The cell envelope structure of bacteria[45]: (a) gram-positive bacteria; (b) gram-negative bacteria

3. Antibody-antigen reactions

An antibody, also known as an immunoglobulin, is a Y-shaped protein produced by the immune system to identify and neutralize foreign objects such as bacteria and viruses (Figure 1.11). The antibody recognizes a unique part of the foreign target, called an antigen. Antigens are usually proteins or polysaccharides in the cell walls, flagella, and toxins of bacteria[45]. Antibodies are typically made of basic structural units, each with two large heavy chains and two small light chains. They are grouped into different isotypes based on which heavy chain they possess, such as IgA, IgD, IgE, IgG and IgM known in mammals[45]. The variation at the tip of the protein allows millions of antibodies, that is the antigen binding site to recognize different antigens. The basic process of antigen detection involves reacting a clinical specimen with an antibody preparation specific for the antigen of interest. If the microbial antigen is present in the specimen, an antigen-antibody interaction occurs. This interaction can then be detected by a number of techniques.

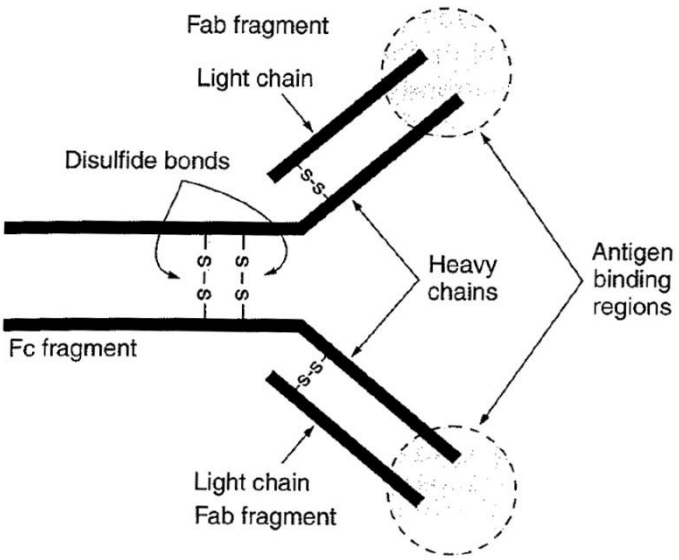

Figure 1.11 Structure of an antibody molecule and its binding sites[45]

1.3.2 Ocular Infections

Because of their location, external ocular structures such as the conjunctiva and cornea are frequently challenged by a variety of potentially pathogenic microorganisms. One of the mechanisms which protects the eye from infection is the tear layer, particularly due to its antimicrobial substances, such as lysozyme, lactoferrin, beta-lysin, and the antibody-complement system of proteins[46]. However, a few microbes can occur in the tear film and further invade and penetrate the intact epithelium of the conjunctiva or cornea, causing an infection. When an infection has started in one layer of the eye, the spread to adjacent layers and tissues can occur quite rapidly. Such spreading can result in devastating and permanent damage to the functional integrity of the eye[45].

Any organism that can invade the internal structures of the eye is capable of causing infection. For example, the red eye, the most common ocular symptom, is the inflammation of the conjunctival tissue, usually caused by *S. aureus* in warm climates or *S. pneumonia* in cool temperature. *S. aureus* and members of the staphylococcal family are the most frequently isolated bacteria from the lid margins. The infection of cornea is usually caused by *P. aeruginosa*, *S. aureus*, and may also be invaded via metastatic spread from the conjunctiva or systemic lesions. Infection of the sclera, known as scleritis, is caused by *P. aeruginosa*, *S. aureus*, *S. pneumonia*, etc. Table 1.3 lists some bacteria recovered from ocular infections.

Table 1.3 Some bacteria associated with ocular infectious diseases[45]

Gram-negative	Gram-positive
Pseudomonas aeruginosa	*Propionibacterium acnes*
Moraxella catarrhalis	*Actinomyces israelii*
Moraxella lacunata	*Staphylococcus aureus*
Aeromonas hydrophila	*Streptococcus pneumonia*
Actinobacillus actinomycetemcomitans	*Staphylococcus epidermidis*
Treponema pallidum	*Chlamydia psittaci*

1.3.3 Traditional Methods for Microbe Detection

By far, the most popular traditional methods are based on culture and colony counting methods, the polymerase chain reaction (PCR), and Enzyme-linked immunosorbent assay (ELISA).

Colony counting methods assume that each colony is derived from an individual cell and it relies on the growth of a microbial population to levels that can be counted, either directly by eyes, or in conjunction with cytometry[47]. Although colony counting methods are the standard strategy in microbiology, they have the limitations of consuming time, required temperature, oxygen content and pressure in liquid or solid media.

Microbe sensing can also relies on nucleic acid detection, based on PCR, a nucleic acid amplification technology. As shown in Figure 1.12(a), a typical PCR cycle consists of a start heat denaturation of the DNA template, the addition of specific primers and primer-template hybrid, and finally DNA strand polymerization and extension. And the presence of the amplified sequence is subsequently detected by gel electrophoresis. The specific primers can be designed and used to target the sequence in the DNA of pathogenic microbes[48]. Moreover, different PCR methods have developed for bacterial detections, such multiplex PCR[49], reverse transcriptase PCR (RT-PCR)[50], real-time PCR[51], PCR-ELISA[52], etc.

ELISA is an enzyme-based immunoassay to detect the presence of a substance in a liquid or wet sample. The “sandwich ELISA” is the most common kind to detect sample antigen, thus to detect the pathogenic bacteria[48]. The basic process is shown in Figure 1.12(b): after a known quantity of specific antibodies is immobilized, the antigen-containing sample is applied to the plate and followed by the enzyme-linked secondary antibodies, and the final step is applying a

chemical that is converted by the enzyme into a color or fluorescent or electrochemical signal which can be detected finally.

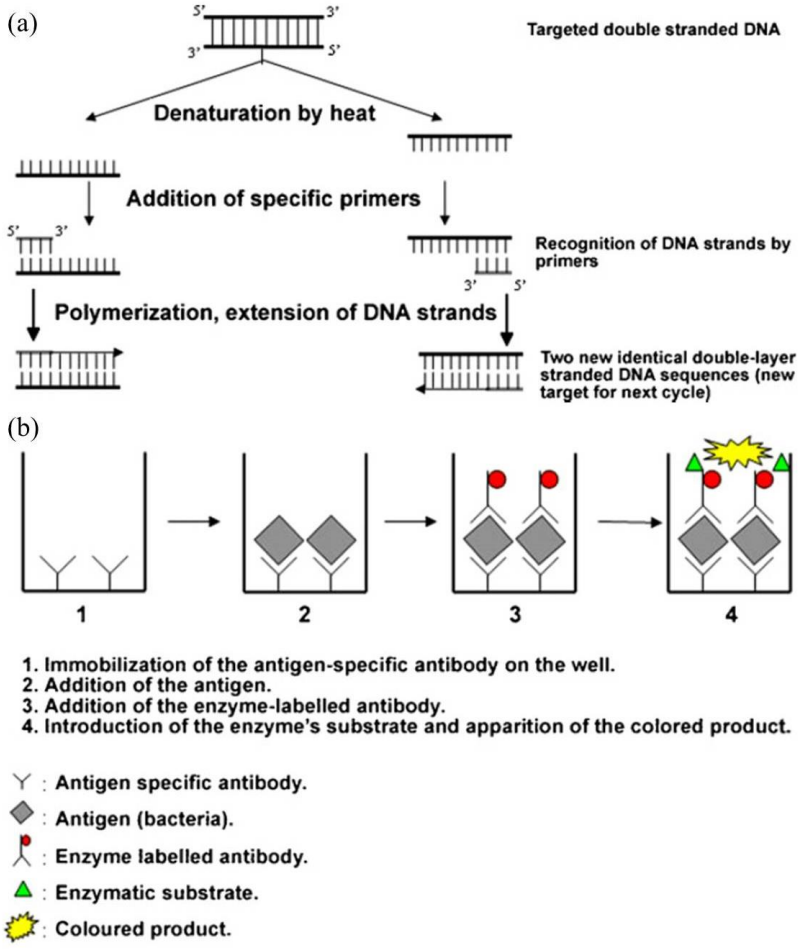

Figure 1.12 Schematic representation: (a) PCR; (b) "sandwich ELISA"[48]

1.3.4 Biosensors for Microbe Detection

As microbe detection is of the utmost importance primarily for health and safety reasons, a wide variety of detection methods have been developed. An ideal device would have the properties of high sensitivity, low detection limit, rapid analysis time, good specificity, portability and automation, etc. The development of microbe detection methods ranges from the traditional methods to modern biosensors.

1. Recognition methods and immobilization strategies

According to the types of biological recognition methods, the biosensors for microbe detection can be categories as label-free sensors, enzyme-based sensors, nucleic acid-based sensors, and antibody-based sensors.

For label-free sensors, microfluidic cells are usually constructed as a chamber to contain the sample of interest. Since the membrane of bacterial cells act as an insulator at low alternating current (AC) frequency, the measurement is performed by directly recording the impedance[53], or based on nanoparticles[54], or using the atomic force microscope[55]. The enzyme-based sensors and the nucleic acid-based sensors are usually the modern biosensors combining ELISA or PCR with electrochemical or fluorescent detection[56].

As the label-free sensors do not have a high specificity, and enzyme-based methods usually suffer from time consumption and complex processes, the use of antibodies in biosensors is currently more popular. Antibodies may be polyclonal, monoclonal or recombinant, depending on their selective properties and the way they are synthesized. The most frequent antibody immobilization routes are shown in Figure 1.13[57]. The physical adsorption method (Figure 1.13(a)), the hydrogel-based immobilization (Figure 1.13(b)) and the Hisx6-tag-mediated immobilization (Figure 1.13(c)) are most common. Figure 1.13(d) shows the immobilization using the silane coupling method, transglutaminase-mediated immobilization, and immobilization using coiled coil interaction. In the silane-coupling method, amino groups in the wild proteins are usually used as a functional group. While in the other three methods, the proteins are fused with a corresponding peptide as an affinity tag respectively: the streptavidin-mediated immobilization (Figure 1.13(e)), protein-mediated immobilization (Figure 1.13(f)), and glutathione/GST-mediated immobilization (Figure 1.13(g)).

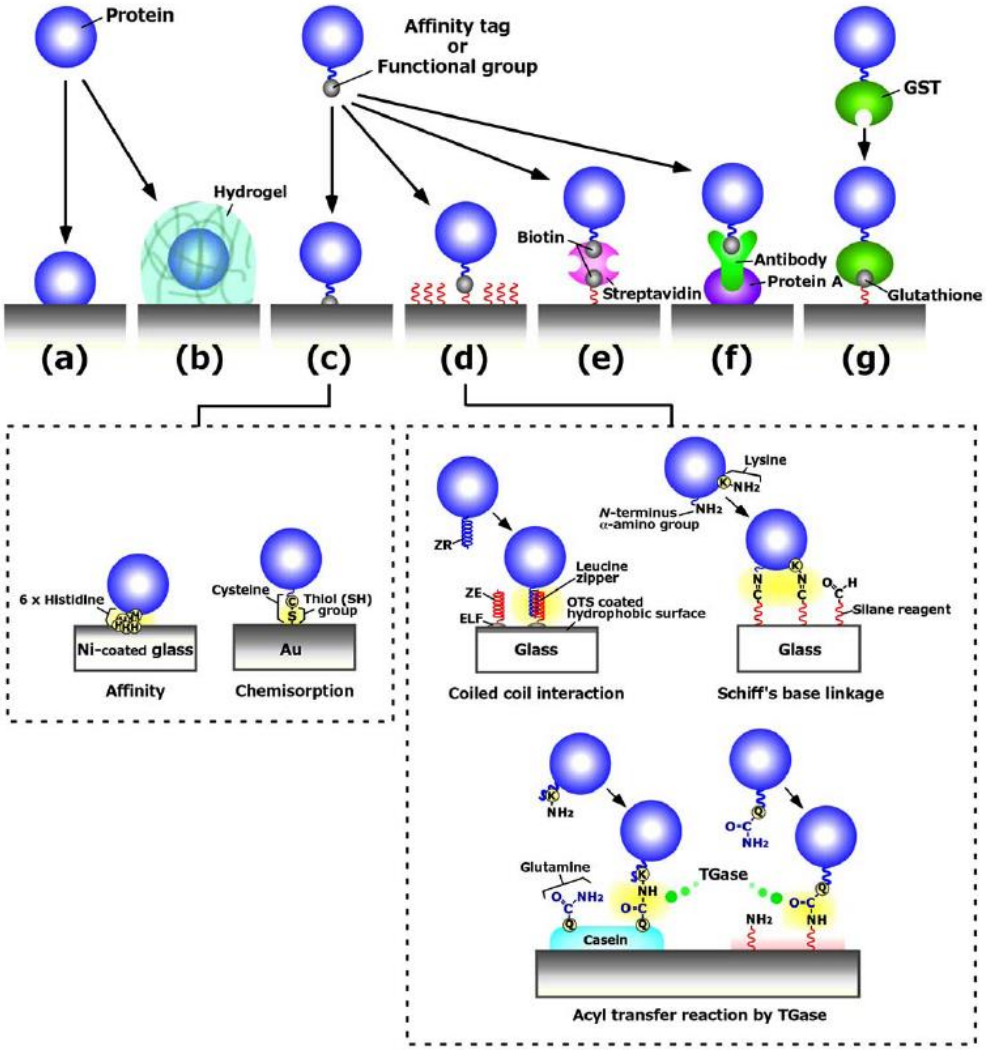

Figure 1.13 Conceptual schemes of various immobilization methods[57]

2. Various transducing systems

The transducing system may be optical, electrochemical, impedance, piezoelectric, magnetic, or based on nanomaterials.

A typical method for optical sensing is fluorescence. Secondary fluorescence represents the emission produced after a molecule is combined with a primary fluorescent molecule called a stain or fluorochrome. Common fluorochromes used for imaging of microbial cells include acridine orange, ethidium bromide, fluorescein isothiocyanate, 5-(4,6-dichlorotriazinyl) aminofluorescein, 4’,6-diamidino-2-phenylindole, europium chelate, magnesium salt of 8-anilino-1-naphthalene sulfonic acid, and calcofluor white M2R. Direct microscopic observation have been performed with fluorescence microscopy, transmission electron microscopy, and

scanning electron microscopy[58]. Surface plasmon resonance (SPR) biosensors, in contrast to fluorescence detection, measure change in refractive index caused by structural alterations in the vicinity of thin film metal surface, based on angular, wavelength or intensity modulation. As SPR offers label-free, sensitive, specific and rapid detection, it has been successfully used for analyzing microorganisms[59].

Electrochemical devices are mainly based on the observation of current or potential changes due to the interactions occurring at the sensor-sample matrix interface. Liao *et al.* have reported an electrochemical DNA biosensor based on biotin-modified capture probe and fluorescein-modified detector probe for rapid identification various uropathogens in clinical urine specimens, *E. coli*, *P. mirabilis*, *P. aeruginosa*, *Enterococococcus species*, and the *Klebsiella-Enterobacter* group[56].

A typical and widely applied method based on piezoelectric effect is the quartz crystal microbalance (QCM). QCM measures a mass per unit area by measuring the change of frequency from a quartz crystal resonator. This surface mass can be further used to determine the affinity of molecules. Such QCM sensors are becoming a good alternative analytical methods in a great deal of applications for microorganism monitor[60]. In addition, some other methods based on magnetic effect have also been reported recently for the development of microbe biosensors [61]. Current development of nanofabrication technology can make the size of a sensing probe comparable to those of bacteria or other target pathogens, which can carry out high throughput detection, such as nanoparticles[62], nanotubes[63] or nanowires[64].

Among the various transducing systems of microbe sensors, impedance measurement or impedance spectroscopy represents a powerful method for the study of conducting material and interfaces, since impedance based biosensors have the advantages of fast response, easy combination with microfabrication processes, and capability to minimize the devices. In this technique, a cyclic function of a small amplitude and variable frequency is applied to a transducer, and the resulting current is used to calculate the impedance at each of the frequencies probed. The amplitude of the current and potential signals and the resulting phase difference between the voltage and current, which depends on the nature of the system under study, dictates the system impedance. This is the basic principle of impedance sensing[48]. And a lot of biosensors have been constructed by impedance spectroscopy[65, 66].

1.3.5 Biofilm Formation and Monitoring

Biofilms are well-recognized phenomenon in industries. In an aquatic environment, microbial cells attach firmly to almost any surface, though the attachment time varies. The immobilized cells grow, reproduce, and produce extracellular polymers, which frequently extend from the cell forming a tangled matrix of fibers which provide structure to the assemblage termed a biofilm[67]. Biofilm is significantly different from other microbial systems due to its microenvironment heterogeneity. A biofilm system is basically composed of five compartments: the substratum, the base film, the surface film, the bulk liquid and the gas, as shown in Figure 1.14.

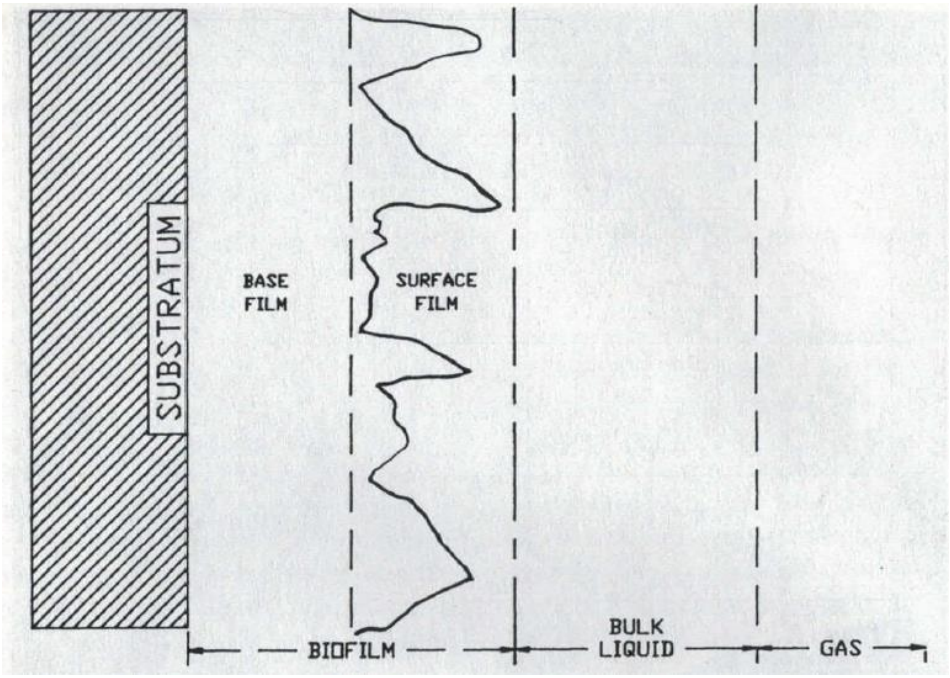

Figure 1.14 The five compartment of a biofilm system[67]

The progression of biofilm accumulation is composed of three different phases: the initial pre-attachment of soluble molecules, such as proteins; the exponential or log accumulation, which is the reversible attachment of cells followed by the secretion of specific polysaccharides and the expression of adhesins; and the final plateau or steady state, which is a stable mature biofilm. In the simplest case, biofilms are composed of microbial cells and their products, like extracellular polymers. *P. aeruginosa* has been extensively utilized as a model organism for the

study of biofilm formation[68], since this bacterium can create a self-generated extracellular polymeric matrix that encases the constituent cells.

There is an increasing industrial demand to monitor biofilm growth, since the biofouling or biocorrosion effects caused by biofilms may lead to serious problems, such as heat transfer losses, product quality deterioration, potable water contamination in distribution systems, infection or clogging of medical devices, and contamination of systems[69]. Biofilm formation on contact lenses, mainly due to the corneal infections or other ocular complications, is associated with poor hygiene of contact lenses, which is frequent in the contact lens-wearing population[70].

In order to monitor biofilm accumulation and activity, direct or indirect methods can be applied. Direct measurement of biofilm can be achieved by direct quantity measurement or microbial activity within the biofilm; and indirect methods usually solve the problem by using specific biofilm constituents or testing effects on biofilm transport properties. Recently, modern techniques have been involved to monitor the biofilm, like optical techniques[71], electrochemical techniques[72], impedance measurements[73], voltammetry and amperometry measurement[74]. Electrochemical techniques have many advantages in monitoring the biofilm formation, especially for contact lenses: they are very sensitive to detect; the data can be rapidly processed; they are environmental friendly and simple to operate; and they are efficient just requiring a small amount of electrical energy[75].

1.4 Summary

In this chapter, the eye structure and components of human tear fluid are first introduced. As there is glucose information in tear fluid, a contact lens with glucose sensors would provide a new way to monitor tear glucose levels in a non-invasive and continuous way. Among various methods, enzyme-based electrochemical sensing is a good option since it is relatively simple, inexpensive, and more specific to glucose. Ocular infection and biofilm formation is also related with eye diseases and daily contact lens wear. A microbe sensor based on electrochemical impedance spectroscopy is preferable to monitor bacteria and biofilm *in situ* as it has good specificity, high sensitivity, low detection limit, and rapid analysis time.

Chapter 2 Glucose Sensors Embedded in Contact Lenses

As introduced in Chapter 1, the non-invasive continuous monitoring of glucose levels are modern appealing vehicles to test blood glucose concentrations. Among different body fluids, tear fluid is very attractive since it is amenable to continuous property, easily accessible and does not require sample collection. The common use of contact lenses is usually for vision correction, while various new concepts have come about for other cosmetic or therapeutic purposes. A contact lens can be integrated with sensors and radio to interrogate the tear fluid, perform an analysis, and wirelessly transmit the results. This contact lens can be built on a polymer substrate, with a biosensor module, telecommunication circuit, antenna and embedded interconnects, leaving the central area clear for unhindered vision. In this chapter, enzyme-based electrochemical glucose sensors have been developed, optimized, integrated with wireless telecommunication circuit, and finally molded to contact lenses.

2.1 Sensing Principles

2.1.1 Basic Electrochemistry

Electrochemistry studies chemical reactions which take place in solution at the interface of an electron conductor and the electrolyte, and which involve electron transfer between the electrode and the electrolyte or species in solution. The collections of interfaces are called electrochemical cells[76]. The overall chemical reaction takes place in a cell, which is made up of two independent half-reactions. Most of the time, only one of the half-reactions is of interest, and the electrode at which it occurs is called the working electrode (WE). The other electrode where the other half-reaction takes place is called the reference electrode (RE). An electric potential is applied between WE and RE to drive charge externally between the electrodes, as shown in Figure 2.1(a). The magnitude of the potential difference at an interface affects the relative energies of the carriers in the two phases, hence it controls the direction and the rate of charge transfer. For electrochemical sensing, in order to get the linearity between the current response and the interested reaction, a stable potential is preferable. But the voltage drop between WE and RE due to the electrolytic conductivity is non-avoidable for two electrode system, and for this reason a three electrode system is preferred for most electrochemical sensing purposes. A third electrode, the counter electrode (CE, sometimes called auxiliary electrode) is employed in the

electrochemical cell working as a current drain, not affecting the behavior of the electrode of interest, as shown in Figure 2.1(b).

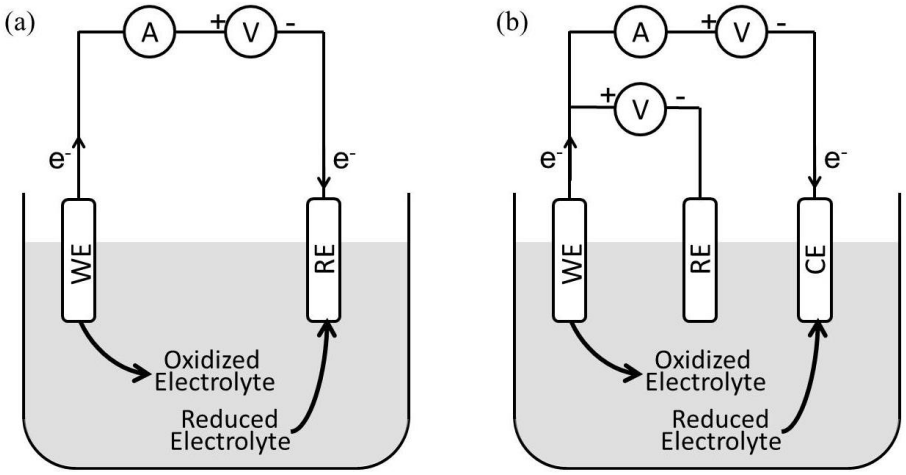

Figure 2.1 Electrochemical cells: (a) two electrode system; (b) three electrode system

2.1.2 Sensing Reactions

The enzymatic reaction based on GOD is mainly composed of two steps: the first one is the enzymatic oxidation of glucose to gluconic acid, followed by the oxidation of H_2O_2 at the WE[18]. The current response is linearly related with the electrons created by the reactions.

$$D-glucose+O_2 \xrightarrow{GOD} H_2O_2+D-gluconolactone$$

$$D-gluconolactone+H_2O \rightarrow D-gluconic\ acid$$

$$H_2O_2 \rightarrow 2H^+ + O_2 + 2e^-$$

2.2 Rectangular-Shaped Glucose Sensors

2.2.1 The Design, Fabrication and Surface Modification of Sensors

1. Material selection

Polyethylene terephthalate (PET) is selected as a start substrate for polymer glucose sensors, because PET plastic is flexible, transparent, biocompatible, and widely used in beverage, food and other health industries. All the microfabrication processes on PET substrate could be transferred to other contact lens polymers with further development.

For electrode metals, we selected Pt as it is biocompatible and commonly used in other medical devices. A more important benefit of Pt is that, the oxidation of H_2O_2 is favored on oxidized Pt surfaces, due to the following scheme[77, 78]:

$$H_2O_2+Pt(OH)_2 \leftrightarrow Pt(OH)_2 \cdot H_2O_2$$

$$Pt(OH)_2 \cdot H_2O_2 \leftrightarrow Pt + 2H_2O + O_2$$
$$Pt + 2H_2O \leftrightarrow Pt(OH)_2 + 2H^+ + 2e^-$$

2. Sensor design

Similar to a standard three-electrode electrochemical cell, the sensor is composed of three electrodes, as shown in Figure 2.2(f). WE is where the reaction of interest occurs; CE acts as the current drain; and RE provides a stable reference potential. WE and CE are designed as concentric rings, in order to minimize resistance between them. The bare plastic surface between the working electrode and the counter electrode is used as a platform to immobilize GOD. This simplifies the fabrication process since there is no need to deposit a specific adherent layer for GOD[79]. WE is a pattern of 50 μm wide rings, and CE is a 75 μm wide ring with an overall surface area greater than WE. In this arrangement, the surface of WE is the point of highest impedance, which ensures that the current signal is strictly determined by conditions at WE. RE is designed as a rectangular bar (1.6 mm × 0.25 mm) near the sensing area. Three large pads (5 mm × 2.5 mm) are used to make electrical connections between an external potentiostat and the sensor for testing.

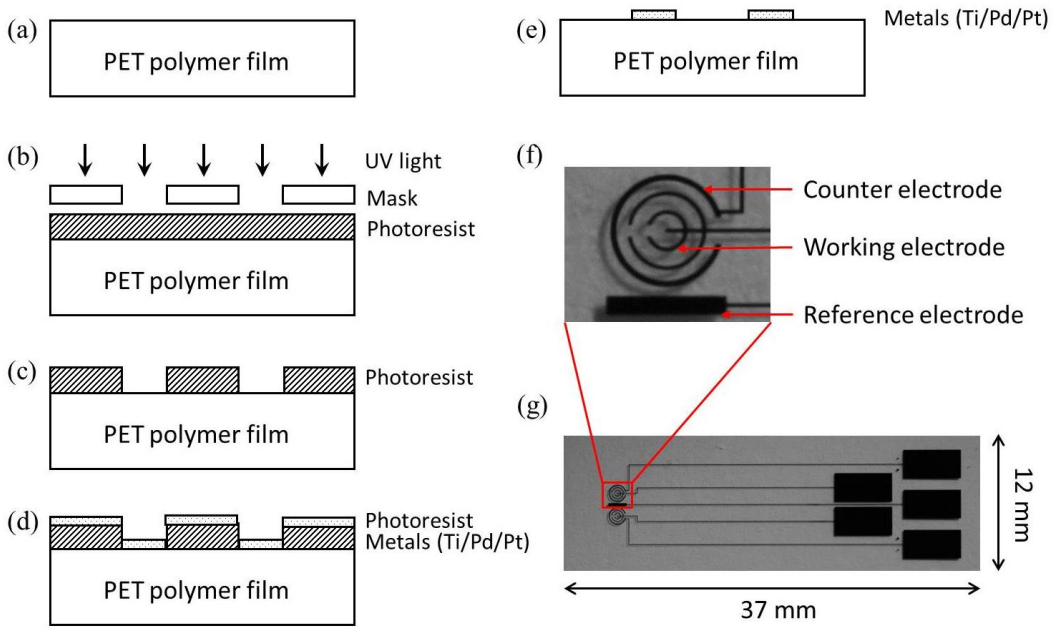

Figure 2.2 The design and fabrication of glucose sensors on PET substrate

3. Fabrication process

The PET polymer (Policrom Inc.) with a thickness of 100 μm was first cut to the standard 4-inch wafer shape using a CO_2 laser cutter. Prior to microfabrication, the polymer wafer was cleaned with acetone, isopropyl alcohol (IPA) and DI (deionized) water in sequence (Figure 2.2(a)). After spin-coating with a layer of photoresist AZ4620 (approximately 5 μm thickness), the wafer was soft baked at 65 ^{O}C for 20 minutes, and then the photoresist was exposed and developed (Figure 2.2(b) and (c)). In the following step, three metals Ti/Pd/Pt (10/20/100 nm) were evaporated in sequence without breaking vacuum (Figure 2.2(d)). After lift-off in acetone for about 20 minutes (Figure 2.2(e)), the 4-inch plastic wafer was cleaned with IPA and DI water, dried with nitrogen gas, and then cut to rectangular shapes (about 37 mm × 12 mm) with scissors (Figure 2.2(g)). It should be noted that the addition of Pd between Ti and Pt is important because Pd works as a metal diffusion barrier layer[80], as well as increases signal stability. The latter effect is most likely due to increased stability of a Ti/Pd/Pt reference electrode, as compared to a Ti/Pt electrode.

4. Surface modification

Prior to surface modification of the sensor, a 50 μL GOD solution was prepared with glucose oxidase type VII (from Aspergillus niger, Sigma) in MES buffer (0.1M MES pH 6.0 – 10% PEG 600, from Fluka) to a concentration 10 mg/mL. After rinsing the sensor thoroughly with DI wafer and drying with N_2 gas, the GOD solution was pipetted onto the sensor area and incubated for 30 minutes. After cleaning loosely bound GOD off the sensor, a 50 μL drop of Nafion Solution (5% by weight percentage, from Clearwater) was pipetted onto the same area and dried in air for about 1 hour.

2.2.2 Flow Injection System Setup

In order to test the first generation of glucose sensors, we built a flow injection system, as shown in Figure 2.3(a). The plastic sensor was sandwiched in a chamber where the thickness of the sample solution layer was defined by a thin nitrile gasket (about 100 μm). Two built-in conduits worked as an inlet from the pump and an outlet to the waste bottle. We employed a FIAlab-3000 fluidic analyzer, which is composed of a bi-directional syringe pump and a six-port multi-position valve, as shown in Figure 2.3(b). The fluidic system allows automated, repeatable delivery of solutions to the flow cell with minimal interruption from valve and port switching, controlled by a computer.

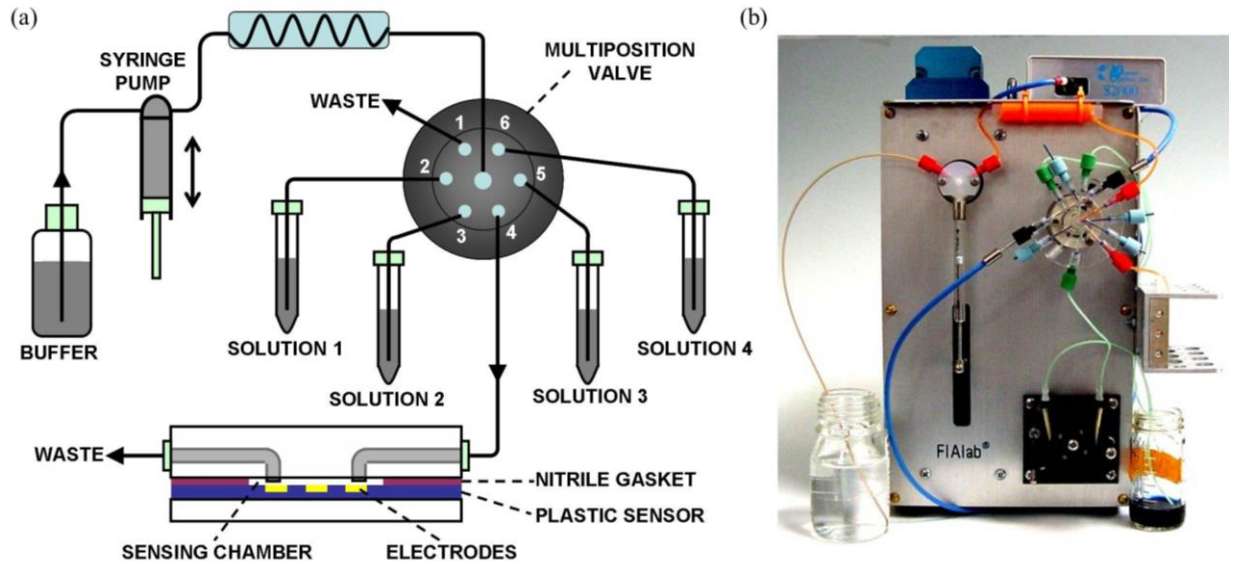

Figure 2.3 Schematic of experiment setup: (a) Experiment setup; (b) FIAlab-3000 Analyzer[81]

To be consistent with physiological pH conditions, the buffer solution was prepared with 130 mM sodium chloride, 10 mM dibasic sodium phosphate and 10 mM monobasic sodium phosphate in DI water, at pH 7.4. The solutions were sonicated for 20 minutes to equilibrate them with ambient pressure to prevent the formation of micro bubbles during test. Different solutions were prepared with glucose, ascorbic acid, lactate and urea, at least 1 hour before test. All the chemicals were purchased from Sigma.

Electrochemical measurements were performed using a BASi Epsilon-EC potentiostat, applying a constant potential of +400 mV between WE and RE. CE was connected to the auxiliary lead of the potentiostat, which serves as a current drain. The signal was recorded for the current flow through WE with sample interval of 1 second.

2.2.3 Results and Discussion

1. The functionality of the sensor

The sensor was first tested for basic functionality continuously with H_2O_2 solutions at different concentrations 20 µM, 40 µM, 60 µM and 80 µM, as shown in Figure 2.4(a). Every cycle comprised dispensing 200 µL H_2O_2 solution followed by 800 µL buffer. The fast response shows that the diffusion rate of H_2O_2 from the solution to the WE surface is very quick. Figure 2.4(b) shows the results for glucose (G) 50 mM, 10 mM, 2 mM with and without ascorbic acid (A) 20 µM, respectively. It demonstrates that GOD has been successfully immobilized on the sensor surface and the sensor shows a reasonable response for different concentrations of GOD.

But for the situation with ascorbic acid added, the interference signal is dominant over the response from glucose. This is a critical problem for sensing glucose in tear film.

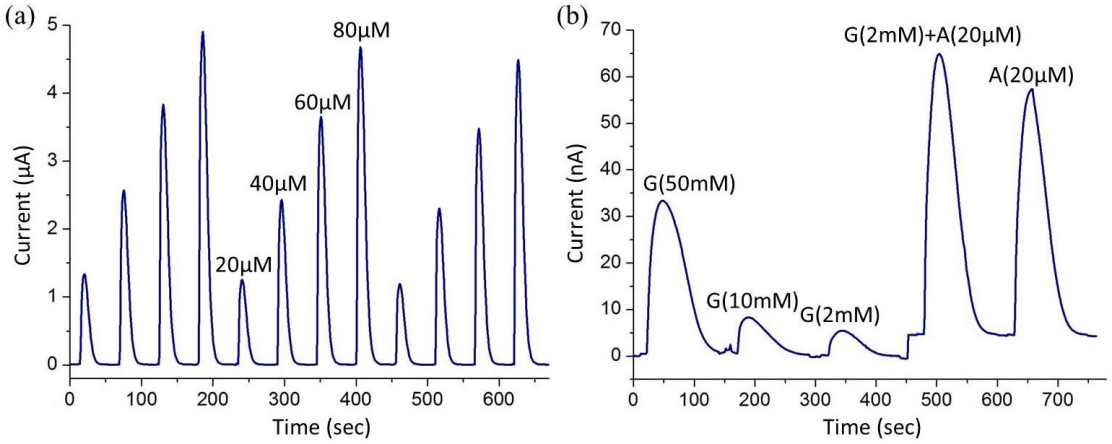

Figure 2.4 Amperometric results for the glucose sensor: (a) the test with different concentrations of H_2O_2; (b) the test with glucose solutions with/without ascorbic acid.

2. The effect of a delay-time test

The above results show that the continuous flow test cannot distinguish glucose from interference chemicals, such as ascorbic acid. In the next step, a delay-time effect was investigated to provide better signal resolution. As the response from glucose is due to the enzymatic reaction of GOD while the response of ascorbic acid is coming from direct oxidation, it is expected that there should be a deviation after a certain delay time in glucose solutions. Figure 2.5 proves the delay-time effect for different glucose concentrations (0, 0.125, 0.25, 0.5 and 1 mM).

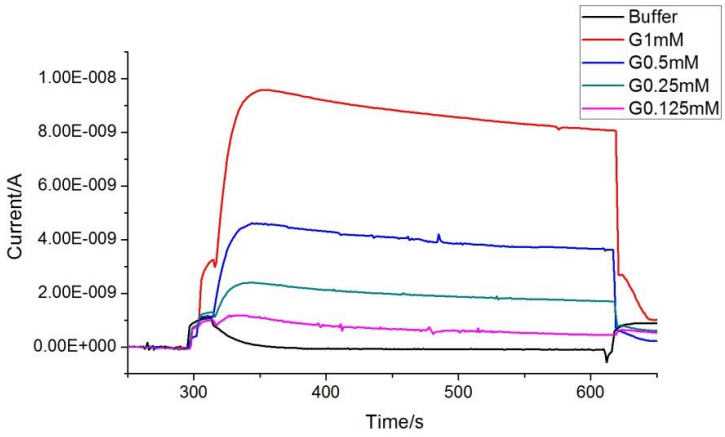

Figure 2.5 The delay-time effect for glucose solutions

The delay-time method was applied to test glucose with and without ascorbic acid (A), as shown in Figure 2.6. It shows that Nafion has certain efficiency of blocking ascorbic acid. The signal of glucose could be calculated from the difference between baseline signals (300 seconds) and delay-time signals (600 seconds).

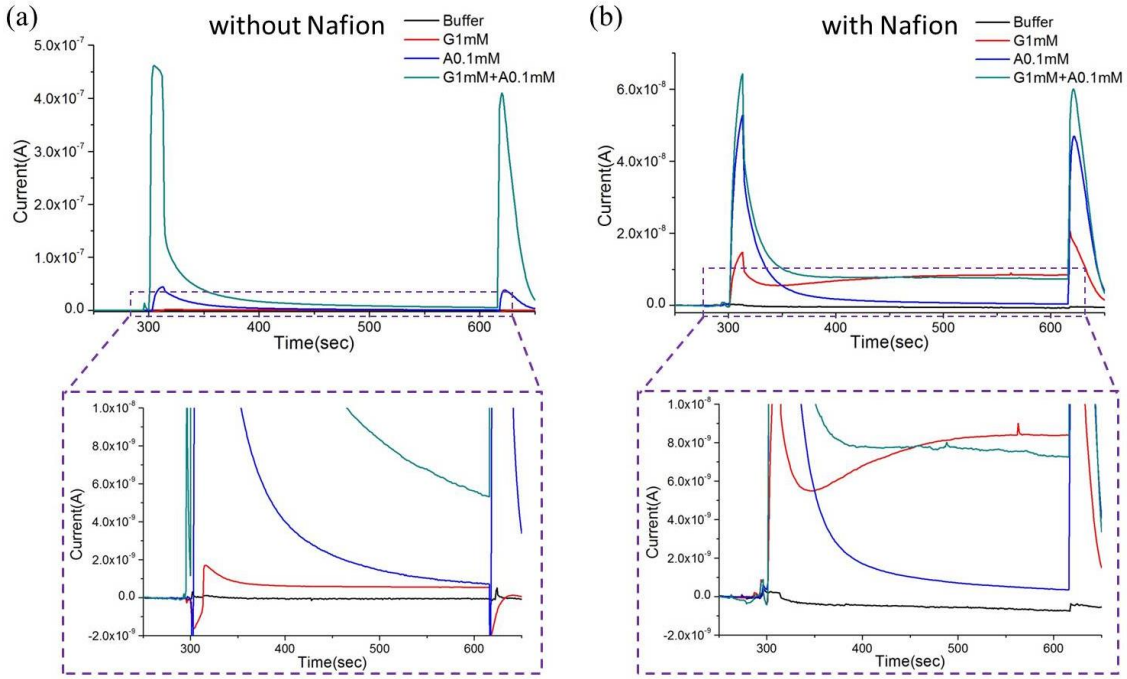

Figure 2.6 The delay-time effect for glucose solutions with ascorbic acid

In the next step, various interferences, such as urea (U), lactate (L) and ascorbic acid (A), were tested together for different concentrations of glucose. Figure 2.7(a) shows the details of the

curve and Figure 2.7(b) is the data based on five independent experiments. The Nafion layer has been employed as a permselective film for our future research.

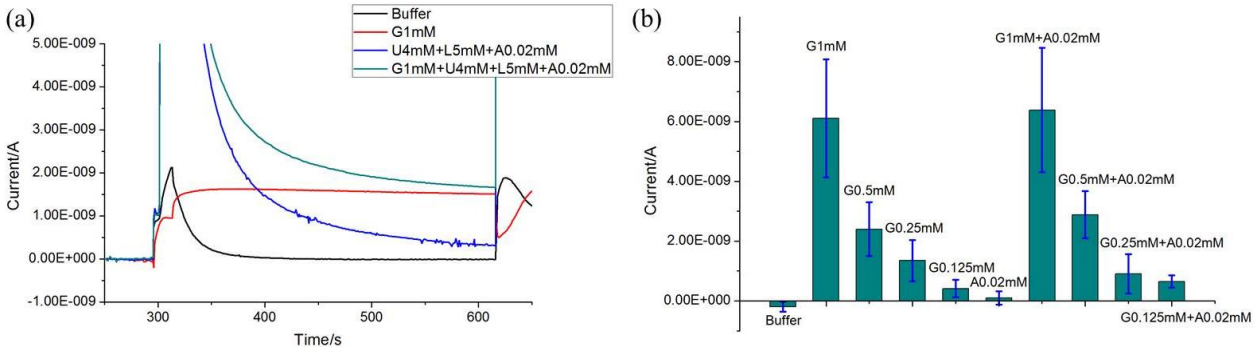

Figure 2.7 Test results of glucose with interference chemicals: (a) enlarged view of the effect of a delay time; (b) the repeatability of the senor (n=5)

2.3 Contact Lens-Shaped Glucose Sensors

2.3.1 The Improvement

Based on the experience of developing the single glucose sensors, in the next stage of the project, the sensor was minimized to the size of a contact lens; and a sol-gel strategy was applied to immobilize GOD more efficiently. The sensors were tested in an open air condition.

1. Sensor design

For this new generation of glucose sensors, all the fabrication processes were adopted from the previous generation, but the shape was designed to resemble into a contact lens, as shown in Figure 2.8(a). The electrodes and three electrical connection pads were placed on the edge of the contact lens, leaving the central area clear in order not to occlude the normal visual path for the user. The whole area of the new sensor was a circle with a diameter of 1 cm. After being fabricated and cut to small pieces with CO_2 laser cutter automatically, the small sensor was heat molded (200^{O}C, 15 seconds) to the shape of contact lens, as shown in Figure 2.8(b). The three large pads were connected to electrical wires by silver conductive epoxy (from MG Chemicals) and then insulated with non-conductive epoxy (from ITW Devcon), as shown in Figure 2.8(c).

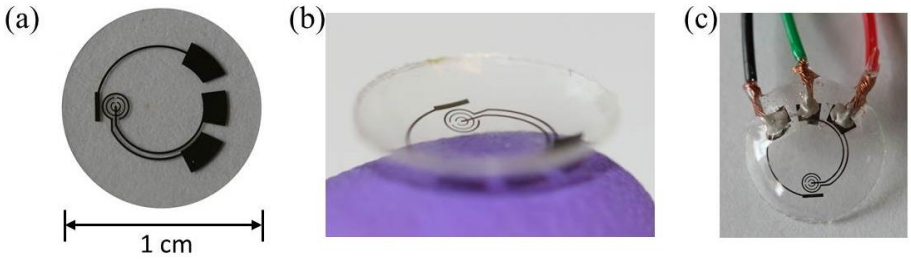

Figure 2.8 Images of contact lens-shaped sensors[82]: (a) a flat sensor; (b) a molded sensor; (c) a hardwired sensor

2. surface treatment

A new method of surface treatment was employed for the second generation sensors. Prior to surface modification, the sensor was rinsed thoroughly with DI water and dried with nitrogen gas. A 30 μL GOD solution (10 mg/mL) was dropped onto the sensor area. Then, the sensor was suspended vertically above a titanium isopropoxide solution in a sealed dish for 6 h to create a GOD/titania sol-gel membrane[83]. After forming the sol-gel membrane, a 30 μL aliquot of Nafion solution was dropped onto the same area of the sensor and allowed to dry in air. Prior to measurement, the sensor was rinsed thoroughly with DI water and kept in buffer solution at 4 ^{O}C. Images of the surface modification sequence are shown in Figure 2.9.

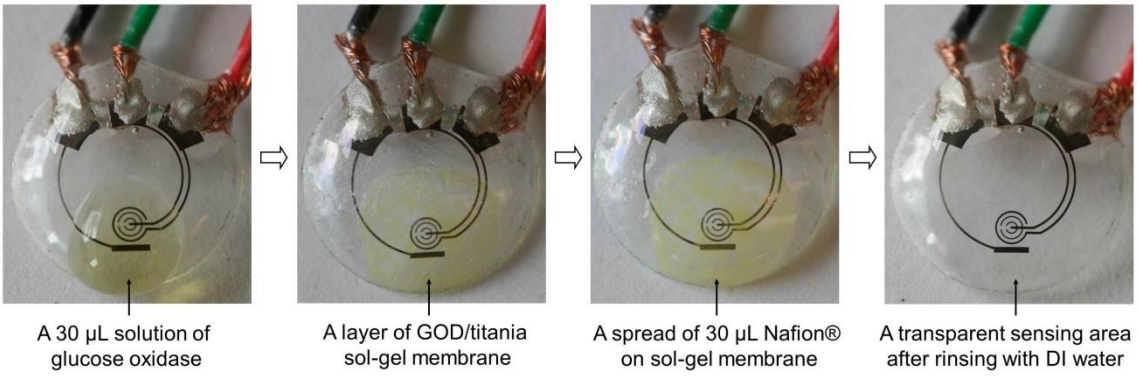

Figure 2.9 Sequential images of sensor pre-treatment with GOD/titania/Nafion[82]

3. system setup

Due to the small size and the molded shape of the new sensors, the flow injection system could not be used to test the sensor, hence a new experiment setup was utilized. As shown in Figure 2.10, the sensor was suspended in buffer solution with a volume of 1.8 mL in a small beaker. Different solutions were added manually by micro pipettes and the solution was stirred continuously by a magnetic stirrer (LUX Scientific Instrument Corp.) to avoid mass transport

limitation. The electrochemical measurements were performed in the same way as before using a potentiostat.

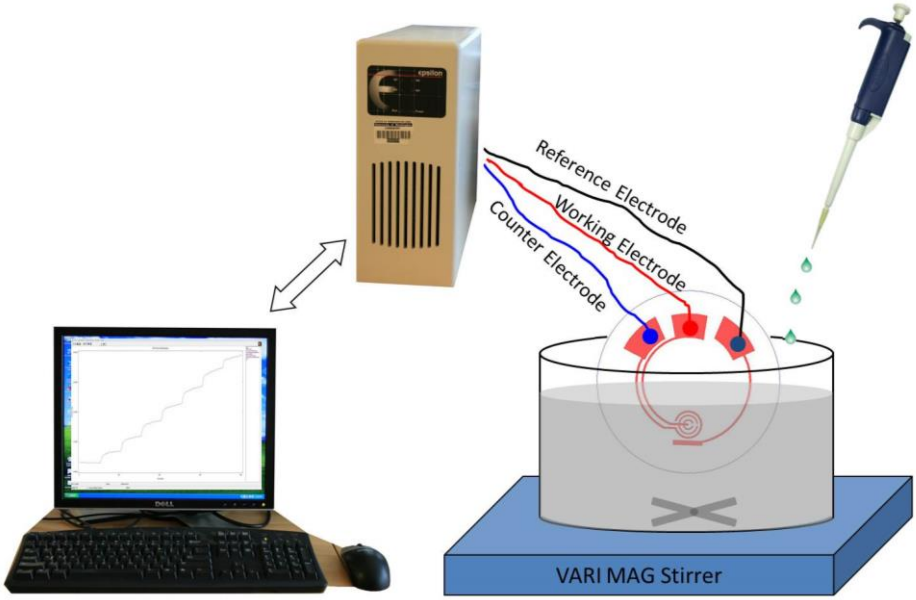

Figure 2.10 Experiment system setup for the beaker test

2.3.2 Results and Discussion

1. Functionality of the sensor

In order to systematically study the pre-treatment of the sensor, we prepared sensors using different procedures. One was just incubated with 30 μL GOD (10 mg/mL) for 30 minutes; another one was prepared with GOD/titania sol-gel film; and the third one was prepared with GOD/titania/Nafion. Figure 2.11 shows the different measured performance for three pre-treatment methods.

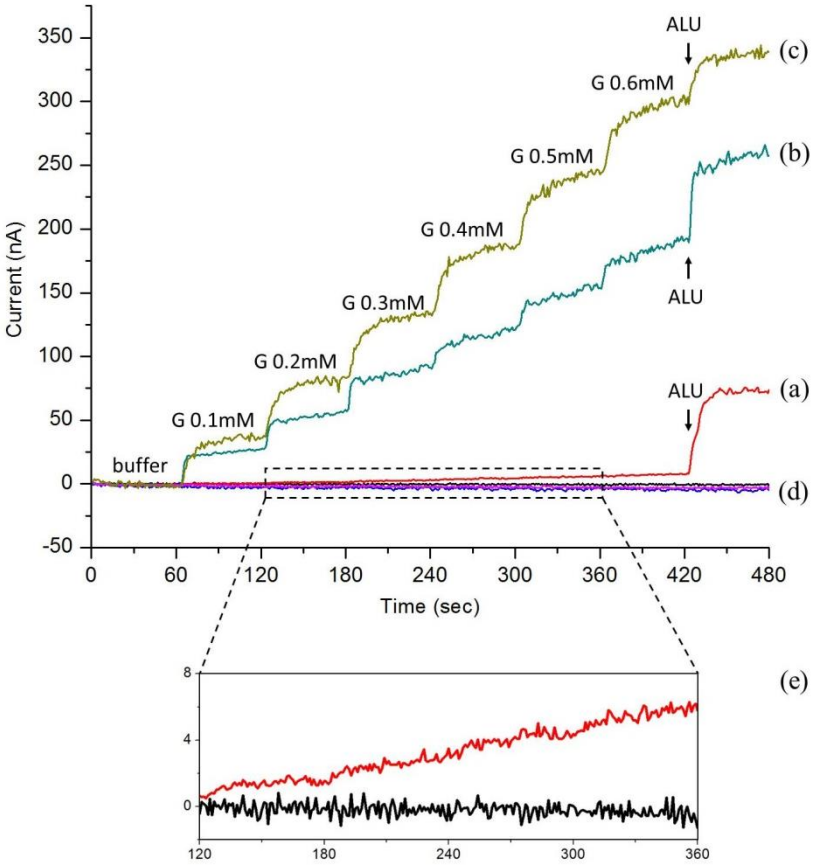

Figure 2.11 The effect of surface treatment and the related measured responses[82]: (a) the sensor just incubated with GOD; (b) the sensor prepared with GOD/titania sol-gel film; (c) the sensor prepared with GOD/titania/Nafion; (d) three controls for the same pre-treatment of (a), (b) and (c); (e) the enlarged view of curve (a) and control of (a) for 120-360 seconds.

As evident from comparing Figure 2.11(a) and Figure 2.11(b), the titania sol-gel film greatly increases the glucose response more than 30 times. As reported, the titania sol-gel film is very efficient for retaining the GOD activity and preventing the enzyme from detaching from the film[83]. This property is due to the large number of hydroxyl groups in titanium isopropoxide, which can form strong hydrogen bonds with the enzyme molecules.

When the sensor was treated with both titania and Nafion coating, as shown in Figure 2.11(c), the glucose signals increased further. This enhancement may be due to the better ability of the titania/Nafion combination film to retain the enzymes than the titania film alone. The main effect of the Nafion coating is to decrease interference, as demonstrated by a 50% reduction in the interference signal after applying Nafion (Figure 2.11(b) and (c)). It has been reported that

different pre-treatment procedures can be used to optimize the permselective characteristics of Nafion coatings[84]. Considering the heat-stability limitations of the PET plastic substrate, it is not possible to anneal it at 210 ^{O}C as suggested in[84] to maximize Nafion permeability. An attempt was made to apply one coat with drying at room temperature (about 20 minutes), several coats allowing 2 minute drying time and also drying at 4 ^{O}C for 10 h[83]. However, no difference was detected between the sensors prepared using different Nafion pre-treatment procedures.

2. Amperometric characterization and calibration curve

Figure 2.12 shows a typical measured amperometric response acquired during successive additions of 0.1 mM glucose every 60 seconds, which is approximately the minimum concentration in the eye surface tear film[3]. Figure 2.12(b) shows the control measurement curve acquired by successive addition of the same amount of buffer (no glucose) verifying the specificity of the sensor response. The calibration curve in Figure 2.12(c) was generated by averaging current values of 30-50 seconds after each addition. A linear relationship between the current and the glucose concentration was observed between 0.1 mM and 0.6 mM (R=0.9988).

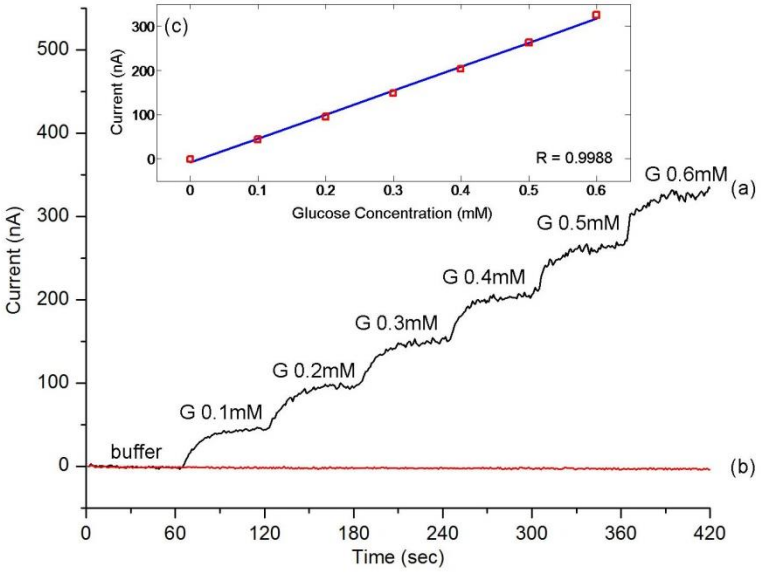

Figure 2.12 Measured amperometric response and calibration curve of the sensor[82]: (a) current signals for glucose (G); (b) current signals for buffer; (c) calibration curve for glucose signals

As WE has a small area of about 0.22 mm^2, the sensitivity of our sensor can be calculated as 240 μAcm^{-2}mM^{-1}, higher than conventional disc electrodes with sol-gel film[83, 85] and nanotube array sensors[86]. The response is very quick, reaching 90% of the maximum value in

less than 20 seconds, which signifies the possibility of its practical application on a contact lens. The small electrode area and the branched WE design provide efficient diffusion conditions, whereas the sol-gel film results in a high enzyme loading due to its three-dimensional porous network.

3. Selectivity, repeatability and stability of the sensor

A typical amperometric test arrangement was used to validate the sensor operation, with successive additions of 0.1 mM glucose first in buffer and then in interference solution, which includes 50 μM ascorbic acid (A), 10 mM lactate (L) and 10 mM urea (U). Figure 2.13(a) shows three independent measurement results from three different sensors. Here, the concentrations of interference chemicals were chosen to exceed the maximum concentrations in tear fluid[3, 87].

The results indicate that the sensor has good interference rejection characteristics, which is attributed to the use of titanium isopropoxide and an additional layer of Nafion. The small error bar for three sensors indicates good repeatability. From another aspect, the current from ALU is almost the same amount as that from glucose 0.1 mM, which makes it more difficult to accurately tell glucose from interferences for very low concentrations of glucose. Comparing the signal difference between glucose in buffer and glucose in interference solution at the same concentration, the difference is 93% for glucose 0.1 mM, and 37% for glucose 0.2 mM, but decreases to less than 20% for glucose more than 0.2 mM, which would be considered clinically accurate for practical measurement[88].

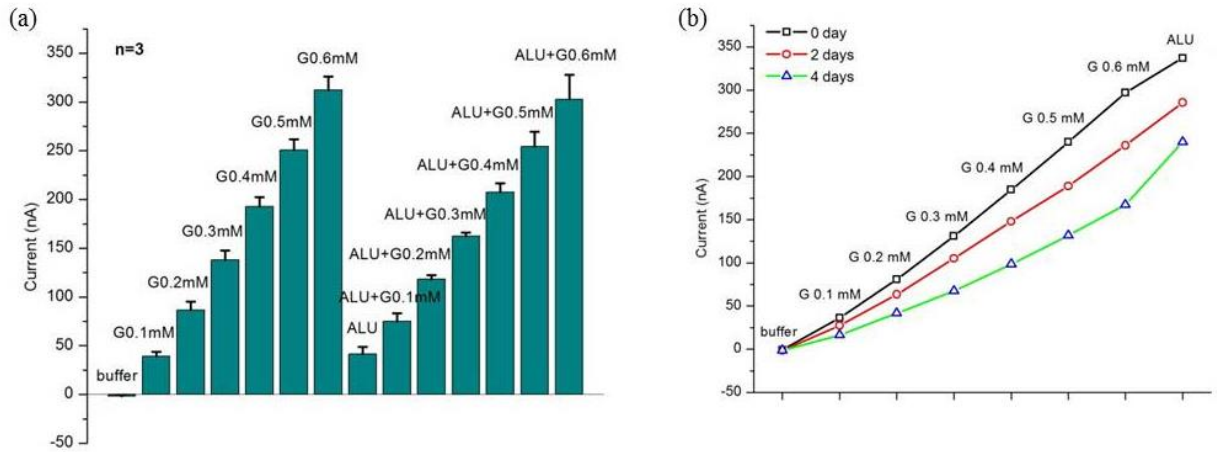

Figure 2.13 The results for sensor performance[82]: (a) measured sensor repeatability and injection rejection (n=3); (b) calibration currents for glucose and interferences for the same sensor right after preparation, 2 days after and 4 days after

In addition, two cases (the unused and used sensors) were studies in order to test the stability of our sensor. The unused sensor can retain its activity for one week if stored in buffer at 4 ^{O}C directly after preparation. The long lifetime is because the sol-gel film can prevent GOD from leaking out and the immobilization process does not influence the biological activity of enzyme, as reported[83, 85]. On the other hand, the activity of a used sensor decreases from measurement to measurement. The used sensor was stored in buffer at 4 ^{O}C between tests and used for about 2 h for each test. As shown in Figure 2.13(b), the sensor can retain nearly 80% of its initial current response after 2 days; it can retain about 55% response after 4 days for glucose, and at the same time the interference signal increases. The decrease of current signals here is probably due to the Nafion component leaching out of the GOD/titania/Nafion film during measurements. Thus an appropriate protection layer for GOD is a direction for future research.

4. Detection limit of the sensor

Figure 2.14(a) shows the detection limit for very low concentrations of glucose 0.01-0.07 mM. The good linearity (R=0.9966) demonstrates that, in the absence of interference species, our glucose sensor can detect a glucose concentration as low as 0.01 mM, which is 1/10 of the minimum concentration in tear film[3, 87].

(a) (b)

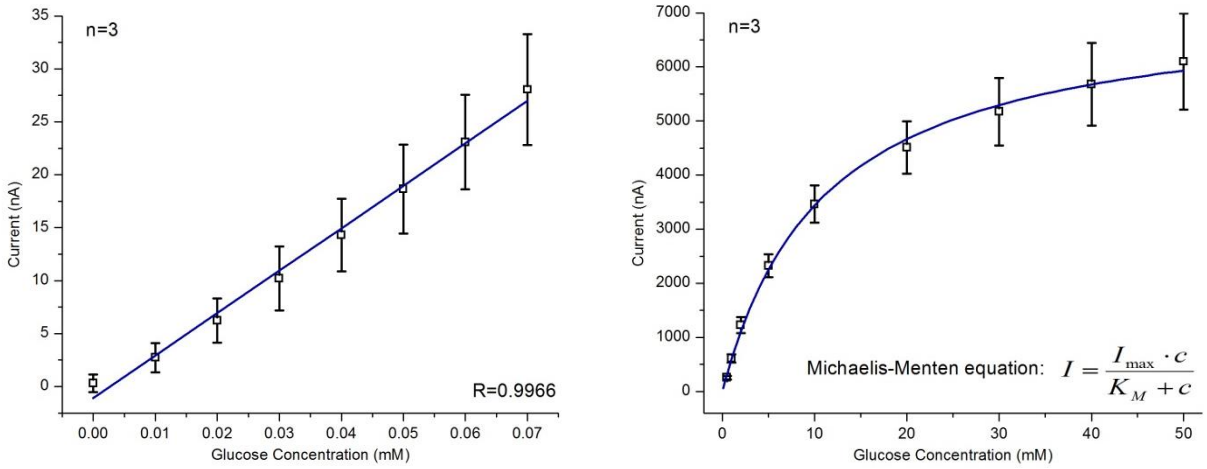

Figure 2.14 Calibration curve for low and high concentration of glucose (n=3)[82]: (a) calibration current and linear fit for low concentrations of glucose (0.01-0.07 mM); (b) calibration currents and Michaelis-Menten fit for high concentrations of glucose (0.5-50 mM)

Figure 2.14(b) shows the calibration curve for high concentrations of glucose (0.5-50 mM). The data is fitted to the Michaelis-Menten equation[89]:

$$I = \frac{I_{max} \cdot c}{K_M + c}$$

where I is the sensor response and c is the glucose concentration. The fit yields a K_M value of 11 mM, which falls within the typical range of glucose sensors[90].

2.4 Development of Dual Glucose Sensors and PDMS Eye Model

Amperometric glucose sensors usually suffer from a lack of selectivity caused by interference chemicals. For a practical sensor, the problem of minimizing signals from interfering chemicals is critical, especially in samples such as the tear fluid where glucose levels are very low (0.1-0.6 mM) compared to blood[3]. As the next approach to developing glucose sensors, a dual sensor design was employed for interference rejection. And a PDMS eye model was utilized to enable the testing of contact lenses in a controlled environment that mimics the eye surfaces.

2.4.1 The Design and Fabrication of Dual Glucose Sensors

There are various kinds of approaches to minimize the interference effect for electrochemical sensing, such as permselective membranes[91], such as a layer of Nafion as used before, self-assembled monolayers[92] and interference-removing enzymes[93]. Another option for interference compensation is a physical approach based on a dual sensor structure where only

one of the identical sensors is treated with active glucose oxidase (GOD) and thus shows a response to glucose. The other one without GOD acts as a control, responding to other electroactive species present in the sample, except glucose. The signal from the control sensor can then be subtracted from the total signal obtained at the enzyme sensor to correct its response[94].

Figure 2.15 shows the design, fabrication and surface treatment of the dual glucose sensor. The dual sensor was designed with two working electrodes (WE), two conjoint counter electrodes (CE), and one common reference electrode (RE), as shown in Figure 2.15(b). WE and CE were designed the same way as the single sensor. The common RE was designed as a bar between the primary sensor and the control sensor with an area of about 1 mm^2. Four large pads (each about 2.5 mm^2) were used to make electrical connections between an external potentiostat and the sensor for testing.

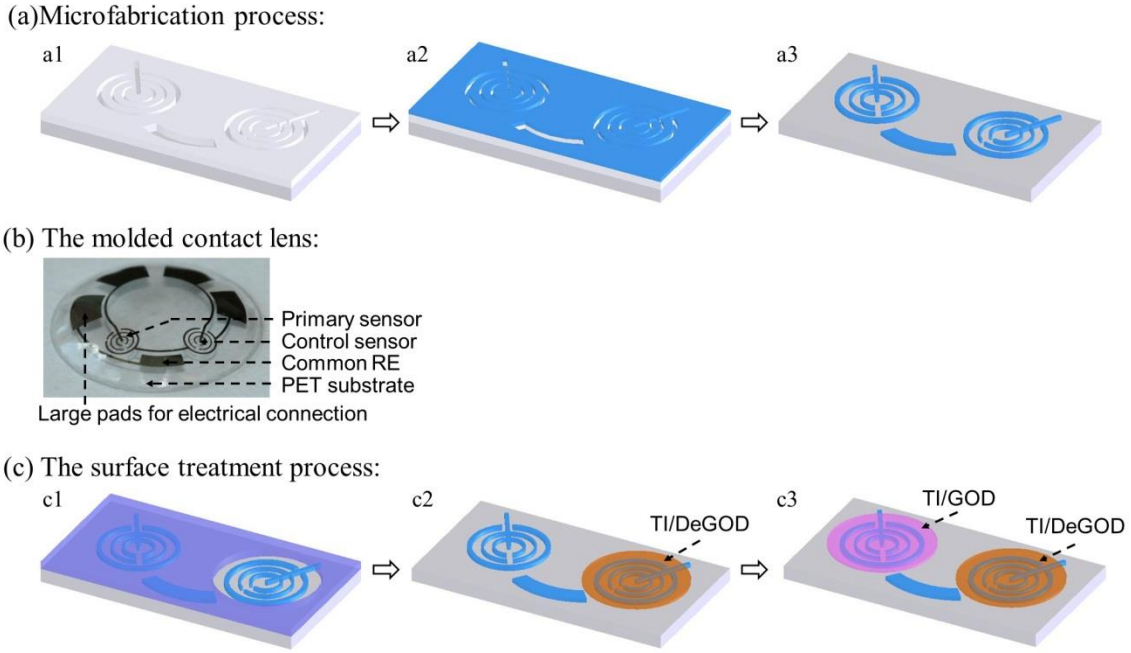

Figure 2.15 The fabrication and surface treatment of the dual sensor[95]: (a) The microfabrication process; (b) The image of lens shape sensor; (c) The surface treatment of the molded sensor.

The fabrication process (Figure 2.15(a)) was the same as single sensors. After the fabrication, four large pads were connected to electrical wires using silver conductive epoxy (from MG Chemicals) in order to connect with a bench top bi-potentiostat (CHI750D, CH

Instruments), and then the connection area was isolated with non-conductive epoxy for convenient continuous flow test.

For the surface treatment step, GOD and deactivated GOD (DeGOD) were prepared for the primary and control sensors, respectively. GOD solution was prepared in MES buffer with a concentration of 10 mg/mL. DeGOD was achieved by heating the GOD solution at 70 ^{O}C for 3 hours[96]. An indicator solution was prepared to determine the DeGOD solution has no enzymatic activity at all, with 100 mM Sodium 4-hydroxybenzoate, 40 mM 4-Aminoantipyrine, and 20 units/mL peroxidase type II. By mixing 100 µL of the indicator solution with 10 µL DeGOD solution, the absence of color change in more than 10 minutes indicated that DeGOD was a completely deactivated enzyme.

As shown in Figure 2.15(c1), the primary sensor was first covered with a piece of flexible semitransparent parafilm, leaving the control sensor open for the surface treatment of TI/DeGOD. A 20 µL DeGOD solution was dropped onto the open area for the control sensor, and then the dual sensor was suspended vertically above evaporating TI solution in a sealed dish for 6 hours, allowing the vapor to create a TI/DeGOD membrane. After that, the parafilm cover was removed, and the sensor was thoroughly cleaned with DI water and dried with N_2 gas (Figure 2.15 (c2)). The next treatment step was carried out in a similar way, except applying GOD instead of DeGOD (Figure 2.15 (c3)). Both TI/GOD and TI/DeGOD membranes had a thickness of about 2 µm measured by P-15 profilometer. After cleaning with DI water and drying with N_2 gas, the sensor was ready to use; and it could be stored in buffer at 4 ^{O}C until measurement.

2.4.2 PDMS Eye Model and System Setup

1. The design and construction of PDMS eye model

In order to test the sensor's functionality under controllable conditions that resemble the eye surface, we designed and fabricated a PDMS model that mimics a human eye (Figure 2.16(a)). By carefully reconstructing the curvature of the cornea, and the tear duct and drain system, we were able to test the sensor functionality in thin liquid layers similar to those of tear film. The PDMS eye model was fabricated using a double molding procedure, starting with a 25 mm diameter glass sphere which has a curvature similar to that of a human eye. A circular indentation was created on the top surface of the model to simulate the edges of eyelids. Thin FEP (fluorinated ethylene propylene) tubing with an internal diameter of 0.5 mm was then

precisely inserted into the final mold to create two liquid inlets and one outlet connecting the backside of the eye model and the internal sidewall of the faux eyelid, simulating the geometry of the tear ducts and drains of a real human eye.

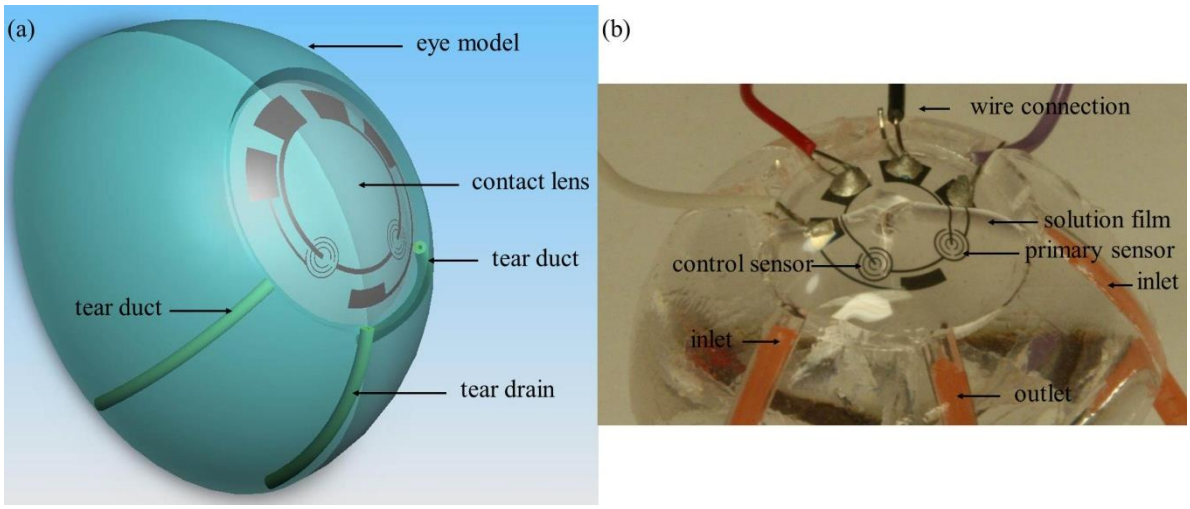

Figure 2.16 Eye model and experiment system setup[97]: (a) schematic of the polymer eye model (b) image of the experiment setup with a contact lens places on the eye model.

2. System setup for measurement

Prior to measurement, the pretreated dual sensor was cleaned, dried and fixed symmetrically to the eye model by non-conductive epoxy, as shown in Figure 2.16(b). We used the FIAlab-3000 fluidic analyzer to automatically deliver different solutions into the two liquid inlets at the same flow rate (each 5 µL/sec). We applied another single syringe pump to aspirate from the common outlet at an equal flow rate (10 µL/sec), thus maintaining a constant solution thickness (about 1 mm) over the sensor. A bi-potentiostat was used to apply a constant potential (+400 mV) between WE and RE, and recording the control current (from the control sensor) and the primary current (from the primary sensor) simultaneously, with a data sampling interval of 1 second.

2.4.3 Results and Discussion

1. Typical continuous amperometric responses of the dual sensor

Figure 2.17 shows a typical amperometric response acquired by delivering different glucose concentrations and interferences ALU (ascorbic acid 50 µM , lactate 10 mM and urea 10 mM). Every delivery cycle is composed of a 200 µL bolus of test solution followed by 800 µL buffer, which avoids signal carry-over between cycles.

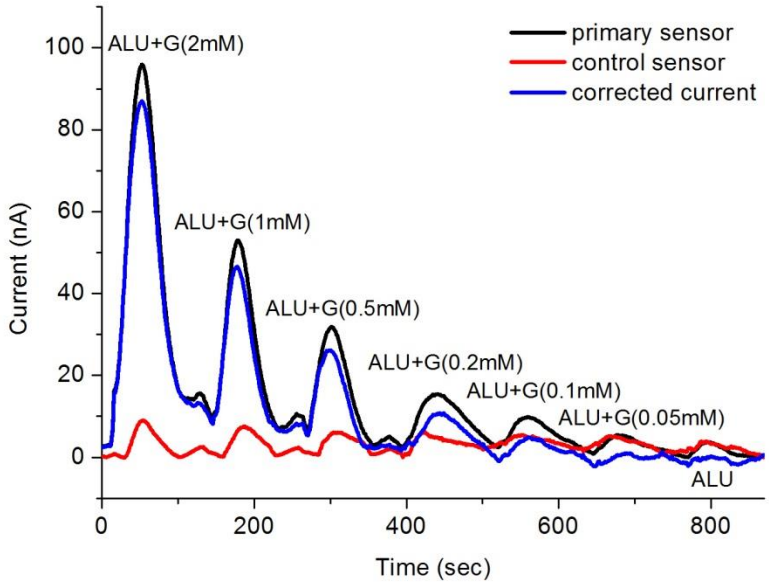

Figure 2.17 The measured continuous response of a dual sensor[95]. The solutions contain different concentration of glucose (G: 0-2 mM) and the same interferences ALU.

The signal given by the primary sensor (the black curve) shows a response to both glucose and interferences, whereas the control sensor (the red curve) only responds to interferences. When a difference signal is calculated, as the blue curve, the interference response is almost entirely removed while the glucose response is preserved. The results indicate that the dual sensor is capable of detecting glucose and rejecting the contribution of interfering molecules. Here, the glucose concentrations are covering the normal values in tear fluid (0.1-0.6 mM), and the interferences exceed the maximum concentrations in tear fluid[3]. Although the thickness of liquid film (about 0.6 mm) and the flow rate (5 μL/sec) are limited by experimental setup and higher than actual situations (about 10 μm, 1.2 μL/min)[98], the basic functionality provides a means of testing sensor performance in conditions that are closer to real life than a stirred beaker.

2. Mimic of eye blinks

In addition to providing mechanical support and a means of fluid delivery, the test setup can mimic eye blinks by manipulating the flow rates of solutions. After each test cycle, delivery to inlets was stopped and aspiration from outlet continued to remove the fluid. After a certain time, aspiration was stopped and delivery was started again, creating a film of fresh fluid. In other words, the fluid film can be removed and replenished in a periodic manner.

As shown in Figure 2.18(a), the flow imbalance changes the thickness of the solution layer to simulate an eye blink. Figure 2.18(b) demonstrates the amperometric response for glucose 0.4 mM in the presence of interferences (ascorbic acid 50 μM, lactate 10 mM and urea 10 mM). Although there is significant fluctuation during mimicking blinks, the current response can return back to normal state. The test illustrates how the setup can be used to investigate the effects of fluctuations in both flow rate and solution film thickness, which is not possible with either manual pipetting application, or in a conventional closed flow cell.

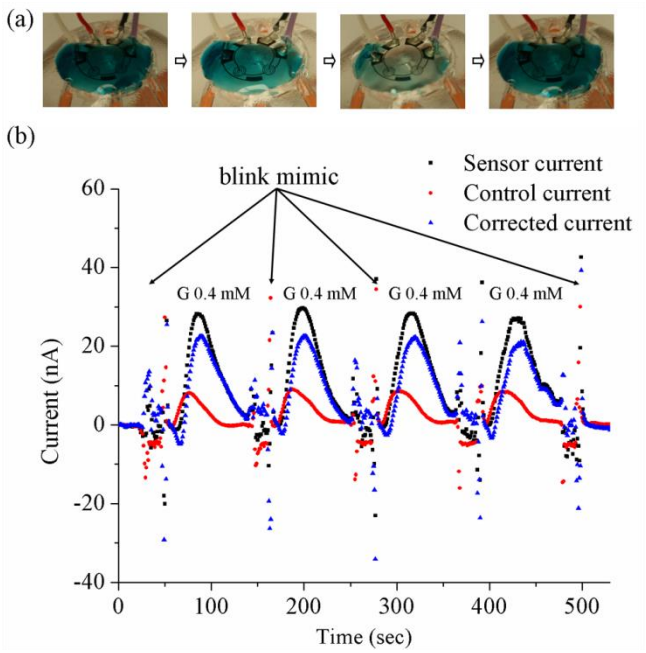

Figure 2.18 Amperometric test by mimicking eye blinks[97]: (a) the change of the fluid layer thickness used to mimic eye blinks; (b) amperometric response for glucose 0.4 mM in the presence of interferences

3. The repeatability, linearity and stability of the sensor

By determining the peaks of the corrected current, three different sensors were studied (Figure 2.19). The sensors were stored in buffer at 4 ^{O}C between tests and used for 2-3 hours during each test. Comparing the signals for glucose 1 mM, the sensor can retain about 97.4% of its initial current response after 12 hours, and 84.3%, 67.2%, 54.2% for 1 day, 2 days and 4 days, respectively. The good stability for the first 12 hours makes the sensors suitable for disposable daily use contact lenses. From another aspect, the unused sensor can retain its activity for up to 1 week if stored in buffer at 4 ^{O}C directly after preparation. The decrease of current signals after

several days testing is probably due to the enzyme leaching out of TI/GOD membrane during measurement. In the near future we will work on polymer encapsulation to provide a possibility to solve the leaking problem. Figure 2.19 also shows a good repeatability between independent sensors and a good linearity for longer tests: R=0.9971 for right after preparation (0 hour), R=0.9980 for 12 hours later, R=0.9982 for 1 day later, R=0.9975 for 2 days later, and R=0.9924 for 4 days later.

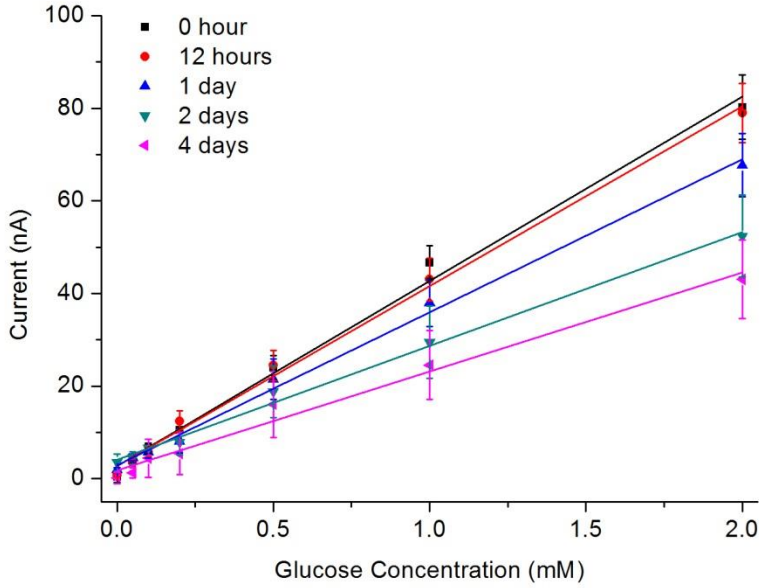

Figure 2.19 The calibration curves right after preparation, 12 hours, 1 day, 2 days, and 4 days later[95]

4. The effect of temperature

Temperature has a significant effect on enzyme activity and it is important to investigate the dependence of current response on this variable. Figure 2.20 shows the effect of temperature for glucose 0.2 mM and 0.5 mM from 5 ^{O}C to 55 ^{O}C (n=3). The response increases when the temperature rises from 5 ^{O}C to 35 ^{O}C, and then decreases as the temperature is further increased. The maximum current response appears at about 35 ^{O}C, which is very near the physiological tear temperature 32-34 ^{O}C[99], but we chose 25 ^{O}C (room temperature) for all the other experiments to simplify lab bench tests.

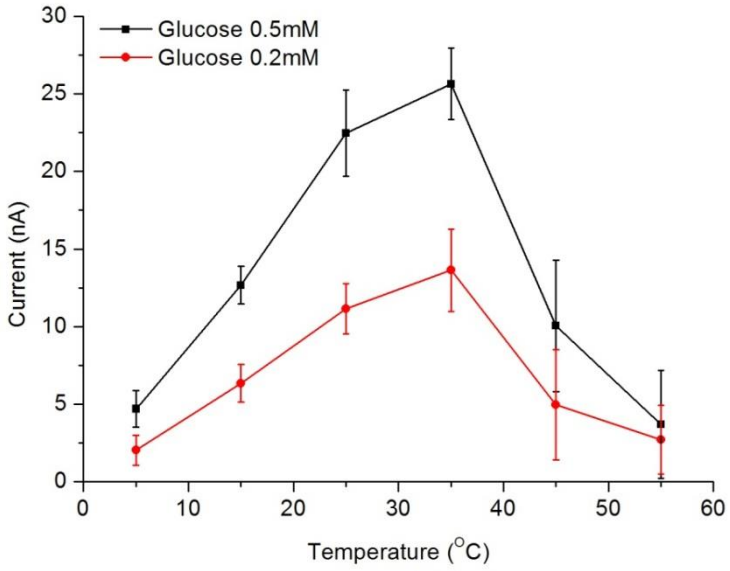

Figure 2.20 Measured effect of temperature variation on system performance[95]

Arrhenius equation can be used to estimate the apparent activation energy (E_a) of the enzyme catalytic reaction[100]:

$$I = A\exp(-\frac{E_a}{RT})$$

where I is the current response, A is a pre-exponential factor specific to the reaction, E_a is the apparent activation energy, R is the gas constant (8.314 $JK^{-1}mol^{-1}$), and T is the absolute temperature. From the data in Figure 2.20, E_a can be calculated as 41 $kJmol^{-1}$ for glucose 0.5 mM and 45 $kJmol^{-1}$ for glucose 0.2 mM. These numbers are similar and comparable with the values reported for other glucose biosensors based on GOD[101].

5. The effect of protein fouling

Compared with artificially prepared glucose test solutions, natural tear fluids are more complex due to a large number of proteins [102]. In order to study the influence of protein fouling on the sensor operation, three typical proteins were added to the glucose solutions (lysozyme 1.9 mg/mL, albumin 0.2 mg/mL and mucin 0.15 mg/mL)[103]. Figure 2.21 shows the results of testing three sensors in solutions without proteins and another three sensors in solutions with proteins. The sensors were first tested right after preparation and again 2 days later. For the test with proteins, we have also tried to store them in protein buffer (lysozyme 1.9 mg/mL, albumin 0.2 mg/mL and mucin 0.15 mg/mL in buffer) between tests. However, no visible difference was

found between normal buffer storage and protein buffer storage, which shows that the signal decreasing is mainly due to the test process, and the storage buffer makes no critical difference.

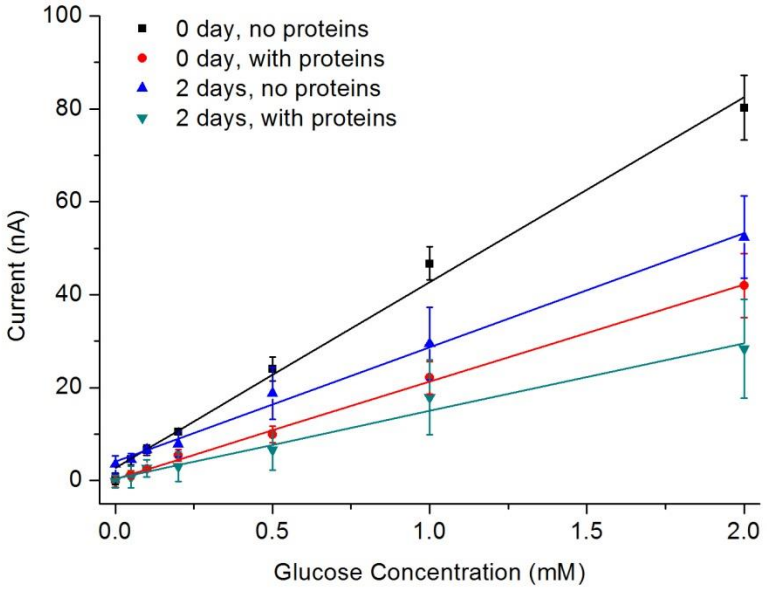

Figure 2.21 Measured effect of protein absorption on system performance[95]

From the data of 0 day in Figure 2.21, the signals with proteins attains about 49.9% compared to that without proteins, the number for 2 days is higher (52.2%). The signal decrease with proteins present is because of the protein-fouling of the sensor surface. The proteins affect the double-layer capacitance and the electron transfer resistance, which leads to the complex impedance change for the electrochemical cell[104]. For this issue, in the future work we will try to apply a polymer network to create a non-fouling surface coating to minimize random protein adsorption.

2.5 Construction of Integrated Contact Lens

Recent advances in portable devices and sensing techniques offer the potential of developing an integrated contact lens with wireless communication circuit to achieve portable glucose sensing or the next generation of human health monitoring. Conducting measurements in a wireless fashion would enable sensor deployment in everyday use. For wireless monitoring, the radio network and telecommunication circuit should have low power consumption, be powered with no external connection, occupy a small area and have a low profile[105]. Our group has experience in integrating silicon chips, an antenna and a micro-LED onto a contact lens and successfully powering and controlling a pixel wirelessly on a live rabbit eye[106, 107].

2.5.1 Read-out/Telecommunication Circuit and Wired Transmission Test

1. Construction of telecommunication circuit and wired connection

Figure 2.22(a) shows the architecture of our custom designed chip which includes rectifier, regulator, bandgap reference circuits, load modulator, pulse generator, and oscillator-based current-to-frequency converter[108]. In conjunction with the antenna, this chip converts the incoming radio frequency wave power to usable DC power for the sensor read-out circuit, operates the sensor, and transmits back the sensor value wirelessly.

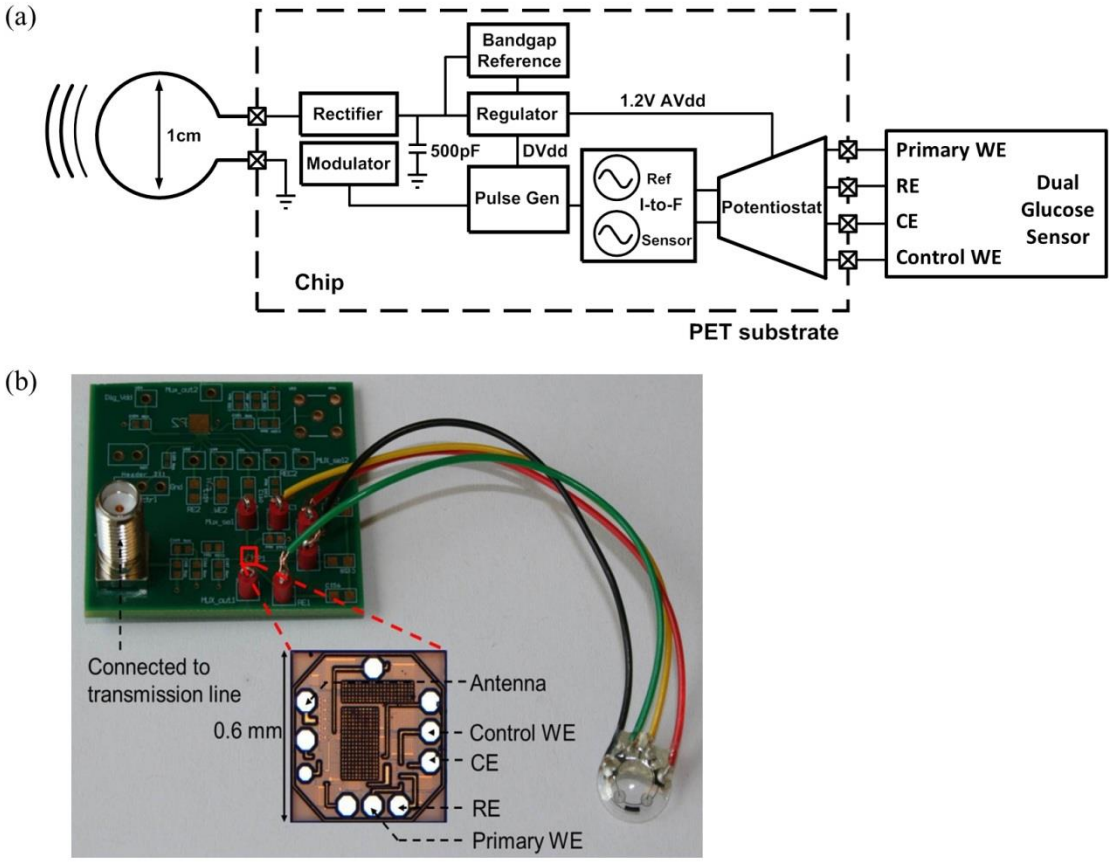

Figure 2.22 The telecommunication circuit and wired transmission connection[95]: (a) System architecture of the communication circuitry; (b) Connection of the dual glucose sensor and the telecommunication circuitry through a PCB

The rectifier was built using Dickson full-wave architecture, which converted the input RF power to a DC voltage. Regulator with a temperature-stable bandgap reference suppressed the supply voltage fluctuation from the incident RF power and provided a +1.2 V supply voltage

to the entire chip. The potentiostat circuits generated a stable +400 mV potential difference between WEs and RE. The sensor currents were injected into a sensing oscillator and a reference oscillator, modulating the frequency of oscillators. A pulse generator compared the output frequency of the two oscillators and generated a pulse period related to the frequency difference. The pulse signals drove the load modulator to reflect the incident RF power (load modulation). The impedance at the input of the chip changed with the pulse signal periodically. Therefore, the sensor current difference was presented by the frequency deviation from the carrier frequency (900 MHz). The readout system was fully integrated in a small chip (0.6 mm × 0.6 mm, 200 μm thickness) without any discrete components (the enlarged view in Figure 2.22(b)). The thickness of the chip can be further reduced, making future contact lens wearable. The chip was wirelessly powered by radiated RF waves from the external power source and consumes 3 μW DC power in operation. The dual sensor and the telecommunication circuitry were first assembled to a PCB (printed circuit board) and connected with a transmission line (Figure 2.22 (b)) to characterize the functionality prior to full integration on the contact lens.

2. Wired transmission results

For preliminary functional test of the wired transmission system, a 900 MHz RF power was delivered to the chip using a low-loss SMA cable. Figure 2.23 shows the output frequency of the wired connection test based on three different sensors (n=3) for glucose 0-1 mM, with a linear correlation R=0.9946.

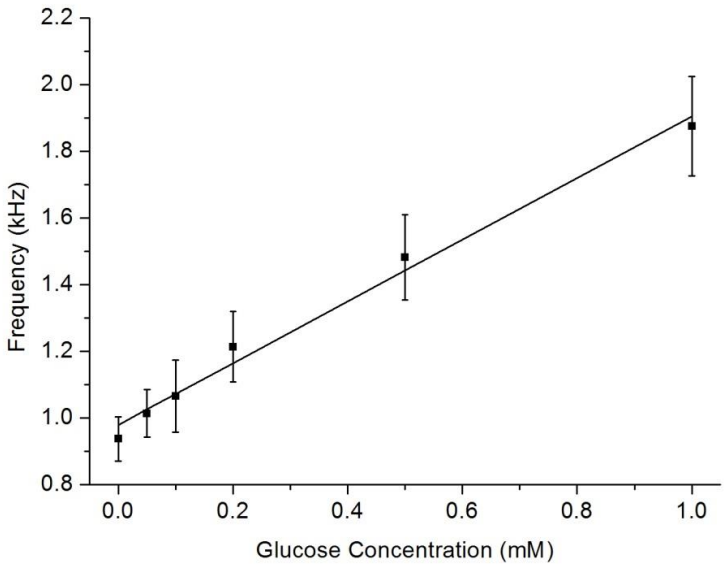

Figure 2.23 The measured frequency responses of wired transmission connection[95]

2.5.2 Integrated Contact Lens and Wireless Transmission Test

1. Construction of integrated contact lens

After concluding the tests for individual system components, an integrated contact lens was built, as shown in Figure 2.24(h). The integrated contact lens is composed of a loop antenna, the read-out/telecommunication circuitry, the dual glucose sensor and the necessary interconnects. The loop antenna was designed for supplying power and signal transmission[106].

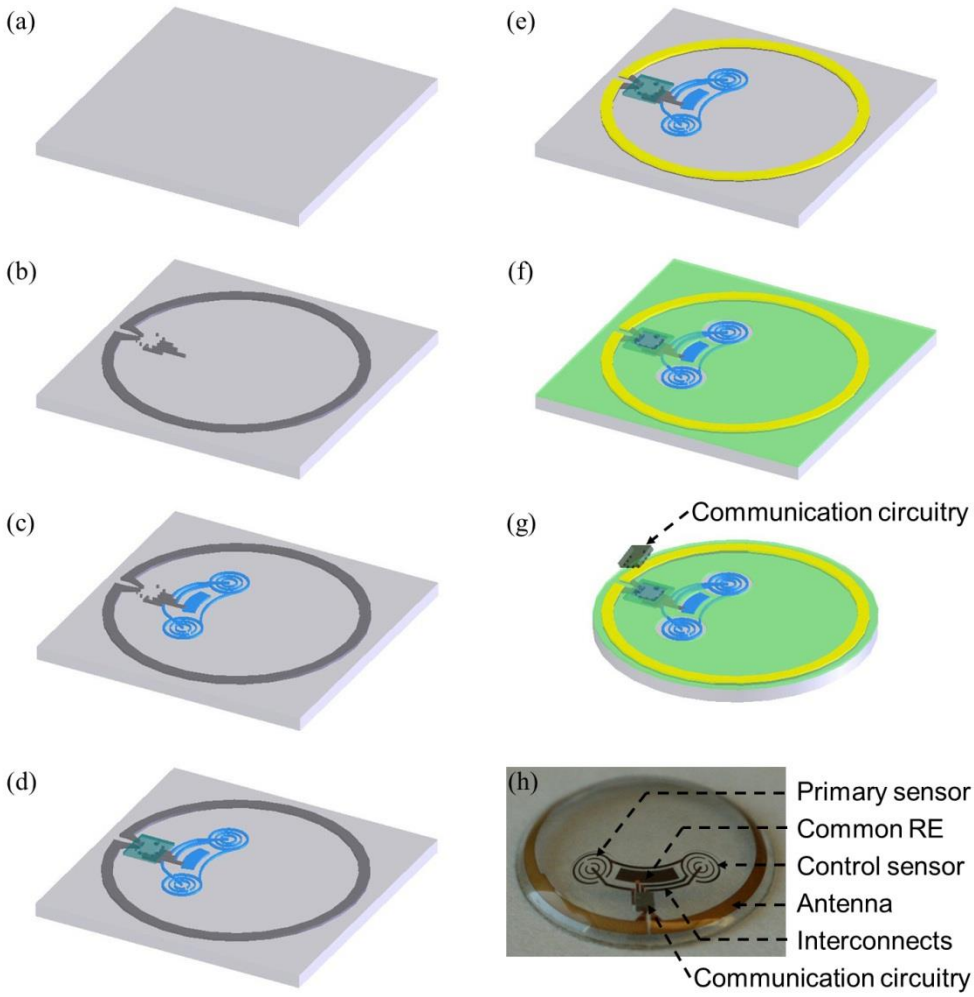

Figure 2.24 The fabrication process flow and image of integrated contact lens[95]

The fabrication of the complete system began with a clean PET wafer (Figure 2.24(a)), a layer of AZ4620 (6 μm) was spin-coated and patterned, and then three layers of metal (Cr 20nm, Ni 80nm, and Au 350 nm) were evaporated in sequence and lifted off to create a pattern for antenna adhesion layer and electrical interconnects (Figure 2.24(b)). Then the differential sensor metal pattern (Ti 10 nm, Pd 20 nm, and Pt 100 nm) was created with photoresist AZ4620 (Figure 2.24(c)). Afterward, a thin layer of SU-8 (1.5 μm) was spin-coated, exposed and developed for electrical insulation and to define solder wetting area (Figure 2.24(d)). Next, a 40 nm Au seed layer was evaporated over the entire wafer. After another AZ4620 photolithography, a 5 μm of Au was created as an antenna with low ohmic loss by pulsed electroplating (1 ms on and 1 ms off) using Pur-A-Gold® 401 formulation (Figure 2.24(e)). After the seed layer of Au was etched off in 5:1 (volume ratio) DI water:Gold Etch TFA, a thick layer of SU-8 (25 μm) was patterned

as a mask to protect the metal structures and to open windows for the dual sensors and silicon chip (Figure 2.24(f)). Then the wafer was cut into lens shape with 1 cm diameter (Figure 2.24(g)).

The next step was the assembly of the silicon chip onto the contact lens via molten-alloy-bridging self-assembly[109, 110]. The metal pads on the silicon chip were electrolessly plated with Ni and Au to create a solderable surface (CVinc Corp.). Then a low temperature indium-based solder (Indium Corp.) was melted and coated on the pads of both the chip and the contact lens. In a heated fluidic bath (70 ^{O}C) with 25 mL ethylene glycohol and 10 μL hydrochloric acid, the chip was aligned over the contact lens (Figure 2.24(g)). And after cooling down in situ, the chip and the contact lens were well bonded together. Afterwards, the integrated lens was heat molded and polished (Figure 2.24(h)). To operate easily with the first prototype of the integrated contact lens, we applied a droplet of non-conductive epoxy to protect the read-out/telecommunication circuitry for further fluidic test. For molecular interference rejection studies, the primary sensor was surface treated with TI/GOD and the control sensor with TI/DeGOD.

2. Wireless transmission results

For wireless setup (Figure 2.25(a)), we used an RF signal generator (Agilent E4438C) to provide a 20 dBm, 900 MHz sinusoidal signal. The signal was fed to an approximately +10 dBi wideband horn antenna (A.H. System, Inc.). Then a 3 dB directional coupler (Krytar Company) was used for the isolation between the input signal and reflected power of the backscatter signal. The directional coupler has four ports: the first port is connected to the signal source, the second port is connected to the antenna to transmit the RF power, the third port is used to receive the reflected signal from the antenna and connected to a spectrum analyzer (RSA3408A, Tektronix Inc.), and the fourth port is terminated with a 50 Ω resistor. We used plastic tweezers to hold the integrated lens in front of the horn antenna (shown in Figure 2.25(a)). The test solutions were pipetted onto the sensor area continuously (one concentration each time), for glucose (G) 0, 0.5 and 1 mM with ALU (ascorbic acid 50 μm, lactate 10 mM and urea 10 mM). We monitored the received signal from the horn antenna using the spectrum analyzer. The frequency deviation between the central carrier frequency (900 MHz) and the first side tone indicates the measured glucose concentration, as shown in Figure 2.25(b).

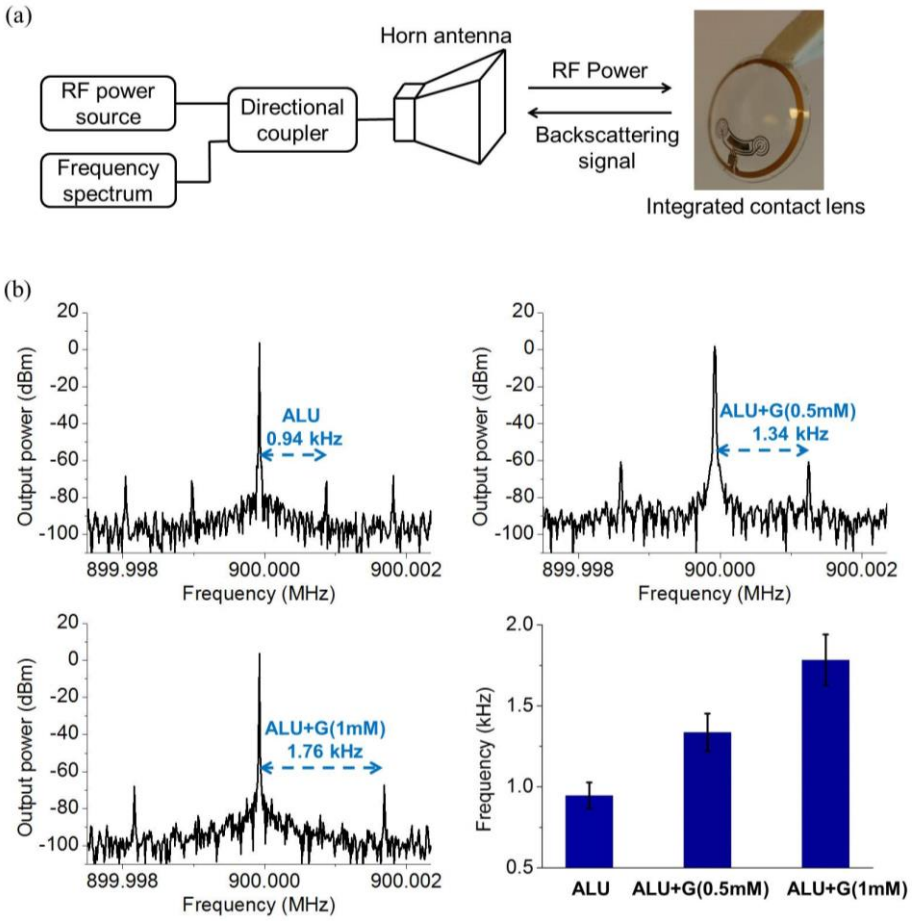

Figure 2.25 The wireless test setup for the fully integrated contact lens and measured wireless data transmission results[95]: (a) Schematic of the test setup for characterization of wireless transmission; (b) Measured wireless transmission results

Figure 2.25(b) shows the wirelessly received spectrum with different glucose concentrations (0, 0.5, and 1 mM). The measured central frequency of the transmitted signal is 900 MHz. The frequency deviation between the carrier frequency and signals are 0.94, 1.34, and 1.76 kHz for glucose 0, 0.5 and 1 mM with interferences, respectively, which shows linearity covering normal tear glucose levels and is in agreement with the wired test data (Figure 2.23). The reproducibility proves a system-level feasibility for the integrated contact lens. The measured operational distance is about 3-4 cm between the integrated contact lens and the horn antenna. The short operating distance is likely caused by impedance mismatch between the antenna and the chip, as well as the low efficiency of the antenna and the rectifier circuit. Further

research is needed to improve the efficiency of wireless transmission and to improve the range of operation for the device.

2.6 Development of Soft Contact Lens

The previous attempts at a contact lens are focused on a hard PET based system. In this section, a soft contact lens is developed based on the common contact lens material pHEMA (poly(hydroxyethyl methacrylate)).

2.6.1 The Selection of Soft Materials

Among various commercial contact lens materials, pHEMA is a popular one due to its high gas permeability, good biocompatibility, insolubility in water, swelling characteristics, and similar flexibility to natural tissue[111, 112]. In our research, pHEMA is selected as our soft lens material because it has other properties that are suitable to develop embedded glucose sensors. 1) pHEMA can also be applied as a polymer matrix for immobilized enzymes in biosensors[113]. The ability to pattern pHEMA by photopolymerization provides a way to quantitatively control the amount of enzyme in order to improve the reproducibility of sensors. 2) pHEMA excels at protecting the electrodes from protein absorption due to its highly hydrophilic nature and tight polymer network[113]. Therefore, pHEMA is an appropriate material to encapsulate glucose sensors in. However, pHEMA is not suitable for multiple microfabrication processes due to its softness and swelling property. Another soft material is needed to work as a substrate for the sensors.

Parylene-C (poly(chloro-p-xylylene)) has desirable properties for microsensor fabrication, especially for implantable devices. It can be easily chemical vapor deposited, possessing a high degree of conformity and uniformity of the membrane[114]. It can tolerate the temperature for metal evaporation and can be dry-etched using oxygen plasma[115]. It has a high level of transparency, biocompatibility and biostability. Unfortunately, parylene-C has very low permeability to gases[116]. To combine the promising properties of both pHEMA and parylene, an improved design is applied for a contact lens-borne glucose sensor. The design features a sensor fabricated on a flexible thin parylene ring, which is subsequently combined with a lens made of oxygen-permeable pHEMA hydrogel.

2.6.2 The First Version of Soft Contact Lens

1. The design, fabrication and surface treatment of parylene sensors

The dual glucose sensor design was adopted and transferred to a fully encapsulated parylene substrate. Since parylene blocks diffusion of oxygen, the sensor was designed in a ring configuration to maximize the fenestration of the oxygen diffusion barrier in the contact lens, as shown in Figure 2.26(a9).

The fabrication of the glucose sensor started by the deposition of a 10 μm Parylene-C layer on a Si wafer (Figure 2.26(a1)). With a layer of positive photoresist (about 6 μm) and O_2 plasma for 30 seconds, three metal layers Ti(10 nm)/Pd(20 nm)/Pt(100 nm) were evaporated and patterned (Figure 2.26(a2)). And then a second 10 μm Parylene-C layer was deposited covering the whole wafer (Figure 2.26(a3)). A Cr(10 nm)/Ni(100 nm) layer was evaporated and patterned to form the first etching mask (Figure 2.26(a4)). The parylene was etched via O_2 plasma (2000W RF) for 7.5 minutes to reach approximately half of the overall device thickness, 10 μm (Figure 2.26(a5)). Then the second etching mask was evaporated and patterned similar to the first etching mask but with openings to the sensor area and contact pads (Figure 2.26(a6)). The second etching step exposed the active area of the sensor, the contact pads and the outline of the device (Figure 2.26(a7)). Oxygen plasma treatment before evaporation step was used to clean and roughen the parylene undercoating.

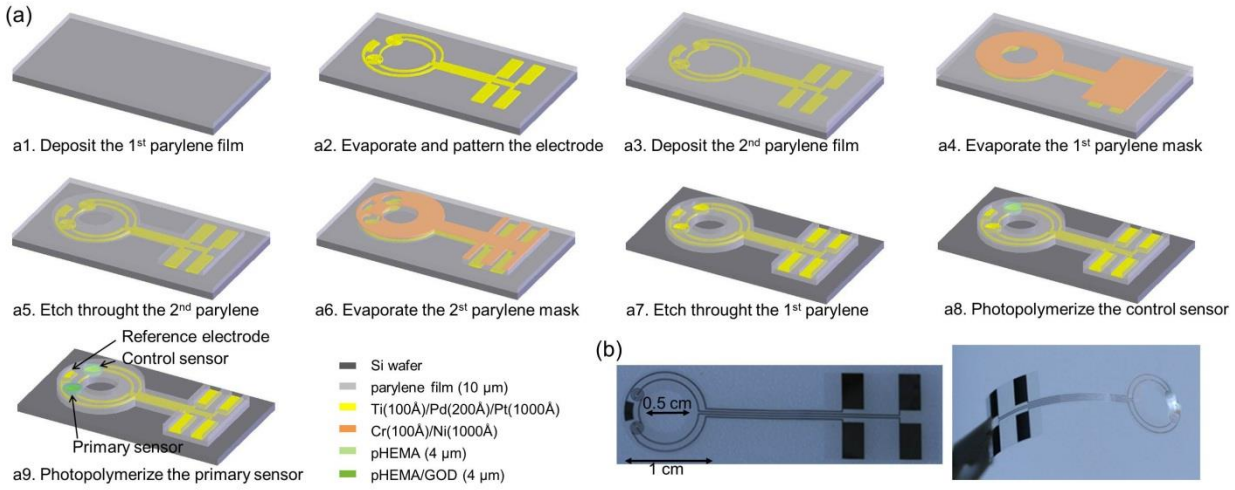

Figure 2.26 Fabrication Process for parylene sensor and images of completed parylene sensors[117]

The immobilization of GOD was done by embedding into a thin film of pHEMA[118]. The pHEMA and pHEMA/GOD were prepared as follows: three chemical components were applied to make pHEMA solution: the monomer hydroxylmethylmethacrylate (HEMA), the crosslinker diethylene glycol dimethacylate (DEGDMA), and the photoinitiator 2,2-dimethoxy-2-

phenylacetophenone (PI). The solutions were prepared with 100:1 molar ratio of HEMA to DEGDMA and 1 wt% of PI. This solution was dissolved in 40% DI to monomer solution (HEMA/DEGDMA/PI) [119]. The pHEMA/GOD solution was prepared the same way, just adding GOD to create a final concentration of 10 mg/mL.

For surface treatment process, a 8 μm pHEMA layer was first spin-coated and selectively photo-polymerized on the control sensor (Figure 2.26(a8)). Next, another 8 μm layer of pHEMA with GOD (10 mg/mL) was separately patterned on the primary sensor (Figure 2.26(a9)). For curing a thin layer of pHEMA or pHEMA/GOD (8 μm), an ABM Contact Aligner was used to apply a 3 minute exposure at 365 nm (24 mW/cm^2), leading to an optically clear polymerization. Finally the parylene sensors were peeled off the silicon wafer simply with tweezers in DI water and dried with N_2 gas, as shown in Figure 2.26(b).

2. Amperometric responses of parylene sensors

The parylene sensors were first tested in a beaker holding a solution volume of 5 mL, with a magnetic stirring bar. The glucose sensor was connected to a bi-potentiostat, applying a constant potential of +400 mV and recording the current with an interval of one second. As shown in Figure 2.27(a), the additions of 0.1 mM glucose (arrow a1) were made sequentially every minute using the basic physiological concentrations of glucose in the tear fluid. In the final injection (arrow a2), 50 μM of ascorbic acid, as an interference chemical, was added to the 0.6mM glucose solution.

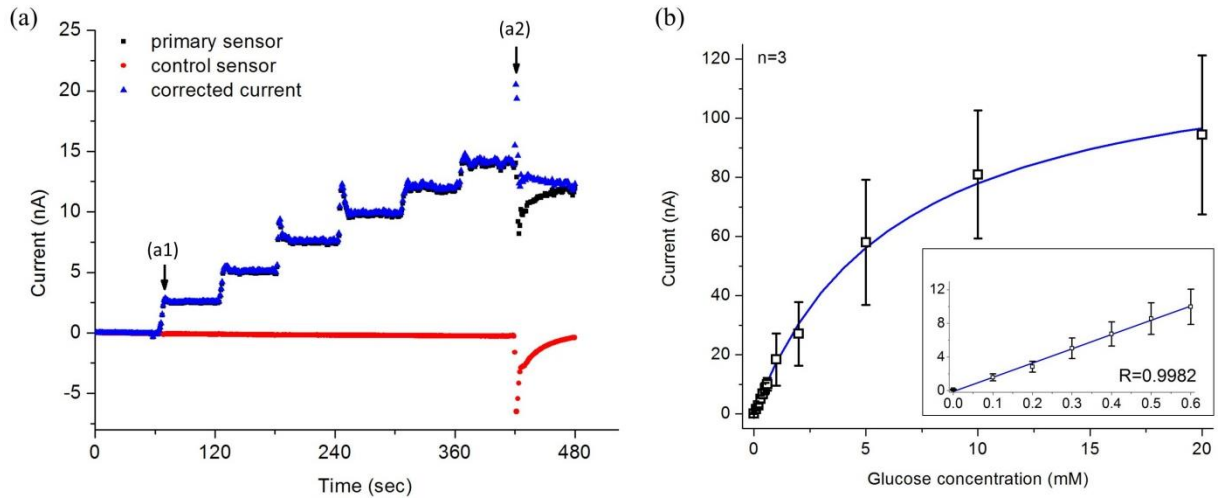

Figure 2.27 Results of pHEMA sensors[117]: (a) current response of the dual sensor; (b) Michaelis-Menten fit for glucose up to 20 mM and the enlarged view of the linear relation for glucose 0.1-0.6 mM

It demonstrate that, the control sensor does not response to glucose, while both sensors have the same response for ascorbic acid. Correcting the response by subtracting the current of the control sensor from the primary sensor, the blue curve shows a good performance for interference injection. Three different sensors were used to get independent measurement results, as shown in Figure 2.27(b). By averaging the corrected current of 30-50 sec after each addition, we get the amperometric response for sensor repeatability. Figure 2.27(b) shows the current results for glucose up to 20 mM. Applying the Michaelis-Menten kinetics model to fit the current response, we can get a Michaelis constant $K_m \approx 6.3$ mM, which is comparable with some previous reports[90]. The enlarged view in Figure 2.27(b) shows the amperometric response for low glucose levels (0.1-0.6 mM). The good linear relationship (R=0.9982) provides potential for real applications in tear fluids.

3. Contact lens molding and results

Forming pHEMA to the contact lens shape utilizes two molds that form the inner and outer concave of the contact lens. An aluminum mold was machined to form the inner concave of the contact lens and polished to a mirror finish. A PDMS mold was cast to form the outer concave of the contact lens. This mold was made by placing the aluminum top mold into a container and pouring a 10:1 ratio of Dow Corning SLYGARD® 184 to hardener, degassed and baked at 85 ^{O}C for 2 hours. The Aluminum mold was then carefully removed from the PDMS mold making a negative of the inner concave. The PDMS mold was plasma treated for 5 minutes

and then treated with a 10mM solution of (3-Aminopropyl) triethoxysilane (APTES) dissolved in ethanol. The APTES solution was pipetted into the concave on the PDMS mold and allowed to dry in a fume hood.

As shown in Figure 2.28(a), encapsulating the parylene sensor was started by filling the PDMS mold with the HEMA solution. The parylene sensor was carefully placed in the mold and centered. The Al mold was pressed into place excess pHEMA solution is pressed out leaving a bubble free layer inside the mold. For curing the pHEMA contact lens molding solution, an ELC-500 (Electro-Lite) UV exposure chamber was used to apply a 9 minute exposure at 365 nm (24-28 mW/cm^2) in an inert nitrogen environment for polymerization. After peeling off from the molds carefully, the hydrogel needed to be soaked in water, usually overnight, to reach the proper hydration of the polymer, as shown in Figure 2.28(b).

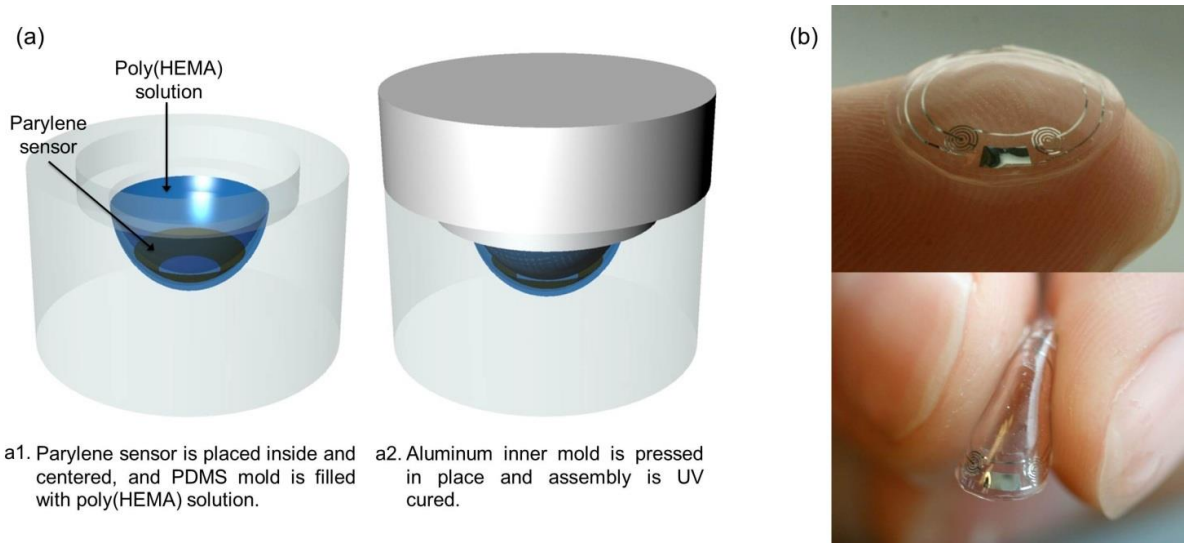

Figure 2.28 Construction of contact lens-based sensors[117]:
(a) Molding process; (b) images of contact lenses

Next, the molded sensors were tested in the same way as parylene sensors, in a beaker of 5 mL buffer with a magnetic stirring bar. The real-time results are shown in Figure 2.29, for both glucose and H_2O_2 responses.

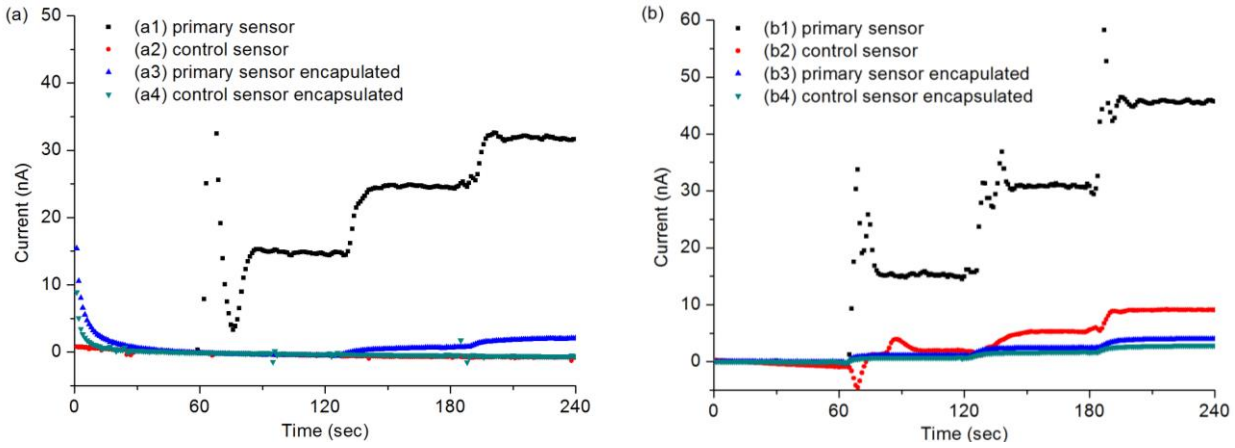

Figure 2.29 Amperometric responses of pHEMA molded sensors:

(a) three additions of glucose 1 mM; (b) three additions of H_2O_2 10 μm

Comparing Figure 2.29(a1) and (a3), the response of the sensor decreased a lot for glucose, and similar phenomenon appears for H_2O_2 as in Figure 2.29(b1) and (b3). It demonstrates that the encapsulating pHEMA layers block the diffusion of both glucose and H_2O_2. This is probably because the thickness of pHEMA during molding process is hard to control, and it is unavoidable to have a very thick layer on top of the sensor area (>10 μm). The thick pHEMA layer does not possess a good permeability as the thin layer of pHEMA/GOD (~8 μm), and it will create a difficult diffusion barrier for both large and small molecules. Another molding problem is that the ring-shaped parylene sensors usually overlap at some spots as the ring shape cannot fit the PDMS mold very well. In the next step, a new shape design and molding process of parylene sensor are carried out to improve the permeability of the molded soft contact lenses.

2.6.3 The Second Version of Soft Contact Lens

1. The improvement of the second version

Since the round ring-shaped parylene sensor always has the folding problem and thick layers while molded in pHEMA, for the second version of parylene sensors, the main part of the sensor is designed as a zigzag shape to maximize the fenestration of the oxygen diffusion barrier, and at the same time to facilitate molding a 2D membrane to 3D shape without the overlapping problem. Figure 2.30 shows the new design of the parylene sensors. In addition, one step molding process cannot promise a very thin layer of pHEMA on top of sensing area in the first

version. Thus, in this step, a new strategy was applied to minimize the thickness of pHEMA layer.

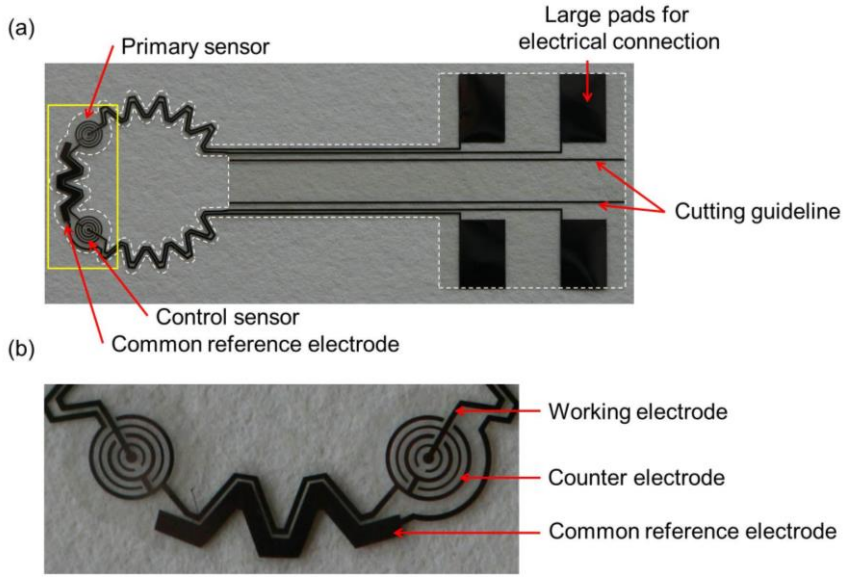

Figure 2.30 The design of the second version of parylene sensors

The fabrication process of the parylene sensors was the same as the first version (Figure 2.26). After the parylene sensor was peeled off and diced along the cutting guidelines, it was ready to be molded to contact lens. The molding process was composed of two main steps: first, a pHEMA lens was produced, followed by incorporating the sensor structure on the lens. Both steps utilize a simplified injection molding technique commonly used in manufacturing hydrogel contact lenses[120]. Here PDMS molds were applied to form the inner and outer surfaces of the contact lens. The PDMS molds were made by curing Dow Corning SLYGARD® 184 and hardener (10:1 in volume) in machined hard aluminum molds, at 80 ^{O}C for 1 hour. And the two PDMS molds were designed to hold a distance of about 500 μm, which mimics the thickness of a contact lens.

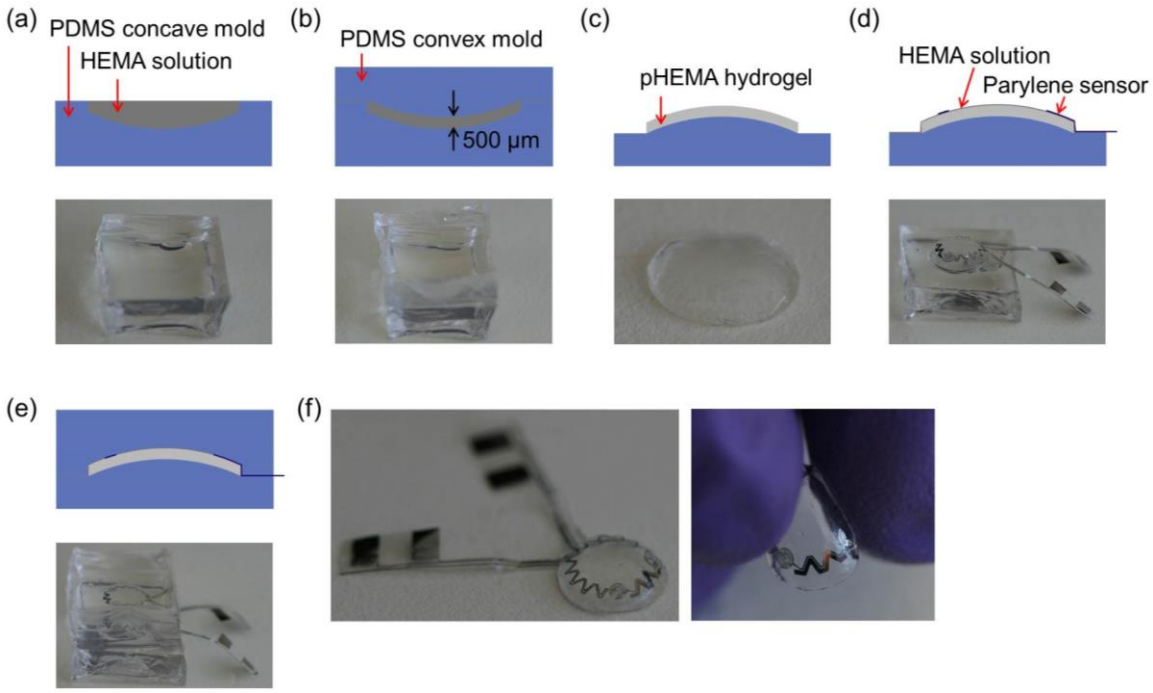

Figure 2.31 The molding process of soft contac lenses

Before polymerization, the PDMS molds were first plasma cleaned for 5 min and then treated with a 10 mM solution of APTES dissolved in ethanol. The APTES solution was pipetted onto the PDMS mold surfaces and allowed to dry in a fume hood to silanize the surface, which aids the release of the contact lens from the mold. As shown in Figure 2.31(a), the PDMS concave mold was filled with the liquid HEMA solution and then covered by a PDMS convex mold (Figure 2.31(b)). The extra HEMA solution was pressed out leaving a bubble-free layer inside the mold. After photopolymerization with UV light in a N_2 environment (365 nm, about 24 mW/cm^2) for 300 seconds, the pure pHEMA contact lens could be easily removed by soaking in DI water for a few minutes (Figure 2.31(c)). Next, the contact lens was put back on the concave mold and the top surface was wetted with HEMA solution. Then the cut parylene sensor was placed on top of the lens and adjusted to the curvature of the lens (Figure 2.31(d)). The whole lens was covered with a PDMS convex mold and photopolymerized again for 5 minutes (Figure 2.31(e)). The whole encapsulated contact lens was soaked in DI wafer for a few minutes and removed. The final soft contact lens with embedded glucose sensors are shown in Figure 2.31(f). The sensors were stored in DI water at 4 ^{O}C until use.

2. Typical amperometric response

The performance of the contact lenses was tested in a beaker with a solution volume of 8 mL, kept under continuous stirring to avoid mass transport limitations. During the test, different concentrations of solutions were pipetted into the beaker and a bi-potentiostat (CHI750D, CH Instruments) was utilized to supply +400 mV on the two WEs, relative to the common RE. The current signals from the WEs were recorded simultaneously every second. Figure 2.32 shows a typical amperometric response to glucose (G 0-1 mM) and interference chemicals: urea (U 10 mM), lactate (L 10 mM) and ascorbic acid (A 0.05 mM). The glucose concentrations are selected by covering the normal values in tear fluid, and the interferences exceed the maximum concentrations in tear fluid[121]. The signal given by the primary sensor (the black curve) shows a response to both glucose and interferences, whereas the control sensor (the red curve) only responds to interferences. When a difference signal is calculated by subtracting the signals of the control sensor from the primary sensor, the interference response is almost entirely removed while the glucose response is preserved, as illustrated by the blue curve.

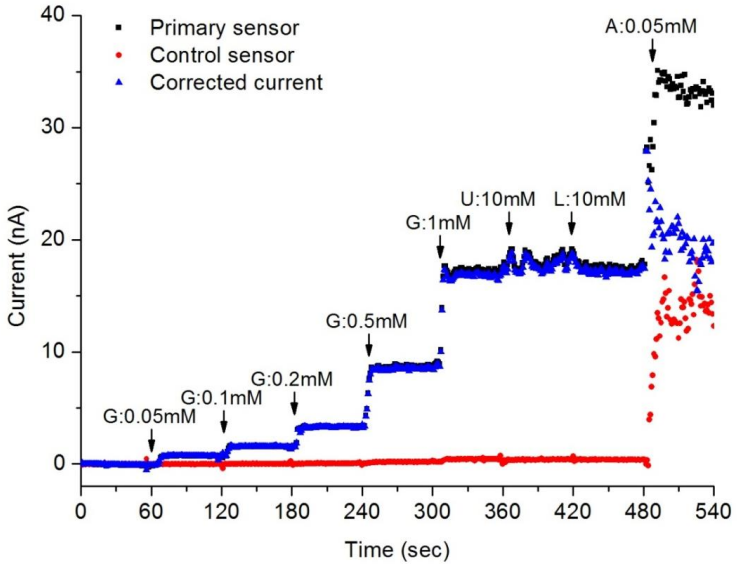

Figure 2.32 Current response of the dual sensor based on the subsequent additions of chemicals

The results indicate that the dual sensor is capable of detecting glucose as low as 0.05 mM. The response from the primary sensor is barely affected by urea or lactate, but a big disturbance is observed in response to ascorbic acid. Although different from previously reported results for the elimination of the ascorbic acid response by using pHEMA[122], our results show that the dual sensor design is successful in rejecting most of the ascorbic acid response.

When using photopolymerization to cure an aqueous solution of HEMA with water as the solvent, the proportion of HEMA can be adjusted from 20% to 90% (in volume)[112]. We chose 40% water because it is the highest diluent concentration that maintains a transparent and homogeneous hydrogel structure after photopolymerization into pHEMA. At the same time, the high amount of water will increase the permeability of pHEMA hydrogel[113]. Here the difference of explosion time for HEMA/GOD or DeGOD (200 seconds) and the molded lenses (300 seconds) comes from the difference of the power and distance from the two UV radiators. The concentration of GOD was selected to be 10 mg/mL as the final concentration in accordance to our previous publications[82, 95], but different concentrations of GOD have been applied to immobilize in pHEMA hydrogel[112, 123]. This could be further investigated in our future research.

3. The linearity and repeatability of the sensor

By averaging the corrected current values of 30-50 seconds after each addition (the blue curve in Figure 2.32), we collected three independent measurement results from three different sensors for both low and high concentrations of glucose. Figure 2.33(a) shows a good linearity of the sensors with R^2 value of 0.9978. Figure 2.33(b) is the calibration curve for high concentrations of glucose up to 50 mM.

The Michaelis-Menten equation was fitted to the high-concentration calibration results, in order to calculate the apparent affinity constant K_m. The equation has the form $I = \frac{I_{max} \times C}{K_m + C}$, where C is the glucose concentration, I is the current response and K_m is the Michaelis constant, corresponding to the glucose affinity for the enzyme GOD[124]. The fit yielded a K_m value of 10.5 mM, which is in accordance with the value of our old immobilization method using titania sol-gel film[82]. Moreover, this value also fits into the range typically observed for glucose sensors[90].

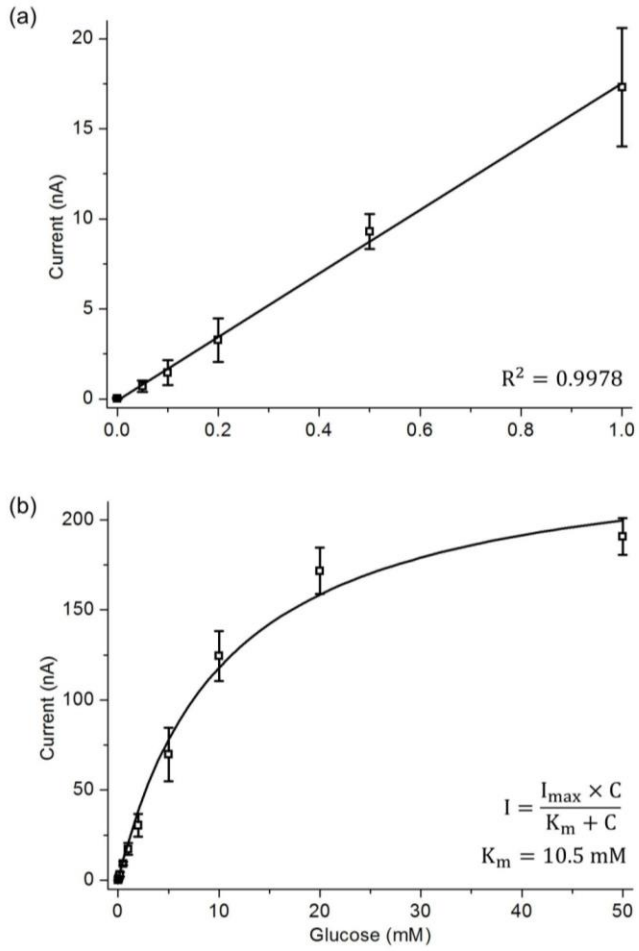

Figure 2.33 Calibration currents for low and high concentrations of glucose: (a) Linear fit for low concentrations of glucose; (b) Michaelis-Menten fit for high concentrations of glucose

Compared to other enzyme immobilization methods, photopolymerization of HEMA/GOD has the advantage of easy patterning and good control of the amount GOD, which makes the fabrication process amenable to commercial production. It has been reported that a prolonged exposure (more than several hours) to UV radiation at 365 nm can lead to a decrease of GOD activity, and deactivation of GOD can also be brought about by the presence of photoiniatiator, crosslinker and DI water[112]. However, our experimental results prove that even if deactivation did occur, the sensor retains sufficient stability and sensitivity for measurements of glucose in tear fluid.

4. The effect of temperature

Temperature has a significant effect on enzyme activity. Figure 2.34 demonstrates the temperature effect for buffer, glucose 0.5 mM and 1 mM from 5 ^{O}C to 55 ^{O}C. The response for

glucose increases when the temperature rises from 5 ^{O}C to 45 ^{O}C, and then decreases as the temperature is further increased to 55 ^{O}C; while the deviation of the current from buffer is unobservable. Different maximum response temperature values have been reported in literature for glucose sensors due to the various microenvironments stemming from different immobilization methods[125]. Here we chose 25 ^{O}C (room temperature) for all the other experiments to simplify lab bench tests.

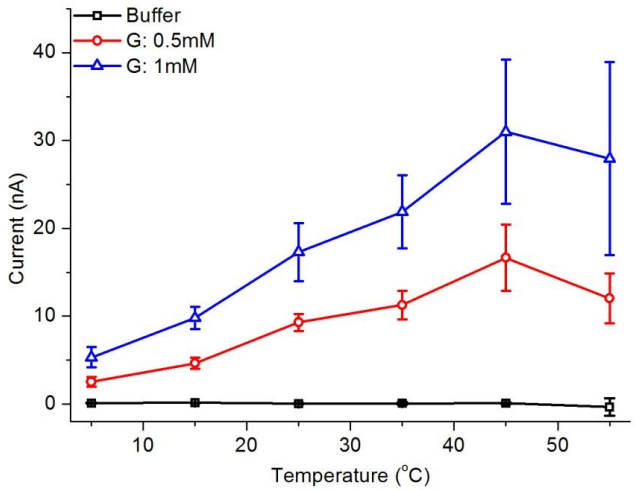

Figure 2.34 Measured effect of temperature variation on system performance

The apparent activation energy (E_a) of the enzyme catalytic reaction can be estimated according to the Arrhenius equation[126]: $I = A\exp(-\frac{E_a}{RT})$, where I is the current response, A is a pre-exponential factor specific to the reaction, E_a is the apparent activation energy, R is the gas constant (8.314 $JK^{-1}mol^{-1}$), and T is the absolute temperature. Here E_a can be calculated as 26.1 kJmol for glucose 0.5 mM and 26.4 kJ/mol for glucose 1 mM. These numbers are similar and comparable with the values reported for other glucose biosensors based on GOD[127] and similar as other reports applying pHEMA immobilized GOD[128].

5. The stability of the sensor and rejection of protein fouling

In order to test the stability of the sensor, we first measured the signals from glucose 0.5 mM continuously for 2 hours. As shown in Figure 2.35(a), the signals from the primary sensor and the control sensor are very stable in the unchanged beaker. In another aspect, three sensors were tested in different days independently. The sensors were stored in buffer at 4 ^{O}C between tests and used for about 30 minute during each test. The black squares and the red circles in

Figure 2.35(b) show the responses to buffer and 1 mM glucose, respectively, from 0 day to 16 days. The sensors can retain about 95.9% of its initial response after 1 day, and 90.2%, 88.2%, 88.1% 68.9% for 2 days, 4 days, 8 days and 16 days, respectively. It shows good stability for at least the first 8 days, which makes the sensors suitable for commercial contact lenses. The stability shows that the polymer network of pHEMA is a suitable matrix to immobilize the GOD enzyme in, and possibly solves the issue of GOD leaching out of the sensor structure. After a longer time, such as 16 days, the average current response decreases to 68.9% of the original signal. The signal decrease is probably caused by gradual enzyme deactivation, and further investigation is still needed to find out the exact deactivation mechanism. It has been reported that pHEMA is not only suitable to immobilize GOD, but also feasible for other enzymes, such as lactate oxidase[129] and cholesterol oxidase[130]. This provides a potential to develop a multiple-target biosensors.

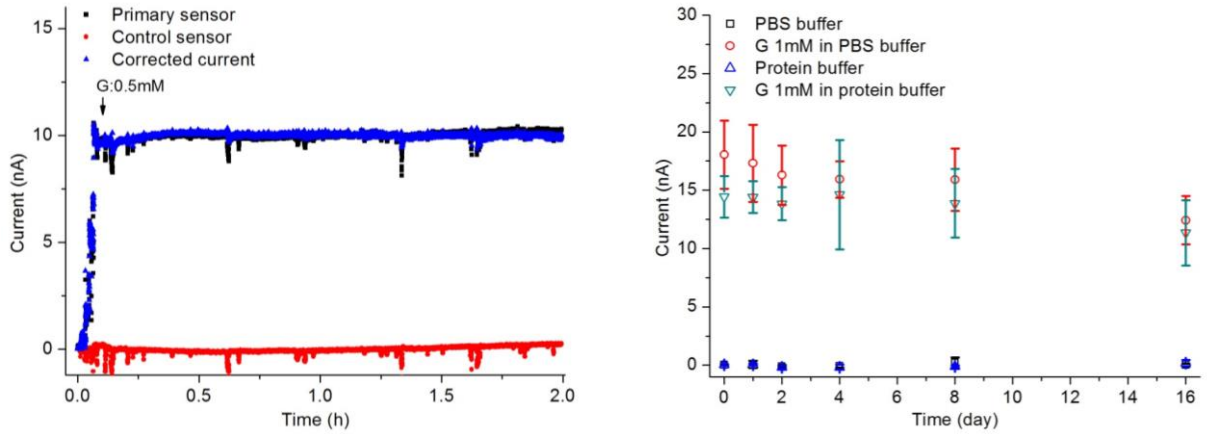

Figure 2.35 The stability and protein effect of the sensor: (a) The real-time response for a sensor continuously measured up to 2 hours; (b) Calibration currents for buffer and glucose 1 mM for three sensors (n=3) tested in PBS buffer and another three (n=3) tested in protein buffer

Besides the stability, the surface resistance to non-specific protein adsorption is also critical for the performance of glucose sensors. Tear fluid contains various proteins, making natural tear composition very complex[131]. In order to study the influence of protein fouling on the sensor operation, three typical proteins were added into the protein buffer to construct a simple artificial tear solution[132]: lysozyme 1.9 mg/mL, albumin 0.2 mg/mL and mucin 0.15 mg/mL. Three sensors were chosen to test and store in protein buffer at 4 ^{O}C in order to tell the degree of protein fouling effect. The blue upward triangles and the cyan downward triangles in Figure 2.35(b) show the

signals from protein buffer only and glucose 1 mM in protein buffer, respectively. Comparison of signals from buffer only, with or without proteins, shows that the signals are similar from 0 day to 16 days. The data for 1 mM glucose, with or without proteins, shows that on day 0, the signal in the presence of proteins is about 80.0% compared to that without proteins. For subsequent measurements in 1, 2, 4, 8 and 16 days, the ratios are 83.3%, 85.1%, 91.8%, 87.2%, 91.4%, respectively. It is unavoidable to have some fluctuation during aging, but it can be concluded that the signals in the presence of proteins can attain a level of about 80-90% in the absence of proteins. This is a considerable improvement over our earlier immobilization strategy[95], and attests to the ability of pHEMA hydrogel to counteract protein fouling.

It is hypothesized that the antifouling ability of pHEMA is tightly correlated with a hydration layer near the surface, because a tightly bound water layer forms a physical barrier to limit protein adsorption and the compression of the long-chain polymer also provides protein resistance due to unfavorable decrease in entropy[133]. Some other reports have combined HEMA with other monomers to adjust the properties of pHEMA layer, such as methacrylic acid[134], methylmethacrylate[135], dimethylaminoethyl methacrylate[128] and ethylene glycol dimethacrylate[136]. Future investigation of including other monomers may provide further improvements in protein fouling rejection.

2.7 Summary

A non-invasive continuous glucose sensor on a contact lens could make personalized medicine cheaper, simpler and more reliable. Based on electrochemical reaction of glucose catalyzed by glucose oxidase, a three micro-electrode system was designed and tested for various generations of glucose sensors. After basic validation of rectangular-shaped and lens-shaped glucose sensors on PET plastic substrates, the sensors were completed with wireless communication circuit and antenna to construct an integrated contact lens to monitor tear glucose levels. A dual sensor design was adopted for interference rejection and an enzyme immobilization with titania sol-gel film was applied to get better sensitivity and repeatability. Finally, the microfabrication of glucose sensors was transfer to a flexible substrate parylene and molded in pHEMA hydrogel to make soft contact lenses. The design of the parylene sensor has been optimized to accommodate a 3D lens shape, and the use of pHEMA for enzyme

immobilization and molding process provides the soft contact lenses with favorable performance characteristics and ease of fabrication, which paves a way for a future commercial product.

Chapter 3 Microbe Sensors Embedded in Contact Lenses

3.1 Sensing Principles

3.1.1 The Electrochemical Impedance Spectroscopy

As introduced before (Section 1.3.4), compared with other microbe sensing methodologies, impedance spectroscopy biosensors have the advantages of fast response, easy combination with microfabrication processes, and capability to minimize the devices. Based on the previous experience of electrochemical glucose sensors, here a sensing method based on electrochemical impedance spectroscopy was employed for microbe sensors.

Electrochemical impedance spectroscopy provides the information of complex impedance, as opposed to a simple magnitude of impedance, and is a powerful method for investigating the interfaces of conductive electrodes. As reported, various impedance biosensors for bacterial cell detection have been constructed by immobilizing antibodies on the electrode surfaces due to the specificity of antibodies to the target cells[137]. These sensors usually probe the attachment of bacterial cells by measuring the change in electrical properties of the sensor due to the insulating properties of the cell membrane. A general electronic equivalent circuit is shown in Figure 3.1(a).

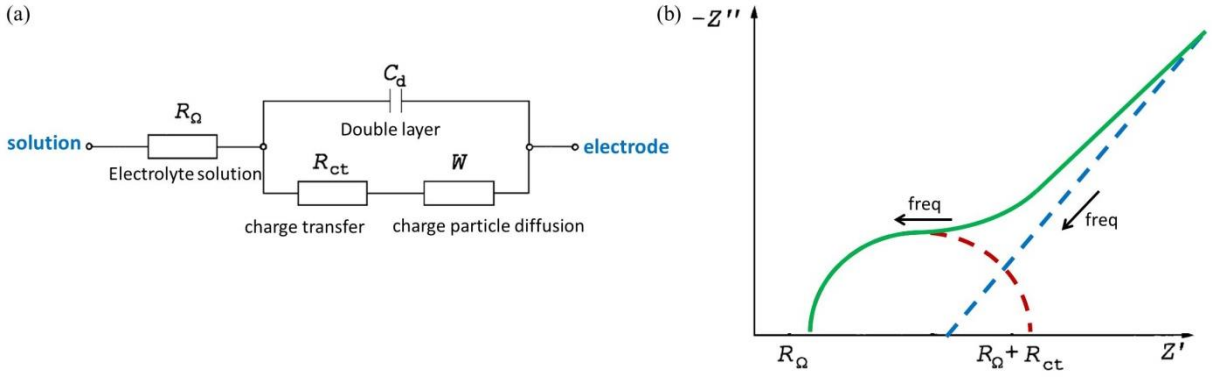

Figure 3.1 Theory of electrochemical impedance spectroscopy[104]: (a) a general equivalent circuit for impedance spectroscopy; (b) schematic impedance spectra presented in the form of a Nyquist plot

R_Ω includes the ohmic resistance of the electrolyte solution and does not vary with changing frequency. C_d is the the capacitance of the double layer. R_{ct} is the charge transfer resistance, existing if a redox probe is present in the electrolyte solution. W is the Warburg impedance, results from the diffusion of ions from the bulk electrolyte to the electrode interface; it represents a kind of resistance to mass transfer. W can be calculated as[138]:

$$W = \frac{R_{ct}K_W}{\sqrt{2\omega}}(1-j)$$

$$K_W = \frac{k_{ox}}{\sqrt{D_{ox}}} + \frac{k_{re}}{\sqrt{D_{re}}}$$

Here, k_{ox} and k_{re} are the rate constants of the oxidation and reduction, respectively. D_{ox} and D_{re} are the diffusion coefficients of oxidized reactant and reduced reactant. As W is proportional to 1-j, the Nyquist plot of W is a straight line at the angle of 45^{O} to the real axis, as the blue dashed line in Figure 1.3(b).

According to the equivalent model, the real part and the imaginary part of the impedance can be expressed as:

$$Z' = R_\Omega + \left(R_{\mathrm{ct}} + \sigma\omega^{-1/2}\right)/Q_{\mathrm{R}}$$

$$Z'' = -\left(\omega C_{\mathrm{d}}\left(R_{\mathrm{ct}} + \sigma\omega^{-1/2}\right)^2 + \sigma^2 C_{\mathrm{d}} + \sigma\omega^{-1/2}\right)/Q_{\mathrm{R}}$$

$$Q_{\mathrm{R}} = \left(\sigma\omega^{1/2}C_{\mathrm{d}} + 1\right)^2 + \omega^2 C_{\mathrm{d}}^2\left(R_{\mathrm{ct}} + \sigma\omega^{-1/2}\right)^2$$

$$\sigma = K_{\mathrm{W}}R_{\mathrm{ct}}/(2)^{1/2}$$

Applying this theoretical analysis, a typical shape of the impedance spectra is presented as the form of a Nyquist plot (the green curve shown in Figure 3.1(b)). The typical curve Z ´~-Z ´´ includes a semicircle region at higher frequencies followed by a straight line for lower frequencies. The semicircle portion corresponds to the process limited by charge transfer, whereas the linear part represents the diffusionally limited electrochemical process. In the case of very fast electron transfer process, the impedance spectrum could include only the linear part whereas a very slow electron transfer step results in a large semicircle region.

For the situation that charge transfer resistance R_{ct} is dominant while Warburg impedance is negligible, such as the semicircle part of the Nyquist plot (the red dashed line in Figure 3.1(b)), then

$$Z' \approx R_\Omega + R_{ct}/(1+\omega^2 C_d^2 R_{ct}^2)$$

$$Z'' \approx -\omega C_d R_{ct}^2/(1+\omega^2 C_d^2 R_{ct}^2)$$

These two equations satisfy that $(Z' - R_\Omega - R_{ct}/2)^2 + (Z'')^2 = R_{ct}^2/4(1+\omega^2 C_d^2 R_{ct}^2)$. For very low frequency, $(Z' - R_\Omega - R_{ct}/2)^2 + (Z'')^2 \approx R_{ct}^2/4$, which is an equation for a circle.

The center of the circle is $(R_\Omega + R_{ct}/2, 0)$, and the diameter is $R_{ct}/2$. It implies that the semicircle diameter equals to the electron transfer resistance R_{ct}, as shown in Figure 3.1(b).

In an electrochemical cell with a redox probe, there is charge transfer across an interface. The bacterial cell attachment or the biofilm formation on the electrode surfaces would retard the interfacial electron transfer kinetics and increase the electron transfer resistance. The difference of obtained resistance R_{ct} could provide the information of the surface cells or biofilms.

3.1.2 Antibody Immobilization

Antibodies help to capture the targeted bacteria, especially for quick assessment. In order to immobilize specific antibodies onto the interdigitated gold electrodes, antibody molecules was first thiolated with S-H group at one end to facilitate the monolayer assembly onto Au surfaces[139]. Two typical bacterium strains, *E. coli* Top 10 (the Lidstrom Laboratory from University of Washington) and *P. aeruginosa* PAO1 (the Harwood Laboratory from University of Washington) were used to test microbe sensors. Anti-E.coli antibody and Anti- *P. aeruginosa* antibody were purchased from Abcam Company.

As shown in Figure 3.2, the antibody (20 µL of 200 µg/mL solution) was first derivatized by 1 hour incubation with 10 µL sulfo-LC-SPDP (40 mM, Sulfosuccinimidyl 6-3'-[2-pyridyldithio]-propionamido hexanoate). Thiolation was completed by adding 35 µL DTT (13 mM, DL-Dithiothreitol) reducing a S-S bond into a S-H group. Finally, 10 µL of the thiolated antibody solution was deposited on the electrode area and incubated at 4 ^{O}C overnight. After rinsing with buffer solution, the sensor was ready to use. Bare sensors were used as control.

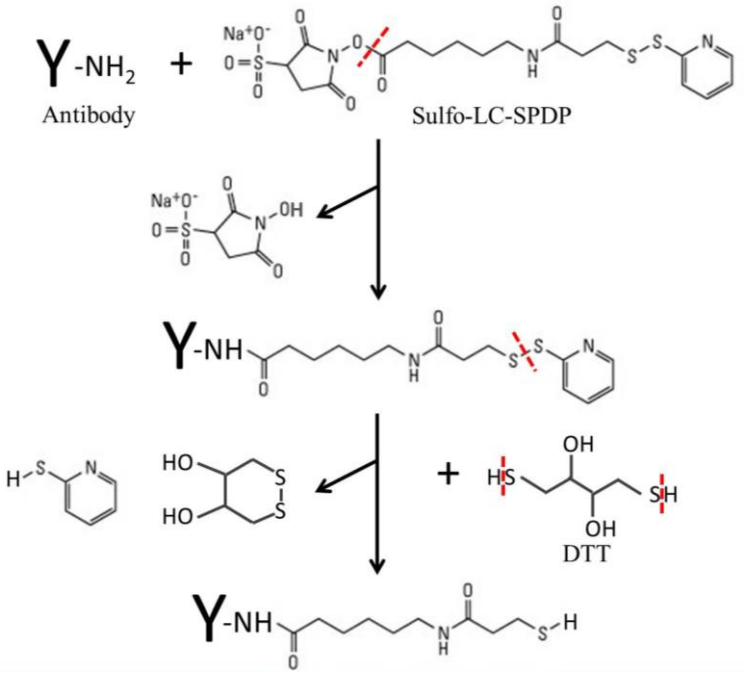

Figure 3.2 The principle of antibody thiolation

3.1.3 Biofilm Formation

P. aeruginosa PAO1 was used to develop biofilms since *P. aeruginosa* is very related with ocular diseases and also it has been extensively utilized as a model organism for biofilm formation due to its self-generated extracellular polymeric matrix[68]. As reported, starvation can induce the biofilm formation of bacteria *P. aeruginosa*, and the growing phase of the biofilm is usually from 12 hour to 24 hours later[140]. After the bacteria attached the Au electrodes through antibody-antigen reaction, the sensors were transferred into a continuous flow cell incubated for up to 24 hours in the presence of 1% normal nutrients at the room temperature, to develop to the matured biofilm. The feed rate is 1 mL/min.

3.2 Microbe Sensors for *E.coli*

As *E. coli* is the most commonly and thoroughly studied model bacterium, *E.coli* Top 10 strain was selected for the design and test of the preliminary microbe sensors.

3.2.1 The Design of the Microbe Sensors

For the detection based on electrochemical impedance spectroscopy, three-electrode design was employed here for the first generation of microbe sensors. As shown in Figure 3.3(a), the sensor is designed as a zigzag shape for future encapsulation in contact lenses. Three large pads (2 mm × 4 mm) are used to make electrical connection with an external potentiostat. The

sensor is composed of a large Au reference electrode (~3.2 mm^2) and two interdigitated Au electrode arrays, each having 48 fingers of 40 μm × 400 μm, with a spacing of 40 μm, as shown in Figure 3.3(b). The key feature of the interdigitated design is to achieve a large active area and improve the sensitivity.

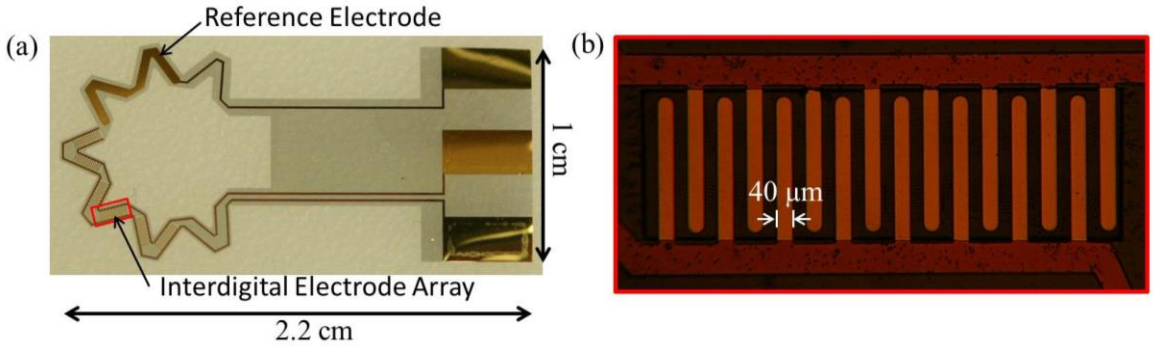

Figure 3.3 The design of the microbe sensor for *E.coli*:
(a) the image of the sensor; (b) the enlarged image of the rectanglar area

The size of the interdigitated electrode must be chosen for different biological entities in consideration of their sizes to achieve a sensitive biosensor for that type of biological entity. Here the width of 40 μm and the spacing of 40 μm are chosen by considering both the bacterium size and the facility of microfabrication. In the future, the width and spacing of interdigitated electrodes could be further reduced to improve the sensitivity.

3.2.2 The Fabrication of the Microbe Sensors

Figure 3.4 shows the fabrication process of the microbe sensor. Beginning with the deposition of the first parylene layer on a silicon wafer (Figure 3.4(a)), the metal layers Ti/Au were evaporated in sequence (Figure 3.4(b)). After a second parylene film covering the whole wafer (Figure 3.4(c)), a layer of Cr/Ni was evaporated and lift-off on parylene film, working as an etching mask (Figure 3.4(d)). The second parylene film was etched with O_2 plasma for 8 min and then the Cr/Ni mask was wet etched (Figure 3.4(e)). Using the same process to etch the parylene down to the silicon wafer (Figure 3.4(f) and (g)), the device was finally released by peeling off sensors by tweezers in water (Figure 3.4(h)). The parylene sensor is very flexible, as shown in Figure 3.4(i).

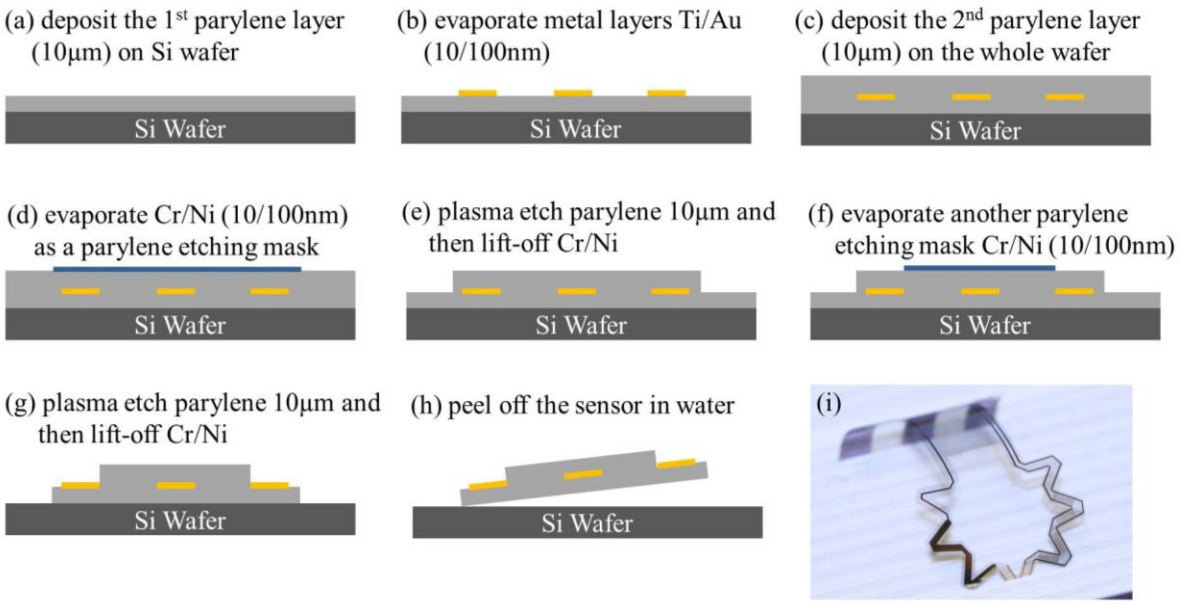

Figure 3.4 The microfabrication process of the microbe sensor

3.2.3 Validation of Microbe Sensors with *E.coli*

After treated with *E.coli* antibody overnight, the sensor was thoroughly cleaned with DI water to remove the unreacted antibody, and dried in air. Then the sensor was immersed in a 5 mL *E.coli* cell culture with different cell concentrations, and incubation was allowed to proceed for 30 minutes at room temperature. Before testing, the sensor was rinsed with phosphate buffer (pH=7.4) to remove non-specially bound cells. Impedance spectrum was carried out in a small beaker with a 10 mL solution of a 10 mM $[Fe(CN)^{6}]^{3-}/[Fe(CN)^{6}]^{4-}$ redox probe. The frequency range is 0.1 Hz-100 kHz with an alternating voltage 10 mV (dc voltage=300 mV).

Figure 3.5 is the comparison of a bare sensor (CTL), an antibody-treated sensor (AB) and AB after binding with *E.coli* (1×10^{5} CFU/mL). It shows that the impedance increases significantly after antibody treatment and increases much further after incubation with *E.coli* solution.

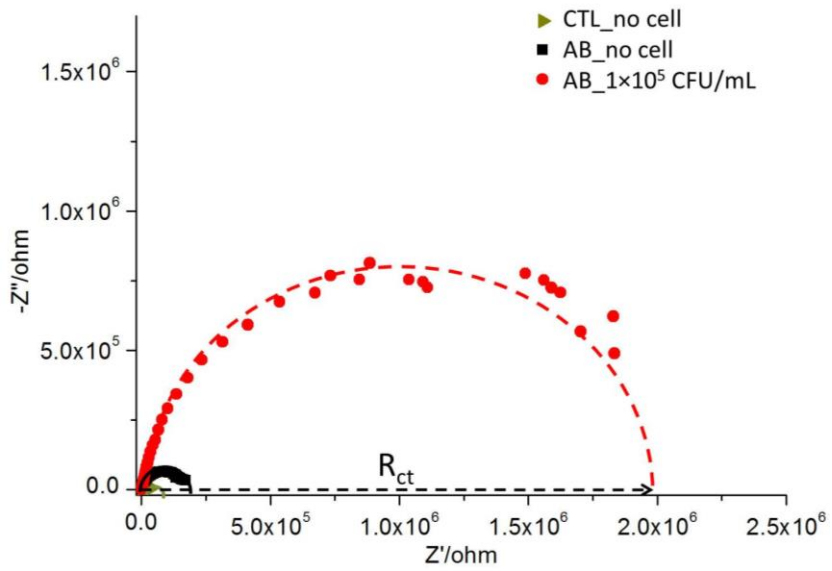

Figure 3.5 The impedance spectra obtained with a bare sensor (CTL), the sensor treated with antibody (AB) and AB after binding with E.coli (1×10^5 CFU/mL)

Figure 3.6 shows the surface photos of AB and CTL after incubation in different E.coli solutions (0, 1×10^6, 1×10^7 CFU/mL). It demonstrates that *E.coli* cells attach onto the antibody-treated electrode surfaces selectively, while non-specific adsorption onto the control surfaces is negligible.

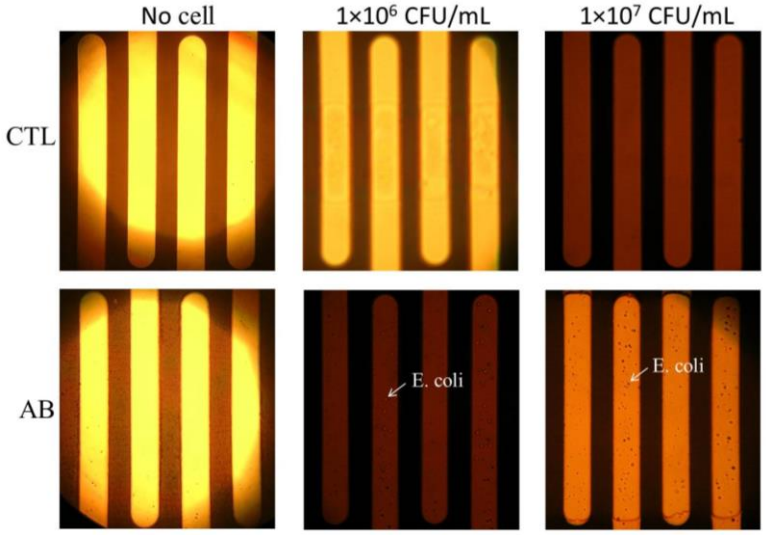

Figure 3.6 Surface images of CTL and AB after incubation in cell media

To validate the sensors with *E.coli*, more concentrations were tested. Figure 3.7 shows the results of impedance spectroscopy for AB and CTL after incubation in different *E.coli* solutions (0, 10^5, 10^6, 10^7, 10^8 CFU/mL). It shows the electron transfer resistance R_{ct} increases

obviously from no cell up to 10^7 CFU/mL, but does not increase significantly from 10^7 to 10^8 CFU/mL. It is probably because the attachment of cells onto the electrode has approached to saturation for high cell concentrations.

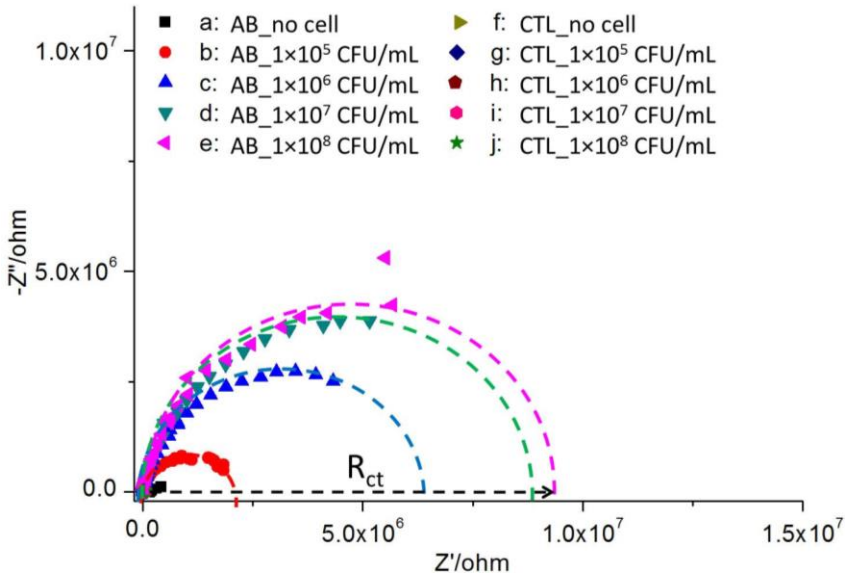

Figure 3.7 Impedance spectroscopy results of AB and CTL for different concentrations of *E.coli*

Figure 3.8 is the enlarged view of the data from CTL. It shows that there is no significant variance for incubation with various *E.coli* concentrations for controls. It proves that non-specific adsorption onto the CTL surface is negligible for the microbe sensors.

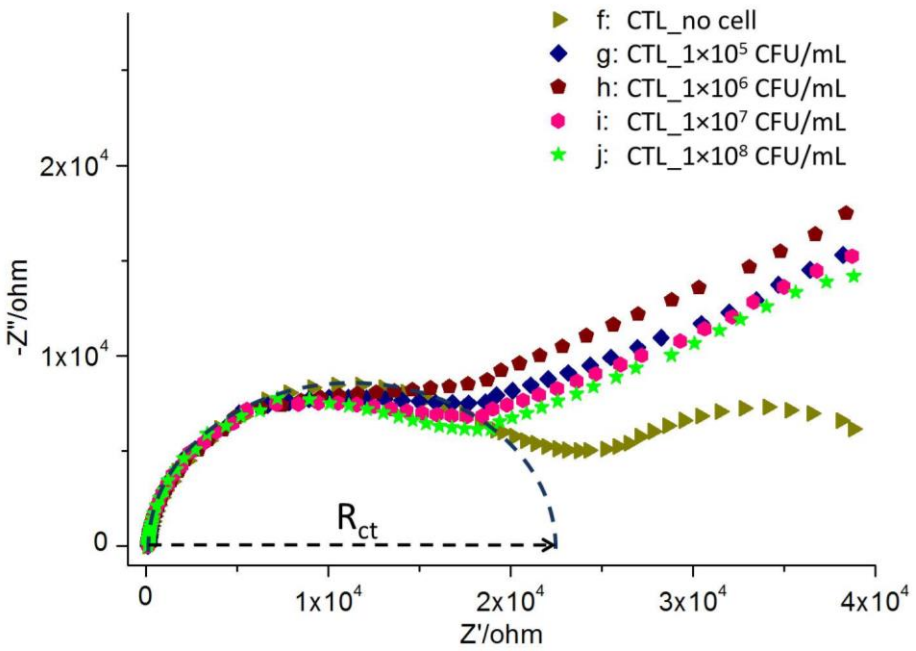

Figure 3.8 Enlarged view of the CTL results

3.3 Microbe Sensors for *P. auroginosa*

Based on the preliminary validation of microbe sensors with *E. coli*, next the sensors are optimized and tested with the targeting bacterium *P. auroginosa*.

3.3.1 The Design, Microfabrication and Molding of the Microbe Sensors

The three-electrode design is similar as the previous microbe sensors for *E.coli*, as shown in Figure 3.9(a). Cutting guidelines are added for future molding processes. Considering the smaller size of *P. auroginosa* compared with *E. coli*, the electrode is designed with 20 μm width (Figure 3.9(c)). The microfabrication process was adopted as microbe sensors for *E.coli*. The sensing area, reference electrode and three large connection pads were open with one parylene layer as substrate, while all the other interconnect wires were sandwiched in two parylene layers. The device was finally released from Si wafer and shows good flexibility, as shown in Figure 3.9(b).

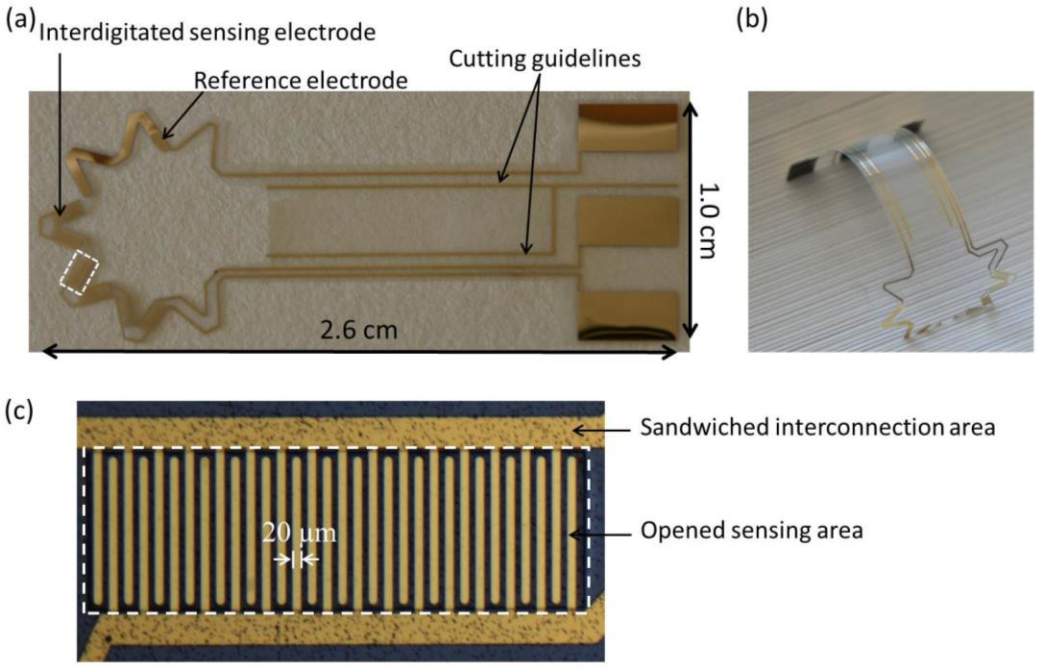

Figure 3.9 Microbe Sensors for *P. auroginosa*

Next, the flexible parylene sensor was molded in pHEMA to make soft contact lenses. The molding process is similar as pHEMA glucose sensors, composing of two steps: a pHEMA lens is first produced and the sensor is incorporated onto the lens. After a pure pHEMA contact lens was gained by a set of PDMS molds, the lens was placed back on the top of the concave mold and wetted with HEMA solution. Then the cut parylene microbe sensor was placed on the lens top and adjusted to the curvature of the lens. After photopolymerized in UV light, the final soft contact lens is shown in Figure 3.10. As impedance sensing of bacteria is mainly based on the surface situation of electrodes, the parylene sensor is preferable to be molded on the outmost layer of the contact lens. Further investigation about sophisticated molding processes should be to done to make the lens surface as smooth as possible.

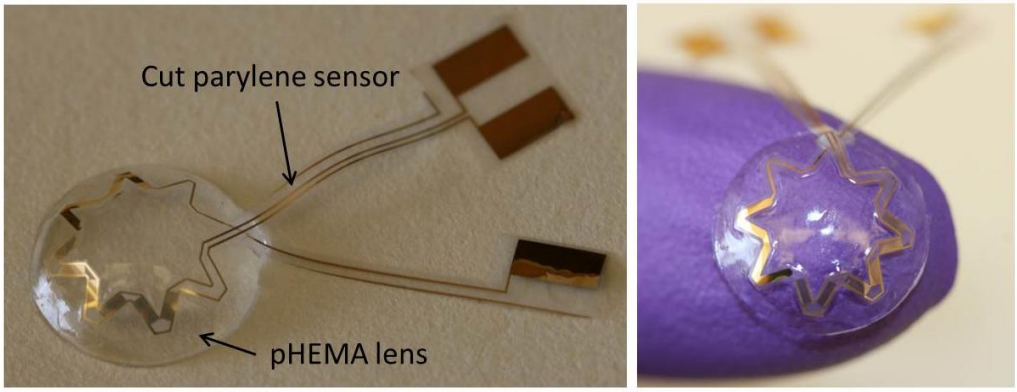

Figure 3.10 Molded soft contact lens with embedded microbe sensors

3.3.2 Antibody Treatment and Attachment Test

Similar as *E.coli* antibody, *P. auroginosa* antibody was first thiolated; and then 10 μL of the thiolated antibody solution was deposited on the sensing area of the molded soft contact lens and incubated at 4 ^{O}C overnight. After rinsing with buffer solution, the sensor was ready to use (AB). Bare sensors were used as control (CTL). As shown in Figure 3.11, after incubation in different *P. auroginosa* media (0, 1×10^{6}, 1×10^{8} CFU/mL), the bacteria attach onto the AB surfaces, while non-specific adsorption onto the CTL surfaces is negligible. The shape of *P. auroginosa* observed by microscopy is rod shaped, which is consistent with reported[141].

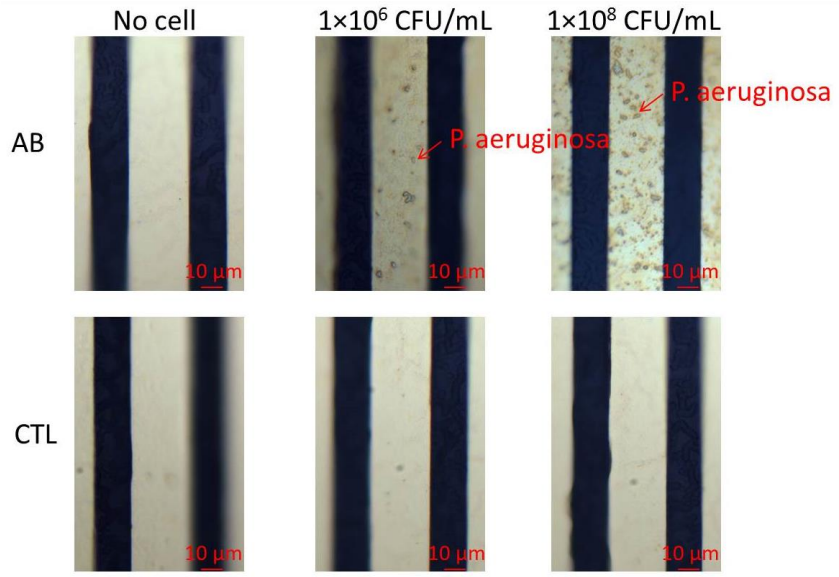

Figure 3.11 Surface images of CTL and AB after incubation in *P. aeruginosa* media

3.3.3 Results and Discussion

After validation of cell attachment by microscopic observation, the sensors were next used for the test of electrochemical impedance spectroscopy. Being treated with *P. auroginosa* antibody overnight, the sensor was thoroughly cleaned with DI water to remove the unreacted antibody, and dried in air. Then the sensor was immersed in a 5 mL *P. auroginosa* cell culture with different concentrations (0, 1×10^5, 1×10^6, 1×10^7, 1×10^8, 1×10^9 CFU/mL) for 30 minutes at room temperature. Before testing, the sensor was rinsed with phosphate buffer to remove non-specially bound cells. The measurement was carried out in a small beaker with a 10 mL solution of 10 mM $[Fe(CN)^6]^{3-}/[Fe(CN)^6]^{4-}$ redox probe. Impedance spectra were recorded in the frequency range of 0.1 Hz-100 kHz with an alternating voltage 10 mV (dc voltage=0 mV).

Figure 3.12 is the comparison of a bare sensor (CTL), an antibody-treated sensor (AB) and AB after binding with *P. auroginosa* (1×10^5 CFU/mL). It shows that the impedance of electron transfer R_{ct} increases significantly after antibody treatment and increases much further after incubation with 1×10^5 CFU/mL *P. auroginosa*. For a specific frequency, such as 1 Hz and 10 Hz, both the real part and the imaginary part of the complex impedance increase due to the increase of cell concentration, which provides a potential to tell the different surface situations in another way.

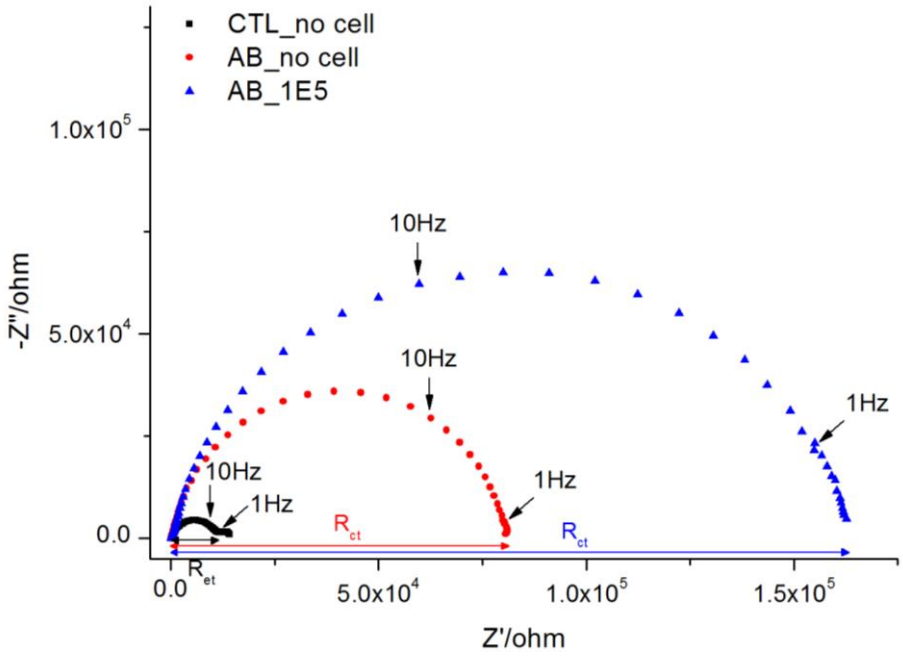

Figure 3.12 The impedance spectra obtained with a bare sensor (CTL), the sensor treated with antibody (AB) and AB after binding with P. auroginosa (1 ×105 CFU/mL)

Next the sensors were validated with more concentrations of *P. auroginosa*. Figure 3.13 shows the results of impedance spectroscopy for antibody-treated sensors (AB) after incubation in different *P. auroginosa* solutions (0, 10^5, 10^6, 10^7, 10^8, 10^9 CFU/mL). It shows the electron transfer resistance R_{ct} increases obviously from no cell up to 10^8 CFU/mL, but does not increase significantly from 10^8 to 10^9 CFU/mL. It is probably due to the saturation of cell attachment for high concentrations.

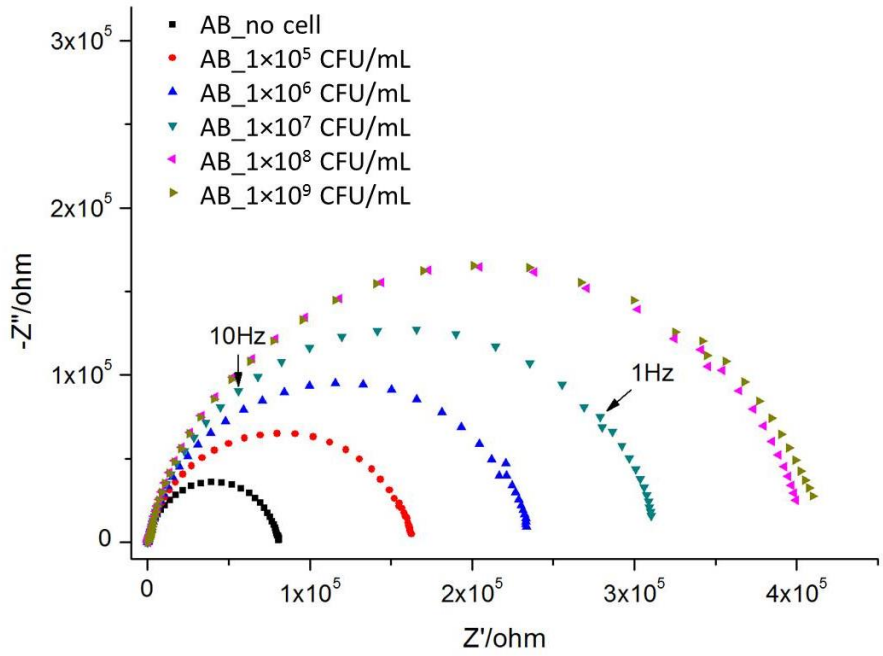

Figure 3.13 The impedance spectra obtained with an antibody treated sensor (AB) after binding with different concentrations of *P. auroginosa* (0-10^9 CFU/mL)

To make sure the impedance difference does not come from the unspecific attachment of *P. auroginosa*. Bare sensors were tested as control (CTL), and Figure 3.14 is the enlarged view of the data from CTL. It shows that there is no significant difference of R_{ct} among various *P. auroginosa* concentrations. It proves that non-specific adsorption onto the CTL surface is negligible for the microbe sensors.

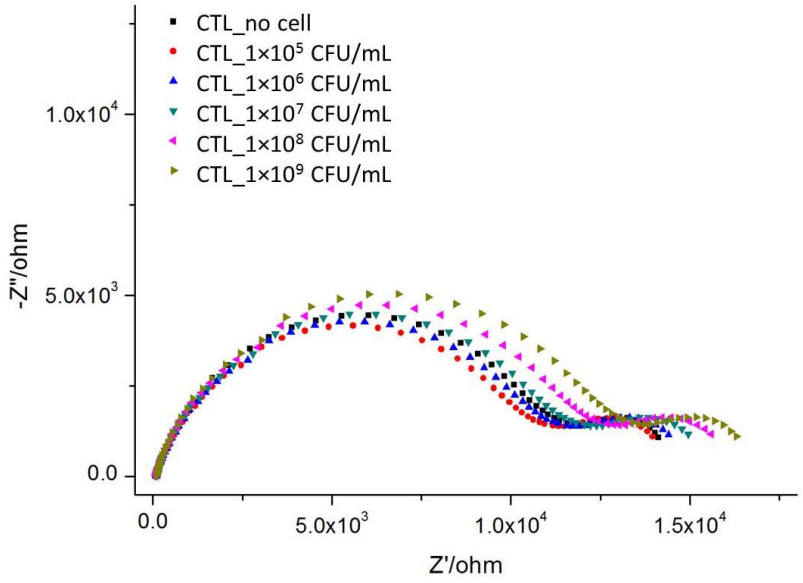

Figure 3.14 The impedance spectra obtained with a control sensor (CTL) after binding with different concentrations of *P. auroginosa* (0-10^9 CFU/mL)

Three different sensors were tested independently to prove the repeatability of the microbe sensors for *P. auroginosa*. By collecting the electron transfer resistance R_{ct}, the average response was gained for bacterium concentrations of 0, 10^5, 10^6, 10^7, 10^8, 10^9 CFU/mL, as shown in Figure 3.15. Compared with the $R_{ct}=9.1\times10^4$ Ω for no cell attachment (just antibody treated sensor), the R_{ct} gained for 10^5, 10^6, 10^7, 10^8, 10^9 CFU/mL equals 1.4×10^5, 1.8×10^5, 2.7×10^5, 3.5×10^5, and 3.6×10^5 Ω respectively. No significantly difference between 10^8 and 10^9 CFU/mL is probably because the attachment of *P. auroginosa* onto the electrode surfaces get saturated for very high bacteria numbers. Here the error bars for three different sensors are a little bit large, that is probably coming from the surface situation for different sensors. For electrochemical impedance sensing, the sensor surface is very critical for the final results, such as the cleanness of the surface, the antibody amount immobilized onto the surface, and the status of cells. There still needs more future research about how to improve the repeatability and electrode surface quality.

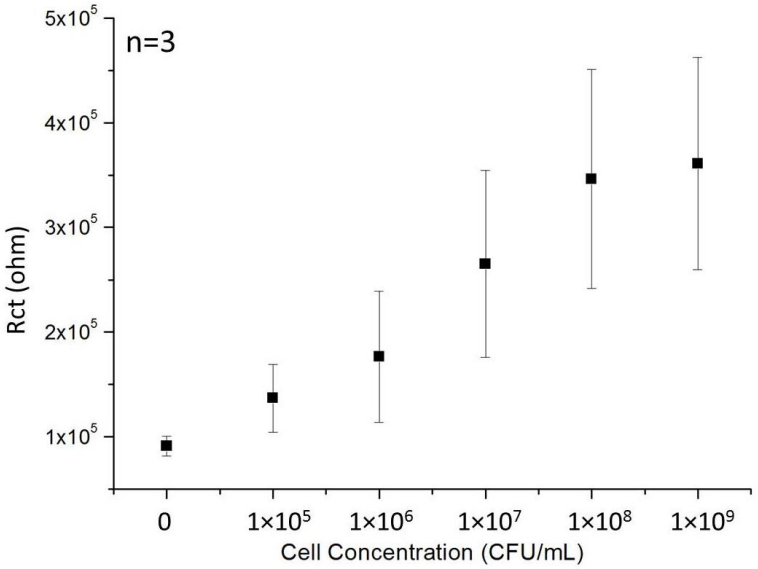

Figure 3.15 The repeatability of microbe sensors for *P. auroginosa* (0-10^9 CFU/mL)

3.4 The Test of Biofilm Formation

Similar as the attachment of bacteria, the development of the biofilm on the metal surfaces are expected to retard the interfacial electron-transfer kinetics and increase the electron-transfer resistance. Biofilms act as insulting films when growing on substrate and the existence of biofilms on the electrode surface would inhibit the electron transfer between the redox probe in the solution and the working electrode. Therefore, the deviation of R_{ct} will reflect the different situation of biofilms.

The experiment was performed like this: the molded sensor was first surface treated with *P. aeruginosa* antibody at 4 ^{O}C overnight, as shown in Figure 3.16(a1). After rinsing with buffer solution to remove the unattached antibody, the sensor was in cell media with the concentration of 1×10^8 CFU/mL for 30 minutes. Figure 3.16(a2) shows that attachment of the cells. Next the biofilm were gained by further incubation in continuous flow cell with 1% LB media up to 24 hours; and the surface situation of 12 hours and 24 hours are shown in Figure 3.16(c) and (d), respectively.

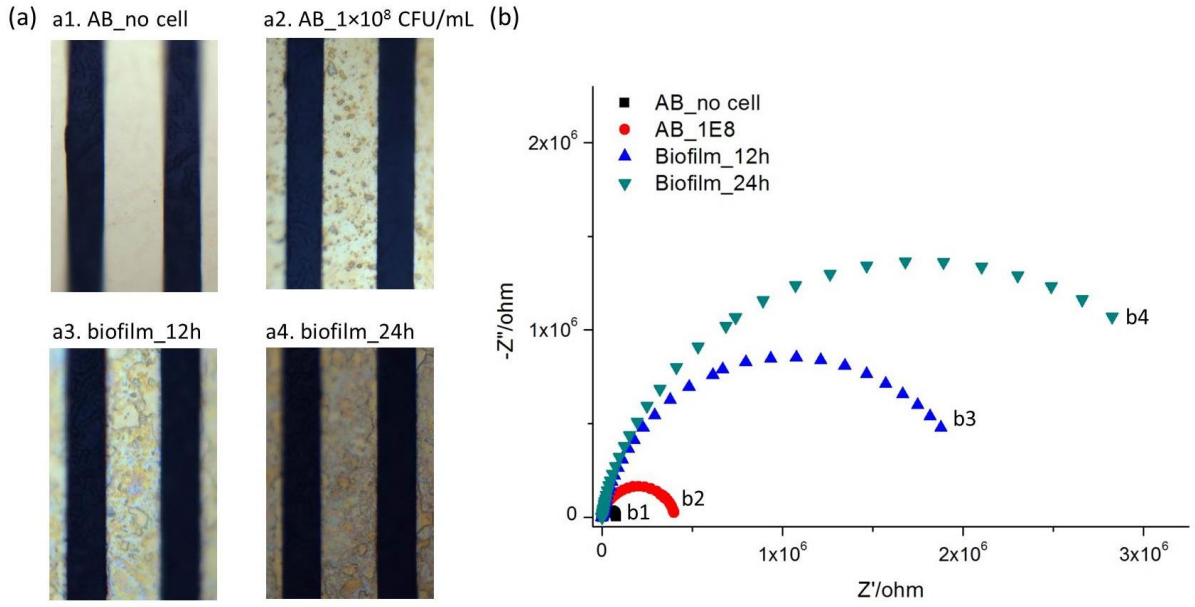

Figure 3.16 The formation and impedance spectra of biofilm:

(a) the microscopic photoes of biofilm formation; (b) the impedance spectroscopy results

The homogeneous biofilm is about 1~2 μm thick and has colonized more than 80% of the metallic surface area after 12 hours incubation. Here all the sensors here are tested after molded, the surface is spherical, not flat enough to provide a good focus for larger area of microscopic observation. The range of Figure 3.16(a) is limited by the spherical surfaces. In future research, more image analyzing techniques need to investigate to for directly observing the three-dimensional structure of biofilms, such as confocal laser scanning microscopy[75].

As shown in Figure 3.16(b), the electron transfer impedance R_{ct} increases from antibody treated sensor to the one incubated with 1×10^8 CFU/mL *P. auroginosa*; and further increases significantly after biofilm formation for 12 hours and 24 hours. The measurement was carried out in the same way as testing cell attachment: in a small beaker with a 10 mL solution of 10 mM $[Fe(CN)^6]^{3-}/[Fe(CN)^6]^{4-}$ redox probe. The impedance spectra were recorded in the frequency range of 0.1 Hz-100 kHz with an alternating voltage 10 mV (dc voltage=0 mV). Here the original concentration of 1×10^8 CFU/mL was selected as the high concentration create biofilm faster than low concentrations; and the attachment of *P. auroginosa* is not saturated, due to the results from Figure 3.15.

Compared with artificially prepared glucose test solutions, As natural tear fluids are composed of a large number of proteins, such as lysozyme, lactoferrin, albumin and IgG[102].

Protein adsorption is an initial event occurring when tear contact with the soft lenses, and the interaction between proteins and electrode surfaces has been found to be sensitive to the surface characteristics of the electrode metals[142], which could provide the false signals for biofilm formation. In order to study the influence of protein fouling on the microbe sensor operation, three typical proteins were added to the incubation buffer: lysozyme 1.9 mg/mL, albumin 0.2 mg/mL and mucin 0.15 mg/mL[103].

The blue dots in Figure 3.17 is the impedance spectroscopy results for the antibody treated microbe sensor after incubation in protein buffer for 30 minutes. All the sensors were tested in a small beaker with a 10 mL solution of 10 mM $[Fe(CN)^6]^{3-}/[Fe(CN)^6]^{4-}$ redox probe; and the impedance spectra were recorded in the frequency range of 0.1 Hz-100 kHz with an alternating voltage 10 mV (dc voltage=0 mV). The impedance of electron transfer R_{ct} increased with the protein incubated sensor, which gives a response between 1×10^8 CFU/mL *P. auroginosa* and 12 hour biofilm formation. This means that the protein fouling will interfere with the signals from cells and biofilms.

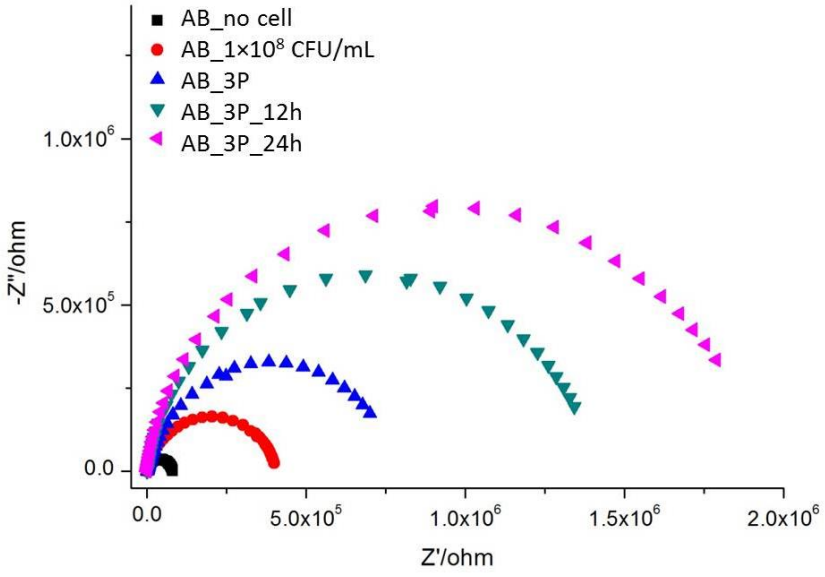

Figure 3.17 The impedance spectra of biofilm formation and protein adsorption

In order to get more results about protein fouling effects, more microbe sensors were tested with proteins. Three sensors were antibody treated and tested with 1×10^8 CFU/mL *P. auroginosa*, 12 hour biofilm formation and 24 hour biofilm formation, as shown in Figure 3.18(a1-a3). Another three sensors were antibody treated and tested with proteins, 12 hour

protein incubation and 24 hour protein incubation, as shown in Figure 3.18(b1-b3). The last three sensors were not surface treated, and tested with proteins, as shown in Figure 3.18(c1-c3).

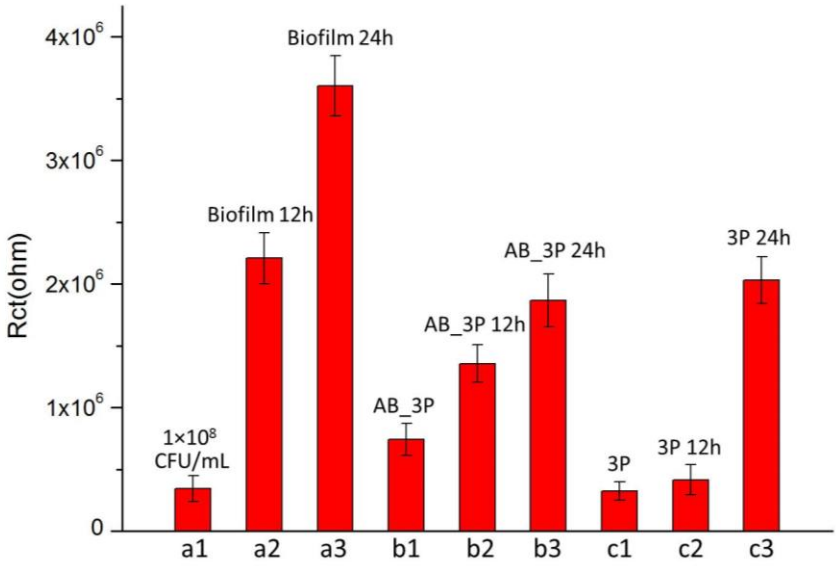

Figure 3.18 The comparison of impedance spectra of biofilm formation and protein adsorption

Compared with the R_{ct} of a1 to a3 (3.5×10^5, 2.2×10^6, and 3.6×10^6 Ω) and the R_{ct} of b1 to b3 (7.4×10^5, 1.4×10^6, and 1.9×10^6 Ω), the signals from protein absorption equals approximate 50% of the impedance from cells and biofilms, which shows that protein fouling is a significant interference for cell/biofilm monitoring. Further investigation need to be focused on avoiding the protein fouling effects for microbe sensors. A dual sensor design, similar as the previous glucose sensors, may provide a potential to delete the interference signals.

3.5 Summary

Based on the sensing method of electrochemical impedance spectroscopy, an interdigitated electrode was designed for the microbe sensor structure, and the antibody-antigen reaction was applied to attach the cells for surface measurement. After preliminary validation of *E.coli*, the microbe sensors were fully investigated with *P. auroginosa* cells for the common concentration of 0-10^9 CFU/mL. In the last part, the microbe sensors were further tested with biofilms induced by *P. auroginosa* and protein fouling effects. Future improvements for microbe sensors will likely include the protein interference rejection, optimized capsulation, and eventual wireless read-out integration.

Chapter 4 Conclusions

In this dissertation, two kinds of biosensors embedded in contact lenses are mainly presented: the glucose sensors have been designed to monitor human tear glucose levels in a continuous and non-invasive way; and the microbe sensors have been constructed to detect bacteria and biofilm in tears *in situ*.

In Chapter 1, a background of the relationship between diabetes, ocular diseases and human tear fluids is introduced. Since a lot of health information can be obtained by analyzing tear fluid, such as the glucose levels for diabetes and the bacterium concentrations for ocular infection, a contact lens with embedded sensors will potentially provide a way to monitor glucose or bacteria in a non-invasive way. Among various methods, electrochemical-based microsensors are relatively simple, inexpensive, and energy efficient. Therefore, electrochemical sensing is employed in the research for both glucose sensing and bacterium/biofilm monitoring.

In Chapter 2, by employing electrochemical reaction of glucose catalyzed by glucose oxidase, various generations of glucose sensors have been designed, based on the three electrode system, fabricated and then tested. A dual sensor design was applied for interference rejection and an sol-gel film was adopted for enzyme immobilization. The plastic sensors showed a good linearity for normal glucose levels in tear (0.1-0.6 mM), as well as repeatability, interference rejection and liability for up to 12 hours. The plastic sensors were next incorporated with wireless communication circuit and antenna to construct an integrated contact lens. The integrated sensors demonstrate a good linearity for glucose 0-1 mM and achieves wireless communication in a few centimeters. Finally glucose sensors were constructed on flexible parylene substrates and then encapsulated in pHEMA hydrogel to make soft contact lenses. The pHEMA was employed for enzyme immobilization, glucose permeability and protein fouling rejection. The embedded sensors exhibited good properties, such as a linearity for glucose 0-1 mM, good stability for more than 8 days and good protein rejection effect.

In Chapter 3, by utilizing electrochemical impedance spectroscopy, an interdigitated-electrode microbe sensor has been demonstrated. By employing antibodies specific to antigens on bacterium surfaces, the capture of bacteria onto electrode was achieved, which would cause a detective deviation of electron transfer resistance. The microbe sensors were validated by detecting two different bacterium strains, *E.coli* and *P. auroginosa*, for concentrations up to 10^9

CFU/mL. The detection limit was as low as 10^5 CFU/mL. Furthermore, by incubated in starvation situation for 12 hours and 24 hours, biofilms were induced and tested using the same microbe sensors by electrochemical impedance spectrometry.

Since the concentrations of tear glucose are reported to have relationship with blood glucose levels and bacterial infection will cause serious eye diseases or disorders, glucose sensors or microbe sensors embedded in contact lenses would make future personalized medicine cheaper, simpler and more reliable. The embedded biosensors could pave a new way to monitor human health in a continuous and non-invasive way during daily life. More research needs to be done to make real and practical products. Further work may include: optimizing the sensor design, testing the biocompatibility, improving the wireless transmission efficiency, and validating the sensors with animal or clinical experiment. Hopefully, the dissertation presented here will be helpful for the further extension of the field of modern medical devices.

References

[1] *Anatomy of the eye*. Available: http://www.ezcontactsusa.com/anatomy-of-the-eye.htm.

[2] R. S. Snell, Lemp, Michael A., *Clinical anatomy of the eye*. Oxford: Wiley-Blackwell, 1997.

[3] E. R. Berman, *Biochemistry of the eye*. New York: Plenum Press, 1991.

[4] S. A. Balasubramanian, D. C. Pye, and M. D. P. Willcox, "Levels of lactoferrin, secretory IgA and serum albumin in the tear film of people with keratoconus," *Experimental Eye Research,* vol. 96, pp. 132-137, 2012.

[5] I. D. Federation. *Prevalence estimates of diabetes, 2010*. Available: http://www.idf.org/.

[6] T. Allman, *Diabetes*. New York: Chelsea House Publishers, 2008.

[7] "Standards of Medical Care in Diabetes-2012," *Diabetes Care,* vol. 35, pp. S11-S63, 2012.

[8] S. Vaddiraju, D. J. Burgess, I. Tomazos, F. C. Jain, and F. Papadimitrakopoulos, "Technologies for continuous glucose monitoring: current problems and future promises," *J Diabetes Sci Technol,* vol. 4, pp. 1540-62, 2010.

[9] G. W. Shaw, D. J. Claremont, and J. C. Pickup, "Invitro Testing of a Simply Constructed, Highly Stable Glucose Sensor Suitable for Implantation in Diabetic-Patients," *Biosensors & Bioelectronics,* vol. 6, pp. 401-406, 1991.

[10] P. H. Kvist, T. Iburg, B. Aalbaek, M. Gerstenberg, C. Schoier, P. Kaastrup, T. Buch-Rasmussen, E. Hasselager, and H. E. Jensen, "Biocompatibility of an enzyme-based, electrochemical glucose sensor for short-term implantation in the subcutis," *Diabetes Technol Ther,* vol. 8, pp. 546-559, 2006.

[11] X. J. Gao, W. Y. Yang, P. F. Pang, S. T. Liao, Q. Y. Cai, K. F. Zeng, and C. A. Grimes, "A wireless magnetoelastic biosensor for rapid detection of glucose concentrations in urine samples," *Sensors and Actuators B-Chemical,* vol. 128, pp. 161-167, 2007.

[12] M. Yamaguchi, M. Mitsumori, and Y. Kano, "Noninvasively measuring blood glucose using saliva," *Ieee Engineering in Medicine and Biology Magazine*, vol. 17, pp. 59-63, 1998.

[13] J. D. Lane, D. M. Krumholz, R. A. Sack, and C. Morris, "Tear glucose dynamics in diabetes mellitus," *Current Eye Research,* vol. 31, pp. 895-901, 2006.

[14] J. T. Baca, D. N. Finegold, and S. A. Asher, "Tear glucose analysis for the noninvasive detection and monitoring of diabetes mellitus," *Ocular Surface,* vol. 5, pp. 280-93, 2007.

[15] W. F. March, A. Mueller, and P. Herbrechtsmeier, "Clinical trial of a noninvasive contact lens glucose sensor," *Diabetes Technol Ther,* vol. 6, pp. 782-9, 2004.

[16] M. X. Chu, T. Shirai, D. Takahashi, T. Arakawa, H. Kudo, K. Sano, S. Sawada, K. Yano, Y. Iwasaki, K. Akiyoshi, M. Mochizuki, and K. Mitsubayashi, "Biomedical soft contact-lens sensor for in situ ocular biomonitoring of tear contents," *Biomedical Microdevices,* vol. 13, pp. 603-611, 2011.

[17] R. Liang, J. Jiang, and J. Qiu, "An amperometric glucose biosensor based on titania sol-gel/Prussian Blue composite film," *Analytical Sciences,* vol. 24, pp. 1425-30, 2008.

[18] M. Miyashita, N. Ito, S. Ikeda, T. Murayama, K. Oguma, and J. Kimura, "Development of urine glucose meter based on micro-planer amperometric biosensor and its clinical application for self-monitoring of urine glucose," *Biosensors & Bioelectronics,* vol. 24, pp. 1336-40, 2009.

[19] J. P. Li, Y. P. Li, Y. Zhang, and G. Wei, "Highly Sensitive Molecularly Imprinted Electrochemical Sensor Based on the Double Amplification by an Inorganic Prussian Blue Catalytic Polymer and the Enzymatic Effect of Glucose Oxidase," *Analytical Chemistry,* vol. 84, pp. 1888-1893, 2012.

[20] D. Huber, M. Talary, F. Dewarrat, and A. Caduff, "The compensation of perturbing temperature fluctuation in glucose monitoring technologies based on impedance spectroscopy," *Medical & Biological Engineering & Computing,* vol. 45, pp. 863-76, 2007.

[21] M. Gourzi, A. Rouane, R. Guelaz, M. S. Alavi, M. B. McHugh, M. Nadi, and P. Roth, "Non-invasive glycaemia blood measurements by electromagnetic sensor: study in static and dynamic blood circulation," *J Med Eng Technol,* vol. 29, pp. 22-6, 2005.

[22] N. D. Evans, L. Gnudi, O. J. Rolinski, D. J. S. Birch, and J. C. Pickup, "Glucose-dependent changes in NAD(P)H-related fluorescence lifetime of adipocytes and fibroblasts in vitro: Potential for non-invasive glucose sensing in diabetes mellitus," *Journal of Photochemistry and Photobiology B-Biology,* vol. 80, pp. 122-129, 2005.

[23] O. W. Lau and B. Shao, "Determination of glucose using a piezoelectric quartz crystal and the silver mirror reaction," *Analytica Chimica Acta,* vol. 407, pp. 17-21, 2000.

[24] A. Matsumoto, N. Sato, T. Sakata, K. Kataoka, and Y. Miyahara, "Glucose-sensitive field effect transistor using totally synthetic compounds," *Journal of Solid State Electrochemistry,* vol. 13, pp. 165-170, 2009.

[25] L. C. Clark, Jr. and C. Lyons, "Electrode systems for continuous monitoring in cardiovascular surgery," *Ann N Y Acad Sci,* vol. 102, pp. 29-45, 1962.

[26] S. Park, H. Boo, and T. D. Chung, "Electrochemical non-enzymatic glucose sensors," *Analytica Chimica Acta,* vol. 556, pp. 46-57, 2006.

[27] A. Heller and B. Feldman, "Electrochemical glucose sensors and their applications in diabetes management," *Chemical Reviews,* vol. 108, pp. 2482-2505, 2008.

[28] C. Y. Li, C. H. Ahn, L. A. Shutter, and R. K. Narayan, "Toward real-time continuous brain glucose and oxygen monitoring with a smart catheter," *Biosensors & Bioelectronics,* vol. 25, pp. 173-178, 2009.

[29] P. D. Bank. (2006). Available: http://www.rcsb.org/pdb.

[30] H. J. Hecht, D. Schomburg, H. Kalisz, and R. D. Schmid, "The 3D structure of glucose oxidase from Aspergillus niger. Implications for the use of GOD as a biosensor enzyme," *Biosensors & Bioelectronics,* vol. 8, pp. 197-203, 1993.

[31] E. Csoregi, C. P. Quinn, D. W. Schmidtke, S. E. Lindquist, M. V. Pishko, L. Ye, I. Katakis, J. A. Hubbell, and A. Heller, "Design, Characterization, and One-Point in-Vivo Calibration of a Subcutaneously Implanted Glucose Electrode," *Analytical Chemistry,* vol. 66, pp. 3131-3138, 1994.

[32] A. Riklin, E. Katz, I. Willner, A. Stocker, and A. F. Buckmann, "Improving Enzyme-Electrode Contacts by Redox Modification of Cofactors," *Nature,* vol. 376, pp. 672-675, 1995.

[33] W. Schuhmann, "Electron-Transfer Pathways in Amperometric Biosensors - Ferrocene-Modified Enzymes Entrapped in Conducting-Polymer Layers," *Biosensors & Bioelectronics,* vol. 10, pp. 181-193, 1995.

[34] H. Muguruma, A. Hiratsuka, and I. Karube, "Thin-film glucose biosensor based on plasma-polymerized film: Simple design for mass production," *Analytical Chemistry,* vol. 72, pp. 2671-2675, 2000.

[35] A. Fang, H. T. Ng, and S. F. Li, "A high-performance glucose biosensor based on monomolecular layer of glucose oxidase covalently immobilised on indium-tin oxide surface," *Biosensors & Bioelectronics,* vol. 19, pp. 43-9, 2003.

[36] K. E. Toghill and R. G. Compton, "Electrochemical Non-enzymatic Glucose Sensors: A Perspective and an Evaluation," *International Journal of Electrochemical Science,* vol. 5, pp. 1246-1301, 2010.

[37] G. L. Cote, M. D. Fox, and R. B. Northrop, "Noninvasive Optical Polarimetric Glucose Sensing Using a True Phase Measurement Technique," *Ieee Transactions on Biomedical Engineering,* vol. 39, pp. 752-756, 1992.

[38] S. F. Malin, T. L. Ruchti, T. B. Blank, S. N. Thennadil, and S. L. Monfre, "Noninvasive prediction of glucose by near-infrared diffuse reflectance spectroscopy," *Clinical Chemistry,* vol. 45, pp. 1651-1658, 1999.

[39] N. C. Dingari, I. Barman, G. P. Singh, J. W. Kang, R. R. Dasari, and M. S. Feld, "Investigation of the specificity of Raman spectroscopy in non-invasive blood glucose measurements," *Analytical and Bioanalytical Chemistry,* vol. 400, pp. 2871-80, 2011.

[40] J. Gun, M. J. Schoning, M. H. Abouzar, A. Poghossian, and E. Katz, "Field-effect nanoparticle-based glucose sensor on a chip: Amplification effect of coimmobilized redox species," *Electroanalysis,* vol. 20, pp. 1748-1753, 2008.

[41] S. M. Borisov and I. Klimant, "Luminescent nanobeads for optical sensing and imaging of dissolved oxygen," *Microchimica Acta,* vol. 164, pp. 7-15, 2009.

[42] S. L. Luo, F. Su, C. B. Liu, J. X. Li, R. H. Liu, Y. Xiao, Y. Li, X. N. Liu, and Q. Y. Cai, "A new method for fabricating a CuO/TiO(2) nanotube arrays electrode and its application as a sensitive nonenzymatic glucose sensor," *Talanta,* vol. 86, pp. 157-163, 2011.

[43] X. Cao and N. Wang, "A novel non-enzymatic glucose sensor modified with Fe(2)O(3) nanowire arrays," *Analyst,* vol. 136, pp. 4241-4246, 2011.

[44] B. D. Davis, *Microbiology,* 4th ed. Philadelphia: Lippincott, 1990.

[45] C. R. Mahon and G. Manuselis, *Textbook of diagnostic microbiology*, 2nd ed. Philadelphia: Saunders, 2000.

[46] D. S. Selinger, R. C. Selinger, and W. P. Reed, "Resistance to Infection of the External Eye - Role of Tears," *Surv Ophthalmol,* vol. 24, pp. 33-38, 1979.

[47] T. Sakakibara, S. Murakami, and K. Imai, "Enumeration of bacterial cell numbers by amplified firefly bioluminescence without cultivation," *Analytical Biochemistry,* vol. 312, pp. 48-56, 2003.

[48] O. Lazcka, F. J. Del Campo, and F. X. Munoz, "Pathogen detection: A perspective of traditional methods and biosensors," *Biosensors & Bioelectronics,* vol. 22, pp. 1205-1217, 2007.

[49] N. K. Tran, D. G. Greenhalgh, T. L. Palmieri, and G. J. Kost, "Multiplex PCR Pathogen Detection in Two Severely Burned Patients With Suspected Septicemia," *Journal of Burn Care & Research,* vol. 32, pp. E172-E177, 2011.

[50] M. Cook and W. H. Lynch, "A sensitive nested reverse transcriptase PCR assay to detect viable cells of the fish pathogen Renibacterium salmoninarum in Atlantic salmon (Salmo salar L.)," *Applied and Environmental Microbiology,* vol. 65, pp. 3042-3047, 1999.

[51] D. Rodriguez-Lazaro, M. D'Agostino, A. Herrewegh, M. Pla, N. Cook, and J. Ikonomopoulos, "Real-time PCR-based methods for detection of Mycobacterium avium Subsp paratuberculosis in water and milk," *International Journal of Food Microbiology,* vol. 101, pp. 93-104, 2005.

[52] I. Hadrich, C. Mary, F. Makni, M. Elloumi, H. Dumon, A. Ayadi, and S. Ranque, "Comparison of PCR-ELISA and Real-Time PCR for invasive aspergillosis diagnosis in patients with hematological malignancies," *Medical Mycology,* vol. 49, pp. 489-494, 2011.

[53] D. A. Boehm, P. A. Gottlieb, and S. Z. Hua, "On-chip microfluidic biosensor for bacterial detection and identification," *Sensors and Actuators B-Chemical,* vol. 126, pp. 508-514, 2007.

[54] S. Y. Lee, T. J. Park, D. K. Kim, H. Kim, N. S. Heo, and S. J. Lee, "Label-free optical biosensors for the detection of food toxin and pathogen using multi-spot nanoparticle

array chip and fusion proteins," *Journal of Bioscience and Bioengineering*, vol. 108, pp. S159-S159, 2009.

[55] J. L. Huff, M. P. Lynch, S. Nettikadan, J. C. Johnson, S. Vengasandra, and E. Henderson, "Label-free protein and pathogen detection using the atomic force microscope," *Journal of Biomolecular Screening*, vol. 9, pp. 491-497, 2004.

[56] J. C. Liao, M. Mastali, V. Gau, M. A. Suchard, A. K. Moller, D. A. Bruckner, J. T. Babbitt, Y. Li, J. Gornbein, E. M. Landaw, E. R. B. McCabe, B. M. Churchill, and D. A. Haake, "Use of electrochemical DNA biosensors for rapid molecular identification of uropathogens in clinical urine specimens," *Journal of Clinical Microbiology*, vol. 44, pp. 561-570, 2006.

[57] T. S. Kazuhiro Nakanishi, Yoichi Kumada, Koreyoshi Imamura, and and H. Imanaka, "Recent Advances in Controlled Immobilization of Proteins onto the Surface of the Solid Substrate and Its Possible Application to Proteomics," *Current Proteomics*, vol. 5, pp. 161-175, 2008.

[58] Y. Li, W. A. Dick, and O. H. Tuovinen, "Fluorescence microscopy for visualization of soil microorganisms - a review," *Biology and Fertility of Soils*, vol. 39, pp. 301-311, 2004.

[59] C. Situ, J. Buijs, M. H. Mooney, and C. T. Elliott, "Advances in surface plasmon resonance biosensor technology towards high-throughput, food-safety analysis," *Trac-Trends in Analytical Chemistry*, vol. 29, pp. 1305-1315, 2010.

[60] A. Arnau, "A review of interface electronic systems for AT-cut quartz crystal microbalance applications in liquids," *Sensors*, vol. 8, pp. 370-411, 2008.

[61] S. P. Ravindranath, L. J. Mauer, C. Deb-Roy, and J. Irudayaraj, "Biofunctionalized Magnetic Nanoparticle Integrated Mid-infrared Pathogen Sensor for Food Matrixes," *Analytical Chemistry*, vol. 81, pp. 2840-2846, 2009.

[62] H. L. Lin, Q. Z. Lu, S. T. Ge, Q. Y. Cai, and C. A. Grimes, "Detection of pathogen Escherichia coli O157:H7 with a wireless magnetoelastic-sensing device amplified by using chitosan-modified magnetic Fe(3)O(4) nanoparticles," *Sensors and Actuators B-Chemical*, vol. 147, pp. 343-349, 2010.

[63] C. Gao, Y. Liu, X. H. Li, and A. Gu, "Carbon nanotube-based nanobiosensor for detection of pathogen DNA in the environment," *Abstracts of Papers of the American Chemical Society*, vol. 240, 2010.

[64] S. Pal, E. C. Alocilja, and F. P. Downes, "Nanowire labeled direct-charge transfer biosensor for detecting Bacillus species," *Biosensors & Bioelectronics*, vol. 22, pp. 2329-2336, 2007.

[65] J. L. Peng, Y. Xu, Y. J. Wu, N. Chuan, J. Gan, and P. Tian, "Determination of E. coli with Electrochemical Impedance on Homemade Microfluidic Chip," *Chinese Journal of Analytical Chemistry*, vol. 39, pp. 1307-1312, 2011.

[66] J. T. La Belle, M. Shah, J. Reed, V. Nandakumar, T. L. Alford, J. W. Wilson, C. A. Nickerson, and L. Joshi, "Label-Free and Ultra-Low Level Detection of Salmonella enterica Serovar Typhimurium Using Electrochemical Impedance Spectroscopy," *Electroanalysis*, vol. 21, pp. 2267-2271, 2009.

[67] W. G. Characklis, Marshall, Kevin C., *Biofilms*. New York: John Wiley & Sons, 1990.

[68] L. Friedman and R. Kolter, "Two genetic loci produce distinct carbohydrate-rich structural components of the Pseudomonas aeruginosa biofilm matrix," *Journal of Bacteriology*, vol. 186, pp. 4457-65, 2004.

[69] H. Ben-Yoava, Freemanb, A., Sternheimc, M., Shacham-Diamand, Y., "An electrochemical impedance model for integrated bacterial biofilms," *Electrochimica Acta*, vol. 56, pp. 7780-7786, 2011.

[70] Y. T. Wu, H. Zhu, M. Willcox, and F. Stapleton, "Removal of biofilm from contact lens storage cases," *Invest Ophthalmol Vis Sci*, vol. 51, pp. 6329-33, 2010.

[71] K. Milferstedt, M. N. Pons, and E. Morgenroth, "Optical method for long-term and large-scale monitoring of spatial biofilm development," *Biotechnology and Bioengineering*, vol. 94, pp. 773-82, 2006.

[72] O. Istanbullu, J. Babauta, H. Duc Nguyen, and H. Beyenal, "Electrochemical biofilm control: mechanism of action," *Biofouling*, vol. 28, pp. 769-78, 2012.

[73] T. Kim, J. Kang, J. H. Lee, and J. Yoon, "Influence of attached bacteria and biofilm on double-layer capacitance during biofilm monitoring by electrochemical impedance spectroscopy," *Water Research*, vol. 45, pp. 4615-22, 2011.

[74] E. Marsili, J. B. Rollefson, D. B. Baron, R. M. Hozalski, and D. R. Bond, "Microbial biofilm voltammetry: direct electrochemical characterization of catalytic electrode-attached biofilms," *Appl Environ Microbiol,* vol. 74, pp. 7329-37, 2008.

[75] J. Kang, Kim, T., Tak, Y., Lee, J.H., Yoon, J., "Cyclic voltammetry for monitoring bacterial attachment and biofilm formation," *Journal of Industrial and Engineering Chemistry,* vol. 18, pp. 800-807, 2012.

[76] A. J. Bard and L. R. Faulkner, *Electrochemical methods : fundamentals and applications*, 2nd ed. New York: Wiley, 2001.

[77] S. B. Hall, E. A. Khudaish, and A. L. Hart, "Electrochemical oxidation of hydrogen peroxide at platinum electrodes. Part 1. An adsorption-controlled mechanism," *Electrochimica Acta,* vol. 43, pp. 579-588, 1998.

[78] S. B. Hall, E. A. Khudaish, and A. L. Hart, "Electrochemical oxidation of hydrogen peroxide at platinum electrodes. Part II: effect of potential," *Electrochimica Acta,* vol. 43, pp. 2015-2024, 1998.

[79] A. P. Fang, H. T. Ng, and S. F. Y. Li, "A high-performance glucose biosensor based on monomolecular layer of glucose oxidase covalently immobilised on indium-tin oxide surface," *Biosensors & Bioelectronics,* vol. 19, pp. 43-49, 2003.

[80] W. Cheng, N. Klauke, H. Sedgwick, G. L. Smith, and J. M. Cooper, "Metabolic monitoring of the electrically stimulated single heart cell within a microfluidic platform," *Lab on a Chip,* vol. 6, pp. 1424-1431, 2006.

[81] F. Instruments. Available: http://www.flowinjection.com.

[82] H. F. Yao, A. J. Shum, M. Cowan, I. Lahdesmaki, and B. A. Parviz, "A contact lens with embedded sensor for monitoring tear glucose level," *Biosensors & Bioelectronics,* vol. 26, pp. 3290-3296, 2011.

[83] J. H. Yu, S. Q. Liu, and H. X. Ju, "Glucose sensor for flow injection analysis of serum glucose based on immobilization of glucose oxidase in titania sol-gel membrane," *Biosensors & Bioelectronics,* vol. 19, pp. 401-409, 2003.

[84] F. O. Brown and J. P. Lowry, "Microelectrochemical sensors for in vivo brain analysis: an investigation of procedures for modifying Pt electrodes using Nafion (R)," *Analyst,* vol. 128, pp. 700-705, 2003.

[85] R. P. Liang, J. L. Jiang, and J. D. Qiu, "An Amperometric Glucose Biosensor Based on Titania Sol-gel/Prussian Blue Composite Film," *Analytical Sciences,* vol. 24, pp. 1425-1430, 2008.

[86] E. M. I. M. Ekanayake, D. M. G. Preethichandra, and K. Kaneto, "Polypyrrole nanotube array sensor for enhanced adsorption of glucose oxidase in glucose biosensors," *Biosensors & Bioelectronics,* vol. 23, pp. 107-113, 2007.

[87] D. R. Whikehart, *Biochemistry of the eye*, 2nd ed. Boston: Butterworth-Heinemann, 2003.

[88] G. S. Wilson and R. Gifford, "Biosensors for real-time in vivo measurements," *Biosensors & Bioelectronics,* vol. 20, pp. 2388-2403, 2005.

[89] F. R. Shu and G. S. Wilson, "Rotating-Ring-Disk Enzyme Electrode for Surface Catalysis Studies," *Analytical Chemistry,* vol. 48, pp. 1679-1686, 1976.

[90] A. Kausaite-Minkstimiene, V. Mazeiko, A. Ramanaviciene, and A. Ramanavicius, "Enzymatically synthesized polyaniline layer for extension of linear detection region of amperometric glucose biosensor," *Biosensors & Bioelectronics,* vol. 26, pp. 790-797, 2010.

[91] T. Hoshi, H. Saiki, S. Kuwazawa, C. Tsuchiya, Q. Chen, and J. Anzai, "Selective permeation of hydrogen peroxide through polyelectrolyte multilayer films and its use for amperometric biosensors," *Analytical Chemistry,* vol. 73, pp. 5310-5315, 2001.

[92] S. E. Creager and K. G. Olsen, "Self-Assembled Monolayers and Enzyme Electrodes - Progress, Problems and Prospects," *Analytica Chimica Acta,* vol. 307, pp. 277-289, 1995.

[93] J. Wang, N. Naser, and M. Ozsoz, "Plant Tissue-Based Amperometric Electrode for Eliminating Ascorbic-Acid Interferences," *Analytica Chimica Acta,* vol. 234, pp. 315-320, 1990.

[94] F. Palmisano, R. Rizzi, D. Centonze, and P. G. Zambonin, "Simultaneous monitoring of glucose and lactate by an interference and cross-talk free dual electrode amperometric biosensor based on electropolymerized thin films," *Biosensors & Bioelectronics,* vol. 15, pp. 531-539, 2000.

[95] H. Yao, Liao, Y., Lingley, A.R., Afanasiev, A., Lähdesmäki, I., Otis, B.P., Parviz, B.A., "A contact lens with integrated telecommunication circuit and sensors for wireless and

continuous tear glucose monitoring," *Journal of Micromechanics and Microengineering,* vol. 22, p. 075007, 2012.

[96] V. N. a. L. Z. Godjevargova T, "Study of the thermal stability of glucose oxidase in the presence of water-soluble polymers," *J. Appl. Polymer Sci. ,* vol. 90, pp. 1393-7, 2003.

[97] A. A. H. Yao, I. Lähdesmäki, and B.A. Parviz, "A dual microscale glucose sensor on a contact lens, tested in conditions mimicking the eye " in *Micro Electro Mechanical Systems (MEMS), 2011 IEEE 24th International Conference on*, 2011, pp. 25-28.

[98] L. S. P. a. B. H, "Tear film rupture " *J. Colloid Interface Sci. ,* vol. 89, pp. 226-31, 1982.

[99] J. P. Craig, I. Singh, A. Tomlinson, P. B. Morgan, and N. Efron, "The role of tear physiology in ocular surface temperature," *Eye,* vol. 14, pp. 635-641, 2000.

[100] C. K. A, *Chemical Kinetics* New York VCH Publishers 1990.

[101] H. G. Xue, Z. Q. Shen, and C. M. Li, "Improved selectivity and stability of glucose biosensor based on in situ electropolymerized polyaniline-polyacrylonitrile composite film," *Biosensors & Bioelectronics,* vol. 20, pp. 2330-2334, 2005.

[102] A. Kuizenga, N. J. VanHaeringen, F. Meijer, and A. Kijlstra, "Analysis of human tear fluid components, inhibiting protein adhesion to plastic surfaces," *Experimental Eye Research,* vol. 63, pp. 319-328, 1996.

[103] D. Mirejovsky, A. S. Patel, D. D. Rodriguez, and T. J. Hunt, "Lipid Adsorption onto Hydrogel Contact-Lens Materials - Advantages of Nile Red over Oil Red-O in Visualization of Lipids," *Optometry and Vision Science,* vol. 68, pp. 858-864, 1991.

[104] E. Katz and I. Willner, "Probing biomolecular interactions at conductive and semiconductive surfaces by impedance spectroscopy: Routes to impedimetric immunosensors, DNA-Sensors, and enzyme biosensors," *Electroanalysis,* vol. 15, pp. 913-947, 2003.

[105] E. Jovanov, A. O. Lords, D. Raskovic, P. G. Cox, R. Adhami, and F. Andrasik, "Stress monitoring using a distributed wireless intelligent sensor system," *Ieee Engineering in Medicine and Biology Magazine,* vol. 22, pp. 49-55, 2003.

[106] J. Pandey, Y. T. Liao, A. Lingley, R. Mirjalili, B. Parviz, and B. P. Otis, "A Fully Integrated RF-Powered Contact Lens With a Single Element Display," *Ieee Transactions on Biomedical Circuits and Systems,* vol. 4, pp. 454-461, 2010.

[107] A. R. Lingley, M. Ali, Y. Liao, R. Mirjalili, M. Klonner, M. Sopanen, S. Suihkonen, T. Shen, B. P. Otis, H. Lipsanen, and B. A. Parviz, "A single-pixel wireless contact lens display," *Journal of Micromechanics and Microengineering*, vol. 21, 2011.

[108] Y. T. Liao, H. F. Yao, A. Lingley, B. Parviz, and B. P. Otis, "A 3-mu W CMOS Glucose Sensor for Wireless Contact-Lens Tear Glucose Monitoring," *Ieee Journal of Solid-State Circuits*, vol. 47, pp. 335-344, 2012.

[109] S. A. Stauth and B. A. Parviz, "Self-assembled single-crystal silicon circuits on plastic," *Proc Natl Acad Sci U S A*, vol. 103, pp. 13922-7, 2006.

[110] E. Saeedi, S. Kim, and B. A. Parviz, "Self-assembled crystalline semiconductor optoelectronics on glass and plastic," *Journal of Micromechanics and Microengineering*, vol. 18, 2008.

[111] P. S., "Contact-lens construction," 1983.

[112] B. Schulz, A. Riedel, and P. U. Abel, "Influence of polymerization parameters and entrapment in poly(hydroxyethyl methacrylate) on activity and stability of GOD," *Journal of Molecular Catalysis B-Enzymatic*, vol. 7, pp. 85-91, 1999.

[113] S. Lu and K. S. Anseth, "Photopolymerization of multilaminated poly(HEMA) hydrogels for controlled release," *Journal of Controlled Release*, vol. 57, pp. 291-300, 1999.

[114] J. P. Seymour, N. B. Langhals, D. J. Anderson, and D. R. Kipke, "Novel multi-sided, microelectrode arrays for implantable neural applications," *Biomedical Microdevices*, vol. 13, pp. 441-451, 2011.

[115] E. Meng, P. Y. Li, and Y. C. Tai, "Plasma removal of parylene c," *Journal of Micromechanics and Microengineering*, vol. 18, 2008.

[116] A. Tanioka, N. Fukushima, K. Hasegawa, K. Miyasaka, and N. Takahashi, "Permeation of Gases across the Poly(Chloro-P-Xylylene) Membrane," *Journal of Applied Polymer Science*, vol. 54, pp. 219-229, 1994.

[117] H. M. Yao, C. ; Afanasiev, A. ; Lahdesmaki, I. ; Parviz, B.A. , "A soft hydrogel contact lens with an encapsulated sensor for tear glucose monitoring " presented at IEEE 25th International Conference on the Micro Electro Mechanical Systems (MEMS), 2012.

[118] B. Z. Yu, C. Y. Wang, Y. M. Ju, L. West, J. Harmon, Y. Moussy, and F. Moussy, "Use of hydrogel coating to improve the performance of implanted glucose sensors," *Biosensors & Bioelectronics,* vol. 23, pp. 1278-1284, 2008.

[119] L. Li and L. J. Lee, "Photopolymerization of HEMA/DEGDMA hydrogels in solution," *Polymer,* vol. 46, pp. 11540-11547, 2005.

[120] K. G.P., "Injection molding process for rotationally asymmetric contact lens surfaces," 1999.

[121] "Evaluation of insulin glargine for the treatment of types 1 and 2 diabetes - Preface," *Current Medical Research and Opinion,* vol. 23, 2007.

[122] A. Abdul-Aziz and F. L. Wong, "Interference elimination of an amperometric glucose biosensor using poly(hydroxyethyl methacrylate) membrane," *Engineering in Life Sciences,* vol. 11, pp. 20-25, 2011.

[123] G. W. Shaw, D. J. Claremont, and J. C. Pickup, "In vitro testing of a simply constructed, highly stable glucose sensor suitable for implantation in diabetic patients," *Biosensors & Bioelectronics,* vol. 6, pp. 401-6, 1991.

[124] L. A.L., D.L., Nelson, M.M., Cox *Lehninger principles of biochemistry*. New York: W H Freeman & Co, 2005.

[125] F. Arslan, S. Ustabas, and H. Arslan, "An amperometric biosensor for glucose determination prepared from glucose oxidase immobilized in polyaniline-polyvinylsulfonate film," *Sensors (Basel),* vol. 11, pp. 8152-63, 2011.

[126] K. A. Conners, *Chemical Kinetics*. New York: VCH, 1990.

[127] H. Xue, Z. Shen, and C. Li, "Improved selectivity and stability of glucose biosensor based on in situ electropolymerized polyaniline-polyacrylonitrile composite film," *Biosensors & Bioelectronics,* vol. 20, pp. 2330-4, 2005.

[128] B. S., D., Narinesingh, A., Guiseppi-Elie, "Kinetics of glucose oxidase immobilized in p(HEMA)-hydrogel microspheres in a packed-bed bioreactor," *Journal of Molecular Catalysis B: Enzymatic,* vol. 18, pp. 69-80, 2002.

[129] M. R. Romero, F. Garay, and A. M. Baruzzi, "Design and optimization of a lactate amperometric biosensor based on lactate oxidase cross-linked with polymeric matrixes," *Sensors and Actuators B-Chemical,* vol. 131, pp. 590-595, 2008.

[130] B. G. Akgöl S., Kacar Y., Denizli A., Arıca M.Y., "Poly(hydroxyethyl methacrylate-co-glycidyl methacrylate) reactive membrane utilised for cholesterol oxidase immobilization," *Polym. Int.,* vol. 51, pp. 1316-1322, 2002.

[131] A. Kuizenga, N. J. van Haeringen, F. Meijer, and A. Kijlstra, "Analysis of human tear fluid components, inhibiting protein adhesion to plastic surfaces," *Experimental Eye Research,* vol. 63, pp. 319-28, Sep 1996.

[132] P. A. S. Mirejovsky D., Rodriguez D.D., Hunt T.J., "Lipid adsorption onto hydrogel contact lens materials. Advantages of Nile red over oil red O in visualization of lipids," *Optom. Vis. Sci.,* vol. 68, pp. 858-864, 1991.

[133] L. L. Chen S., Zhao C., Zheng J., "Surface hydration: principles and applications toward low-fouling/nonfouling biomaterials," *Polymer,* vol. 52, pp. 5283-5293, 2010.

[134] L. B. Garrett Q., Garrett R.W, "Hydrogel lens monomer constituents modulate protein sorption," *Invest Ophthalmol. Vis. Sci.,* vol. 41, pp. 1687-1695, 2000.

[135] A. Denizli, H. Yavuz, and Y. Arica, "Monosize and non-porous p(HEMA-co-MMA) microparticles designed as dye- and metal-chelate affinity sorbents," *Colloids and Surfaces a-Physicochemical and Engineering Aspects,* vol. 174, pp. 307-317, 2000.

[136] C. G. Gomez, G. Pastrana, D. Serrano, E. Zuzek, M. A. Villar, and M. C. Strumia, "Macroporous poly(EGDMA-co-HEMA) networks: Morphological characterization from their behaviour in the swelling process," *Polymer,* vol. 53, pp. 2949-2955, 2012.

[137] L. Yang and R. Bashir, "Electrical/electrochemical impedance for rapid detection of foodborne pathogenic bacteria," *Biotechnology Advances,* vol. 26, pp. 135-150, 2008.

[138] F. Scholz and A. M. Bond, *Electroanalytical methods : guide to experiments and applications*. Berlin ; New York: Springer, 2002.

[139] V. Escamilla-Gomez, S. Campuzano, M. Pedrero, and J. M. Pingarron, "Gold screen-printed-based impedimetric immunobiosensors for direct and sensitive Escherichia coli quantisation," *Biosensors & Bioelectronics,* vol. 24, pp. 3365-3371, 2009.

[140] D. Schleheck, N. Barraud, J. Klebensberger, J. S. Webb, D. McDougald, S. A. Rice, and S. Kjelleberg, "Pseudomonas aeruginosa PAO1 preferentially grows as aggregates in liquid batch cultures and disperses upon starvation," *Plos One,* vol. 4, p. e5513, 2009.

[141] B. G. Iversen, "Contaminated mouth swabs caused a multi-hospital outbreak of Pseudomonas aeruginosa infection," *J Oral Microbiol*, vol. 2, 2010.

[142] M. Q., S.A., Fadl-allah, N.S., El-Shenawy, "Electrochemical impedance spectroscopy study of the adsorption behavior of bovine serum albumin at biomimetic calcium-phosphate coating," *International Journal of Electrochemical Science*, vol. 7, pp. 4510-4527, 2012.